REPORT DOCUMENTATION PAGE

Form Approved OMB NO. 0704-0188

1. REPORT DATE (DD-MM-YYYY)	2. REPORT TYPE	3. DATES COVERED (From - To)
30-03-2015	Final Report	9-Aug-2010 - 8-Jan-2014

4. TITLE AND SUBTITLE
Final Report: Rare Earth Doped GaN Laser Structures Using Metal Modulated Epitaxy

5a. CONTRACT NUMBER
W911NF-10-1-0329

5b. GRANT NUMBER

5c. PROGRAM ELEMENT NUMBER
611102

6. AUTHORS
Andrew Steckl, Mingyu Zhong

5d. PROJECT NUMBER

5e. TASK NUMBER

5f. WORK UNIT NUMBER

7. PERFORMING ORGANIZATION NAMES AND ADDRESSES
University of Cincinnati
51 Goodman Dr.
PO Box 210222
Cincinnati, OH 45221 -0222

8. PERFORMING ORGANIZATION REPORT NUMBER

9. SPONSORING/MONITORING AGENCY NAME(S) AND ADDRESS (ES)
U.S. Army Research Office
P.O. Box 12211
Research Triangle Park, NC 27709-2211

10. SPONSOR/MONITOR'S ACRONYM(S)
ARO

11. SPONSOR/MONITOR'S REPORT NUMBER(S)
57881-EL.4

12. DISTRIBUTION AVAILIBILITY STATEMENT
Approved for Public Release; Distribution Unlimited

13. SUPPLEMENTARY NOTES
The views, opinions and/or findings contained in this report are those of the author(s) and should not contrued as an official Department of the Army position, policy or decision, unless so designated by other documentation.

14. ABSTRACT
A new growth scheme named Phase Shift Epitaxy (PSE) was developed. PSE is a periodic and dynamic growth scheme, which desynchronizes the host material growth with dopant incorporation by adjusting delays between shutters operation, frees the doping condition from limited host material growth condition confined by stoichiometry. PSE takes advantage of various surface conditions during each cycle. The overall uncompromised host quality and dopant can be introduced strategically at desired surface condition. This technique is first applied to Eu doping of GaN. Doping Eu in Ga rich condition leads to 10x enhancement of the photoluminescence

15. SUBJECT TERMS
GaN, phase shift epitaxy, doping, p-type, rare earths

16. SECURITY CLASSIFICATION OF:			17. LIMITATION OF ABSTRACT	15. NUMBER OF PAGES	19a. NAME OF RESPONSIBLE PERSON
a. REPORT	b. ABSTRACT	c. THIS PAGE			Andrew Steckl
UU	UU	UU	UU		19b. TELEPHONE NUMBER 513-556-4777

Report Title

Final Report: Rare Earth Doped GaN Laser Structures Using Metal Modulated Epitaxy

ABSTRACT

A new growth scheme named Phase Shift Epitaxy (PSE) was developed. PSE is a periodic and dynamic growth scheme, which desynchronizes the host material growth with dopant incorporation by adjusting delays between shutters operation, frees the doping condition from limited host material growth condition confined by stoichiometry. PSE takes advantage of various surface conditions during each cycle. The overall uncompromised host quality and dopant can be introduced strategically at desired surface condition. This technique is first applied to Eu doping of GaN. Doping Eu in Ga rich condition leads to 10x enhancement of the photoluminescence efficiency of Eu ions at a specific peak (620 nm) and 50% enhancement of the overall PL efficiency compared with optimum traditional MBE condition. PSE is also used for Mg doping of GaN to achieve p-type conductivity. Mg self-compensation effect is postponed to higher Mg concentration when Mg is doped in N rich condition and thus high hole concentration (2.4E18cm-3) is achieved. The highest Mg concentration by PSE is comparable to the highest concentration ever published thanks to the suppression of self-compensation effect. Phase Shift Epitaxy is thus proved effective in doping of GaN. PSE grown active layer (GaN:Eu) and p-type layer are tested in devices such as GaN p-n junction and GaN:Eu LED.

Enter List of papers submitted or published that acknowledge ARO support from the start of the project to the date of this printing. List the papers, including journal references, in the following categories:

(a) Papers published in peer-reviewed journals (N/A for none)

Received		Paper
03/27/2015	1.00	M. Zhong and A. J. Steckl, . GaN:Eu Metal Migration Epitaxy, JSAP Applied Physics Express, (12 2010): 121002. doi:
03/27/2015	2.00	M. Zhong, J. Roberts, W. Kong, A. S. Brown, A. J. Steckl. p-type GaN grown by phase shift epitaxy, Applied Physics Letters, (01 2014): 12108. doi: 10.1063/1.4861058
TOTAL:	**2**	

Number of Papers published in peer-reviewed journals:

(b) Papers published in non-peer-reviewed journals (N/A for none)

Received		Paper
TOTAL:		

Number of Papers published in non peer-reviewed journals:

(c) Presentations

Number of Presentations: 2.00

Non Peer-Reviewed Conference Proceeding publications (other than abstracts):

Received Paper

TOTAL:

Number of Non Peer-Reviewed Conference Proceeding publications (other than abstracts):

Peer-Reviewed Conference Proceeding publications (other than abstracts):

Received Paper

TOTAL:

Number of Peer-Reviewed Conference Proceeding publications (other than abstracts):

(d) Manuscripts

Received Paper

TOTAL:

Number of Manuscripts:

Books

Received Book

TOTAL:

Received Book Chapter

TOTAL:

Patents Submitted

Patents Awarded

Awards

Graduate Students

NAME	PERCENT_SUPPORTED	Discipline
Mingyu Zhong	1.00	
FTE Equivalent:	**1.00**	
Total Number:	**1**	

Names of Post Doctorates

NAME	PERCENT_SUPPORTED
FTE Equivalent:	
Total Number:	

Names of Faculty Supported

NAME	PERCENT_SUPPORTED	National Academy Member
Andrew Steckl	0.08	
FTE Equivalent:	**0.08**	
Total Number:	**1**	

Names of Under Graduate students supported

NAME	PERCENT_SUPPORTED
FTE Equivalent:	
Total Number:	

Student Metrics

This section only applies to graduating undergraduates supported by this agreement in this reporting period

The number of undergraduates funded by this agreement who graduated during this period: 0.00

The number of undergraduates funded by this agreement who graduated during this period with a degree in science, mathematics, engineering, or technology fields:..... 0.00

The number of undergraduates funded by your agreement who graduated during this period and will continue to pursue a graduate or Ph.D. degree in science, mathematics, engineering, or technology fields:..... 0.00

Number of graduating undergraduates who achieved a 3.5 GPA to 4.0 (4.0 max scale):..... 0.00

Number of graduating undergraduates funded by a DoD funded Center of Excellence grant for Education, Research and Engineering:..... 0.00

The number of undergraduates funded by your agreement who graduated during this period and intend to work for the Department of Defense 0.00

The number of undergraduates funded by your agreement who graduated during this period and will receive scholarships or fellowships for further studies in science, mathematics, engineering or technology fields: 0.00

Names of Personnel receiving masters degrees

NAME
Total Number:

Names of personnel receiving PHDs

NAME	
Mingyu Zhong	
Total Number:	**1**

Names of other research staff

NAME	PERCENT_SUPPORTED
FTE Equivalent:	
Total Number:	

Sub Contractors (DD882)

Inventions (DD882)

Scientific Progress

Gallium nitride is a well-known wide bandgap III/V semiconductor, commonly used in blue LEDs and lasers and increasingly in high power electronic devices. Indeed, GaN is sometimes being referred as the next important semiconductor material after silicon. GaN has two crystal structures: zinc blende and wurtzite. While both structures are direct recombination type semiconductors (lending themselves to efficient optical emission), zinc blende GaN is meta-stable (unstable above 600 °C) and high quality crystals are difficult to achieve. Wurtzite GaN is the most studied and in this work, the growth and doping study involves only wurtzite GaN Compared with other semiconductor material, wurtzite GaN has a very high critical breakdown field of 3MV/cm, making it very promising in next generation of high power devices.

Our group at the University of Cincinnati has been investigating for some time rare-earth-doped GaN electroluminescent devices. GaN also serves as an excellent host material for rare earth elements (Eu, Er, Tm, etc.) for luminescence application and for other transition metals (Mn, Gd, etc.) for potential magnetic application. These RE-doped thin films display truly amazing emission peaks from rare earth ions, which are strong and very sharp, insensitive to environment, and thus useful in a range of opto/electronic applications. The magnetic properties of these materials are found to have potential usage in areas such as quantum computing. We have been working very hard to improve the optical emission efficiency of these devices. Most importantly, if these doped GaN are thin films can be prepared with extremely low defect density (similarly to conventional semiconductors), then important devices with attractive characteristics can eventually be obtained. There is an increasing body of evidence that indicates that defects in these doped thin films play a very strong role in the energy transfer. For example, co-doping of Si, Mg with Eu in the active region of the device is found to be useful in improving the device efficiency. The main focus of this research has therefore become the quest to incorporate dopant impurities that can be optically active without simultaneously generating additional defect structures.

The ways in which atoms are incorporated into the lattice or the formation of favorable structure depends very strongly on the ratio of Group III to Group V elements, the so-called III/V ratio. This ratio determines the surface condition during growth: either Ga-rich or N-rich, depending on whether the III/V ratio is greater or smaller than 1. In general, one always needs to find an optimized growth condition for a doped material, which is usually different from the growth condition of undoped material. This difference in optimum conditions for growth of undoped vs doped layers results a trade-off between desired dopant structure formation efficiency and host material quality. Traditionally, similar research could proceed with design of experiment, choosing substrate temperature, III/V ratio for host, real time surface condition, dopant concentration, etc., as variables and choosing the thin film quality parameters (XRD FWHM, PL intensity, mobility, etc.) as the desired response. However, these variables are inter-dependent, making interpretation of the results rather obscure even with a huge amount of data.

In response, we have developed a novel growth scheme that we named phase shift epitaxy (PSE). PSE is a periodic and dynamic growth scheme, which desynchronizes the host material growth from dopant incorporation by adjusting delays between shutters operation. This approach frees the doping condition from limited host material growth condition that is confined by stoichiometry requirements. Inspired by similar dynamic growth schemes such as metal migration epitaxy (MME), PSE takes the advantage of various surface conditions during each cycle and the overall uncompromised host quality and dopant can be introduced strategically at desired surface condition. This new technique is first applied to Eu doping of GaN. Doping Eu in Ga rich condition leads to 10 times enhancement of the photoluminescence efficiency of Eu ions at a specific peak wavelength (620 nm, belonging to a specific Eu site in the GaN lattice) and 50% enhancement of the overall PL efficiency compared with optimum obtained by traditional MBE condition.

PSE was also utilized for Mg doping of GaN to achieve p-type conductivity. Mg self-compensation effect is postponed to higher Mg concentration when Mg is doped under the N-rich condition. Using PSE growth with Mg doping, a high hole concentration (2.4E18cm-3) was achieved. The highest Mg concentration demonstrated by PSE is comparable to the highest concentration reported previously, thanks to the suppression of self-compensation effect. In studying the Mg doping of GaN with PSE, we found that the incorporation of Mg under the N-rich condition greatly suppressed the self-compensation effect. The self-compensation is believed to originate from the formation of Mg clusters. In other words, doping Mg atoms in the N-rich condition helps improve the distribution uniformity of Mg.

PSE grown active layer (GaN:Eu) and p-type layers were successfully incorporated in two types of devices - GaN p-n junction diodes and GaN:Eu LEDs – resulting in promising electrical and optoelectronic characteristics.

Looking ahead to related applications of the PSE technique, InGaN alloys with high In content produce In clusters that are blamed for carrier localization, which in turn results in a greatly reduced he current efficiency of InGaN quantum well LED at high current density. This problem is similar to Mg doping of GaN except that In content could be as high as 40-50 atomic %. Indium and gallium are not perfectly miscible, thus when Indium content increases, In cluster concentration and size also increase. PSE with In incorporation under N-rich conditions may very likely provide a solution to improve the In distribution uniformity, so that long wavelength “green” or “red” InGaN quantum well LEDs may have higher current efficiency and less efficiency droop.
In terms of rare earth doped GaN, our study indicates that simply improving the quality of the host material is not the optimum approach. On the contrary, researchers should look more into co-doping rare earth elements with other impurities since defect levels play a big role in the energy transfer.

We conclude that phase shift epitaxy has been thus proven effective in the doping of GaN. Importantly, PSE could also be applied to the growth of alloy semiconductors (InGaN) in which high In content can lead to non-uniformity of In distribution and the onset of clusters. In conclusion, we believe that PSE can be a very effective tool in thin film doping and has the potential to achieve much higher quality doped films than other growth schemes.

Technology Transfer

Doped GaN grown by Phase Shift Epitaxy, fabrication and characterization of GaN:Eu LED

A dissertation submitted to the

Graduate School

of the University of Cincinnati

in partial fulfillment of the

requirements for the degree of

Doctor of Philosophy

in the Department of Electrical Engineering and Computing Systems

of the College of Engineering

by

Mingyu Zhong

B.S. Beijing University of Aeronautics and Astronautics, 2007

October 2013

Abstract

A novel growth and doping scheme in Molecular Beam Epitaxy (MBE) named Phase Shift Epitaxy (PSE) is developed and described in this thesis. PSE is a periodic and dynamic growth scheme which desynchronizes the host material growth and the dopant incorporation by adjusting delays between shutter operations. PSE frees the doping procedure from the limited growth conditions of the host material, making it a very effective technique for determining the optimum surface condition for a particular dopant. In order to demonstrate its advantages over traditional MBE growth, PSE techniques were applied to the doping of GaN (activated layer of GaN:Eu LED) and Mg doping of GaN (p-type). The optimum PSE condition for GaN:Eu with Eu doped in a Ga-rich surface condition, was shown to lead to over 50% enhancement of the photoluminescence efficiency of Eu ions compared with the optimum traditional MBE condition. Luminescence from a specific Eu location was significantly increased. With the PSE growth of p-type GaN:Mg, Mg self-compensation effect was significantly suppressed at high Mg concentration when Mg is doped in an N-rich condition. A high hole concentration (2.4E18cm^{-3}) is achieved with the optimum PSE condition for Mg doping. Even with a relatively high compensation donor level and a relatively poor template quality, this hole concentration result is comparable to the highest concentration, thanks to the self-compensating effect of PSE. Phase Shift Epitaxy is thus demonstrated to be a very effective tool in the doping of GaN, as well as other compound semiconductors.

The PSE-grown active layer (GaN:Eu) and the p-type layer are also tested in devices such as GaN p-n junction and GaN:Eu LED in order to prove its feasibility in device fabrication.

Acknowledgment

I would like to express my heartfelt gratitude to Professor Andrew Steckl, my dear friend as well as mentor. He has been so inspirational, supportive, and patient that I feel truly blessed. During these six years, Dr. Steckl has given me freedom and encouragement to pursue my research and has provided me with many insights related to my work. I would also like to thank the members of my PhD committee--Dr. Joseph T. Boyd, Dr. Jason C. Heikenfeld, Dr. Thomas D. Mantei, and Dr. John M. Zavada--for their suggestions and their helpful career advice.

I would like to thank Dr. Rui Wang for generously sharing his knowledge and experience in MBE, SIMS and nitride semiconductors. The discussions I was fortunate enough to have with Dr. Han You, as well as his assistance in system maintenance, were truly helpful. My thanks also go out to my fellow lab-mates: Daewoo Han, Duk Young Kim, Hans Dietrich, Srikoundinya Punnamaraju, Ben Pierce, Nick Bedford, Eliot Gomez, Adam Zocco, Sumit Purandare, Vishak Venkatraman, and Hua Li. It was such an enjoyable and rewarding experience working with all of you.

I would never have contemplated pursuing this career if not for my parents, Wei Zhong and Lianyu Ma, who instilled within me a love of creative pursuit and of science, both of which, I hope, inspire this thesis. Neither would this thesis have been possible without the love and support of my beloved fiancée, Yan Li. You have been with me all the way and I am so grateful.

Contents

Chapter 1. Introduction

GaN is an important wide band gap semiconductor material frequently used in optoelectronic applications such as LEDs and Lasers. It also serves as an excellent host material for foreign atoms in various applications: such as Rare earth (RE) elements (Eu, Er, Tm, etc.) for luminescence applications and other transition metals (Mn, Gd[34], etc.) for potential magnetic applications. Because in most cases the optimum conditions (surface condition, concentration, etc.) for each dopant are different, doping of GaN or any other material is usually considered a separate subject in the field of crystal growth. For example, the optimum III/N condition for un-doped GaN was found to be around III/N ratio =1, while in the case of Mg doping of GaN, different III/N conditions are usually used. Even in the specific case of Mg doping of GaN, diverse conclusions have been published. (Details will be given in Chapter 5.) A better understanding of the doping process is thus urgently needed. In this thesis, a new MBE process called Phase Shift Epitaxy was developed to serve this purpose.

In the traditional MBE process, molecular beam sources are kept ON continuously during the growth and the layers are grown after the surface reaches its static state. Different from the traditional MBE process, Phase Shift Epitaxy is a dynamic process that allows the existence of abundant surface conditions (from extremely N-rich to extremely Ga-rich) in each growth cycle, and in the meantime keeps the overall III/N ratio equal to 1. A careful control of dopant shutter would allow the incorporation of dopant under various surface conditions with minimum influence on the host lattice growth. This allows us to separate the optimization process of host lattice growth and doping. Optimum surface conditions for host lattice and doping are usually different and there is a “difficult to avoid” trade-off in conventional MBE doping. For example,

suppose the extreme N-rich condition is preferred for a particular dopant. (Under N-rich condition, dopant-related defects have the highest formation energy.) III/V=1 is the optimum condition for the host lattice. The optimum condition of this specific doped GaN is then slightly N-rich. Apparently, the slightly N-rich condition is not a perfect condition for either process. PSE allows one to simultaneously incorporate dopant and grow host lattice with different III/V ratios, making it a desirable growth process for high-quality doped GaN and other materials.

In our group at the University of Cincinnati, we have a long research history of using Rare Earth (RE) doped GaN for photonic applications. The optimization of doped GaN growth is a very important process for our group and the development of PSE technique thus allows us to meet various needs. The goal of the study of RE doping of GaN is to use GaN:RE as the active layer in LED; in this thesis, efforts have thus been made to fabricate GaN:RE LED devices with optimized PSE-grown layers.

The research aims of this thesis are:

1. Optimize the growth process for Eu doping and Mg doping of GaN with PSE.
2. Demonstrate the LED and p-n junction devices with PSE-grown layers, to prove the feasibility of this technique in device fabrication.

The thesis is constructed as follows: In the first chapter, a general description of the research background will be given, as well as a summary of the thinking behind the development of PSE techniques. Chapter 2 contains a description of the MBE system and of the characterization and fabrication techniques that are used in this thesis. Chapter 3 deals with the optimization of un-doped GaN with PSE. Since the host lattice quality for PSE can be independently optimized, the product from the study of un-doped GaN growth using PSE can be inherited and utilized in the

following chapters about GaN doping. Chapters 4 and 5 are concerned with Eu doping of GaN and Mg doping of GaN, respectively. Till this point, the three layers of a GaN:Eu LED (p-type layer, Eu-doped active layer, and Si-doped n-type layer) are optimized or readily available to us. In Chapters 6 and 7, the previously optimized materials are put together to construct a p-n junction and LEDs. These devices and their performance will be described. The last chapter concerns future work and suggestions for improvement on the current experiment.

In this chapter, we will start with general GaN characteristics, the growth method and current research status. Then a brief examination of rare-earth doped GaN and the application of this material in LED devices will be presented. Next, a novel technique for semiconductor doping called Phase Shift Epitaxy (PSE) and its advantages over the conventional MBE growth process will be discussed in detail. Finally, a comparison is made between PSE and similar techniques.

1.1 GaN and Related Devices

Gallium Nitride (GaN) and other III Nitrides have attracted attention due to their direct wide band gap nature and robust chemical properties. These properties (see Table 1.1) make GaN a very good candidate for opto-electronic and high-power applications such as high brightness blue LED, Laser and HEMT. Although research on GaN was begun in the early 20th century, [1-4] an efficient blue LED was not produced until 1995. [5]

GaN has two crystal structures: Zinc Blende and Wurtzite. The two structures are both direct type semiconductor, but since Zinc Blende GaN is meta-stable (unstable above 600 °C), high quality Zinc Blende structure is difficult to achieve. Wurtzite GaN is the most studied and will

be utilized in the present growth and doping study. The structural properties of these two GaN are listed below (Table 1.2). Compared with other semiconductor material, Wurtzite GaN has a very high critical breakdown field of 3MV/cm (Table 1.2) [6,7], making it very promising in next- generation high power devices.

Material	Bandgap (eV)	Electron Mobility (cm^2/Vs)	Hole Mobility (cm^2/Vs)	Critical Field Ec (V/cm)	Thermal Conductivity sT (W/m·K)	Coefficient of Thermal Expansion (ppm/K)
InSb	0.17, D	77,000	850	1,000	18	5.37
InAs	0.354, D	44,000	500	40,000	27	4.52
GaSb	0.726, D	3,000	1,000	50,000	32	7.75
GaN	3.44, D	900	10	3,000,000	110 (200 Film)	5.4-7.2
Ge	0.661, I	3,900	1,900	100,000	58	5.9
Si	1.12, I	1,400	450	300,000	130	2.6
SiC (3C, b)	2.36, I	300-900	10-30	1,300,000	700	2.77
SiC (6H, a)	2.86, I	330 - 400	75	2,400,000	700	5.12
SiC (4H, a)	3.25, I	700		3,180,000	700	5.12
diamond	5.46-5.6, I	2,200	1,800	6,000,000	1,300	0.8

Table 1. Properties of various semiconductors

Property/material	Cubit GaN (β-GaN)	Hexagonal GaN (α-GaN)

Structure	Zinc Blende	Wurzite
Stability	Meta-Stable	Stable
Lattice Parameters at R.T.	0.45 nm	a=0.3189 nm c=0.5185 nm
Density at R.T.	6.10 g.cm-3	6.095g.cm^{-3}
Bandgap	3.24 ev (direct)	3.44 ev (direct)

Table 1.2 Basic properties of GaN with different structures

GaN devices are usually grown on Ga-face GaN (Figure 1.1), since the thin film quality grown on Ga face is usually much more favorable than on N-face. In addition, Mg doping in N-face GaN is problematic, making it difficult to grow devices on N-face GaN. While some claim that building devices on M-plane and R-plane improves the LED efficiency by reduction of the quantum stark effect, [8] these semi or non-polar substrates have not been used in production due to their high cost.

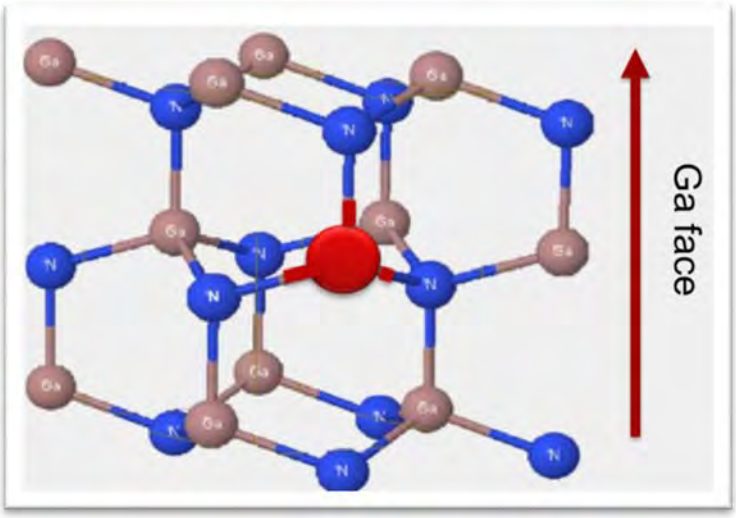

Figure 1.1 Wurzite GaN structure. The arrow indicates the Ga-face direction (0001). The opposite direction is N-face(000-1).

The lack of native substrate makes it very hard to obtain high quality GaN thin films. Lattice constant mismatch and thermal coefficient mismatch are two very important factors that significantly affect the crystal quality. The most commonly used substrate is sapphire, and the film grown on top of it generally has a dislocation density around 1E8/cm^2-1E10/cm^2. Sapphire is not only expensive but also highly resistive, making device fabrication difficult and costly. Extra steps (such as ICP dry etching or laser lift-off) also need to be taken to expose the bottom layer for electrode contact. Silicon, which has a higher mismatch to GaN, is a cheaper alternative. However, the dislocation density is usually approximately from 1E9/cm^2 to1E11/cm^2; the high-threading dislocation density degrades the device performance significantly. The joint effect of the 19% lattice mismatch and the 50% thermal expansion coefficient mismatch makes GaN growth on Si substrate very challenging. Not only will threading dislocations be generated during growth, but the thermal expansion mismatch can result in cracks if there is no effective stress release buffer layer. SiC has the lowest lattice mismatch (3.5%), and it is a semiconductor material. The GaN film quality on SiC is generally better, and the fabrication cost is relatively low for a vertical device (SiC as electrode contact), but SiC is much more expensive than sapphire, limiting its application to high-end devices. In recent years, bulk GaN substrates have become available in the market. These bulk GaN substrates are generally grown by HVPE on the sapphire substrate or in an ammonothermal process with GaN seed. Even though HVPE offers quite a high growth rate (100μm/h), it still requires hours or days to get a usable substrate. The ammonothermal process is much slower (10-50 μm/h) but it offers very low threading dislocation density (~1E4-1E5/cm^2). The

dislocation density of a bulk GaN substrate can be significantly reduced by LEO technology, [9-16] which enables vertical growth at selected areas on the substrate using a mask (usually SiN_x) and enhances lateral growth so that segregated terraces coalesce to form a new flat surface. The mask will stop the propagation of threading dislocations underneath it, and lateral growth is dislocation-free; thus, the defect density can be greatly reduced. This process to fabricate high-quality bulk GaN substrate is extremely inefficient. For these reasons, the cost of bulk GaN is high when compared with other substrates.

Bulk GaN vs. Non-Native Substrates				
	GaN on Bulk GaN†	**GaN on SiC**	**GaN on sapphire**	**GaN on Silicon**
Lattice Constant Mismatch	0%	3.5% mismatch	14% mismatch	17% mismatch
Dislocation Density	10^4 - 5 x 10^6 / cm^2	1 x 10^9 / cm^2	5 x 10^9 / cm^2	1 x 10^{11} / cm^2
Thermal Conductivity	2.5 W/cm-K	1.3 W/cm-K	1.2 W/cm-K	1.0 W/cm-K

Table 1.3 Threading dislocation densities in GaN films grown on different substrates

1.2 Growth Techniques for GaN

There are several techniques available for epitaxial growth of GaN. The most commonly used technique in industry is MOCVD, which delivers a satisfactory quality and relatively fine control of the growth with a high growth rate (2 μm/hr). Multiple wafers can be placed in the chamber at the same time; thus MOCVD is suitable for mass production. However, it has several

disadvantages. Since it is gas phase deposition, turning the gas stream on and off requires a relatively long time and a sharp hetrojunction interface is difficult to obtain. It is also very hard to monitor the growth, due to limited in-situ characterization techniques. Process gas is extremely toxic and requires special attention during operation and maintenance. A high substrate temperature (above 1000 °C) is needed for the reaction, which requires special chamber design and chamber material selection.

Another technique widely used in industry for GaN growth is HVPE. HCl is introduced to the surface of Ga, which contains a quartz boat to pick up Ga. GaCl and NH_3 reaction takes place on the substrates to form GaN and HCl. Extra HCl is evaporated due to a high substrate temperature. The advantage of HVPE is that its growth rate is very high (100-200 μm/hr), making it useful for bulk GaN substrate growth. However, the high growth rate compromises the ability to fine control growth and thus it is not suitable for device fabrication.

MBE is another well-developed technique for thin film growth. First of all, an ultra-high vacuum chamber is used such that molecules or atoms can travel a long distance inside the chamber. Molecular beams are released from a source and directed to the substrate. For GaN growth, Ga is evaporated from a high temperature cell equipped with a PBN crucible. Two kinds of N source are commonly used. The NH_3 gas source is relatively simple, but high substrate temperature (800 °C) is required for efficient NH_3 decomposition. The N_2 plasma source provides relatively efficient cracking, and active N is delivered directly to the substrate without extra decomposition effort, and so the growth temperature can be reduced to around 600-700 °C. MBE equipped with a gas source is usually referred to as Gas Source MBE. If a plasma source is used to crack Nitrogen, the system or process is usually referred to as Plasma Assisted MBE (PA-MBE).

GaN contains many structural and point defects caused largely by lattice mismatch. These defects notably alter the electrical and optical properties of the host material and can seriously degrade the performance and reliability of devices. Furthermore, long after the first single crystal GaN was synthesized by H. P. Maruska and J. J. Tietjen,[17] all films have shown extremely high electron concentration (>1E19cm^{-3}) even without intentional doping. The problems were at first attributed to the high density of N vacancies formed during the film growth. Later, based on state-of-the-art first principle calculations, n-type doping nitrogen vacancies were shown to be too high in energy to be incorporated during growth, while silicon and oxygen from the chamber contamination readily form donors. [18] Besides, the photoluminescence of GaN usually exhibits strong and broad yellow luminescence centered around 2.2 ev. Only recently has this donor-acceptor type emission featuring a broad peak been found to be C-related. [19]

1.3 RE-doped GaN

RE elements play a very important role in optoelectronic and photonic applications. They are used in solid-state lasers as emitting elements and in color lamps and displays as phosphors. The RE elements have a partially filled inner ($4f^n$) shell shielded from its surroundings by completely filled outer ($5s_2$ and $5p_6$) orbits. Due to the shielding effect, the intro $4f^n$ shell transitions result in very sharp optical emissions. In the case of Er-doped optical fiber amplifiers, Er ions are pumped to a higher state by photon excitation. Usually, the pump light has a wavelength of

980-1450 nm. The light excites the erbium ions into the 4I 13/2 state. Once the population inversion is achieved, a 1.5 μm wavelength light can be amplified via stimulated emission.

Unlike glass fiber, GaN is a semiconductor and thus doped RE ions can be electrically activated. Secondly, RE ions are trivalent and readily take the Ga sites in the GaN lattice. For this reason, RE ions can be safely introduced into the lattice without the introduction of extra defect structures. In addition, RE doping for optoelectronic applications is simpler than the delicate control of quantum wall thickness, so that GaN:RE LED is potentially easier to grow than conventional quantum well LEDs.

For several years, research on RE doping of GaN was ongoing in our lab. We have obtained photoemission with different colors from different RE elements in GaN, and we have demonstrated that almost the entire color map can be covered by doping different RE ions into GaN.[20-24] Figure 1.2 shows the transitions responsible for visible emission from GaN doped with different RE ions.

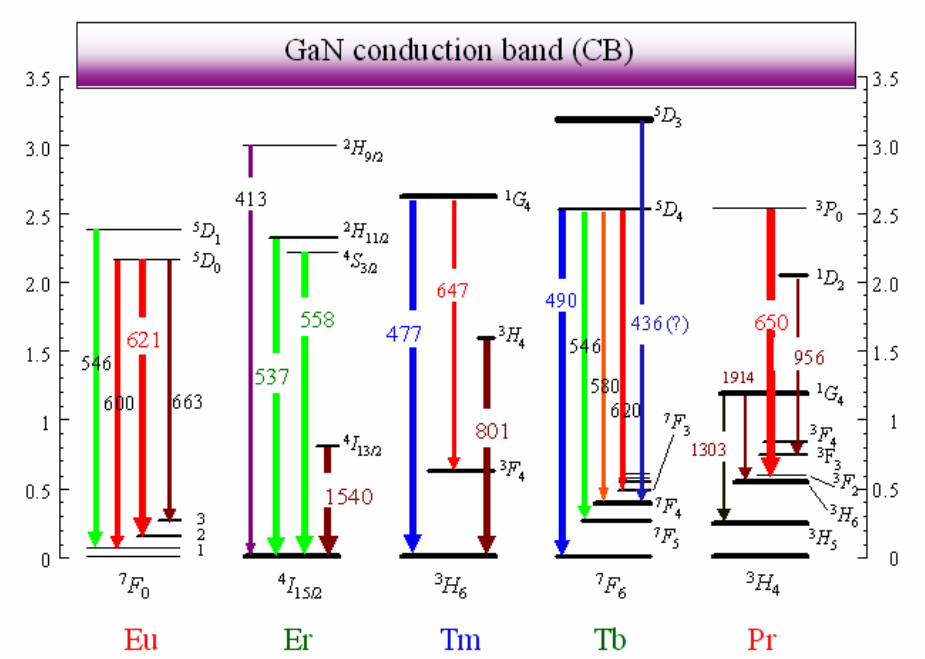

Figure 1.2 The transitions responsible for visible emission from GaN doped with different RE ions

RE doping into GaN can be achieved through ion implantation. However, the implantation of such heavy elements usually results in lattice damage, some of which cannot be healed by post annealing. Another way to incorporate RE into a GaN lattice is in-situ doping, i.e. introducing RE elements during growth. In this thesis, we focus on in-situ doping of RE elements using MBE.

1.4 GaN:RE Electroluminescence Devices (ELDs)

Both DC and AC devices were studied in nano-lab. AC electroluminescence devices were found to have higher efficiency than DC electroluminescence devices. [25] However, all of these devices

have very high threshold voltages and low efficiencies. Other GaN:RE LEDs with a thinner MBE- grown active layer have a lower threshold voltage but still very low efficiency.[26]

In Japan, relatively high efficiency has been achieved by Nishikawa, et al. [27,28] with atmosphere MOCVD. Similar results have been published using MBE, but with the active layer co-doped with Mg and Eu. [29]

Typical LED behavior from relatively high efficiency GaN:Eu LEDs [27,29] suggests that the electron-hole recombination is responsible for the RE excitation. On the other hand, high threshold voltage from the DC and AC ELD devices suggests that the impact of hot carriers is responsible for the activation of Eu ions. The energy released from electron-hole recombination is indirectly transferred to the RE ions through defect levels. Photoluminescence resulting from Mg Eu co-doping samples suggests a very complex process involving electron-hole recombination and several defect levels. [29]

1.5 Considerations in Conventional MBE Growth

Before introducing Phase Shift Epitaxy, it is necessary to discuss some basic considerations regarding conventional MBE. Similar to other growth techniques, MBE-grown film quality is highly sensitive to substrate temperature, Ga and N flux, substrate lattice and contamination level. However, it is not very sensitive to chamber pressure since the pressure during growth is usually below 1E-4 Torr and so has an insignificant effect on the transportation of Ga or N.

The determination of the substrate temperature of an MBE growth is usually related to the stability of the liquid metal layer on the surface as well as the stability of the final product. For example, since the decomposition of GaAs occurs at a higher temperature, the growth rate is

significantly reduced and so the growth of GaAs is usually carried out at a substrate temperature of 500-600 °C. In the case of InN, the In metal layer on the surface has a very high desorption rate and thus growth at a higher substrate temperature requires a great amount of compensation of In flux. Also, with high Indium flux compensation, Indium film stability is compromised because Indium Nitride starts to decompose with thick Indium surface coverage. Thus, for InN, the substrate temperature is usually in the area of 500 °C. Since Ga has a lower desorption rate than Indium, GaN growth temperature is higher, usually from 600-750 °C. If the nitrogen source is NH_3 instead of N_2 plasma, the NH_3 decomposition rate is also a serious concern. In this case, a substrate temperature of at least 800 °C is required for NH_3 decomposition and growth is usually carried out at N-rich condition to ensure the stability of Ga (similar to MOCVD). Growth with NH_3 source in MBE is similar to MOCVD growth in the sense that decomposition of the precursor at the surface is required and an N-rich condition is used.

The substrate temperature also affects impurity incorporation. In an Ultra High Vacuum (UHV) chamber pumped with a cyro pump, trace gasses coming from the out-gassing of the chamber wall usually consist of H_2 and CO in the range of 1E-14 Torr to 1E-13 Torr. N_2 gas impurity can be reduced with a "point of use" purifier, which is very effective in removing the impurities in N_2(except CH_4). The plasma tube is also an important source of impurity. (For example, Boron is released from the PBN crucible, although at a very slow rate.) All of these concerns make it very hard to get a low impurity level in the reaction chamber. For this reason, the substrate temperature is usually kept as high as possible to lower the sticking coefficient of impurities. Another advantage of increasing substrate temperature is that in this way the surface mobility of each species can be maximized.

The most important factor of MBE growth of GaN is III/V ratio. Different optimum III/V ratios are usually reported for different growth processes, depending on substrate temperatures. To avoid confusion in the future, the relationship between III/V ratio and film growth must be described in detail.

III/V can also be described according to whether it is Ga- or N-rich, by its Ga Monolayer (ML) thickness, and sometimes with a number. In the case of GaN MBE, extra Ga (with a maximum growth rate and higher ML) on the surface acts as a surfactant to help smooth the surface. This is the reason why the optimum III/V ratio of GaN MBE growth is sometimes reported as slightly higher than 1. However, at a higher substrate temperature, due to the above-mentioned metal stability issue, the III/V ratio is kept slightly lower than 1 in order to stabilize Ga. The stability of Ga in N-rich condition is described in detail in Reference 30. Generally speaking, without knowledge of the substrate temperature, the ideal III/V ratio is 1 (stoichiometry).

In the case of N-rich condition, Ga ML thickness is less than 1 and Ga mobility is limited, since its moving to another location requires breaking a relatively tight Ga-N bond. Thus, the GaN surface is rough and full of structural defects, due to incomplete Ga ML and limited Ga mobility on the surface. We must be clear that this applies to low-mid temperature (550-700 °C) growth. At high temperature, Ga mobility is higher and an N-rich condition does not necessarily result in a rough surface. In the case of a Ga-rich condition (more Ga than in the case of optimum condition), Ga ML thickness is too high and thus Ga droplets form on the surface. In this case, surface roughness increases and N vacancies are easily formed because of the extra Ga on the surface.

In the optimum, slightly Ga rich-condition, extra Ga acts as surfactant to smooth the surface. At the beginning of the growth, Ga on the surface will increase to its static state a few seconds after the Ga shutter is turned on. This transition to a static state can be easily observed and roughly measured by the variation of RHEED pattern intensity. To be more accurate, the transition time can be calculated with the rate equation shown below:

$$\frac{dM}{dt} = F - G - D \qquad \text{eq. 1.1}$$

In this equation, M is metal (Ga) ML thickness, t is time, F is the incoming flux of metal (Ga), and G and D are growth rate and desorption rate, respectively. This differential equation will be discussed in detail in Chapter 5 and the predicting power of this differential equation will be shown. It is interesting that the existence of the static Ga ML in conventional MBE growth makes this process somewhat similar to Liquid Phase Epitaxy (LPE).

1.6 Phase Shift Epitaxy and Other Dynamic Growth Schemes

The concept of Phase Shift Epitaxy derives from a set of simple questions. As we know from the previous section, a unity III/N ratio is considered the optimum condition. However, should we assume that this optimum growth condition for GaN is also the optimum growth condition for doping? Supposing X is dopant and X_aN_b is an unwanted defect to be minimized, which condition (Ga- or N-rich) helps minimize its formation? If X_aN_b turns out to have useful properties, which condition helps promote its formation? These questions have no meaning in conventional MBE growth, since even if an N-rich condition is useful for doping, the film is still

grown under a condition approaching the optimum condition for un-doped GaN. We are therefore almost certain that the "optimized" condition for a certain doping is the result of a trade-off if there is a difference in the optimum conditions for doping and host lattice.

PSE is used to solve this problem of trade-off. In this dynamic growth scheme, active nitrogen flux is always ON but the Ga shutter is opened and closed periodically. If Ga flux is kept higher than that which is used in optimum condition, Ga ML thickness on the surface will vary from 0 to beyond its optimum thickness. When the Ga shutter is closed, extra Ga surface will be consumed by nitrogen or be evaporated. In this way, the Ga ML thickness iterates through N-rich condition and Ga-rich condition, but overall there is no extra Ga accumulated nor is the structure seriously damaged by N-rich condition. In fact, the resulting film has very good quality and surface smoothness. [31] More importantly, dynamic growth schemes like these provide us with different surface conditions (Ga-rich and N-rich) in each cycle. The idea of Phase Shift Epitaxy is to incorporate dopant only when a certain surface condition is satisfied.

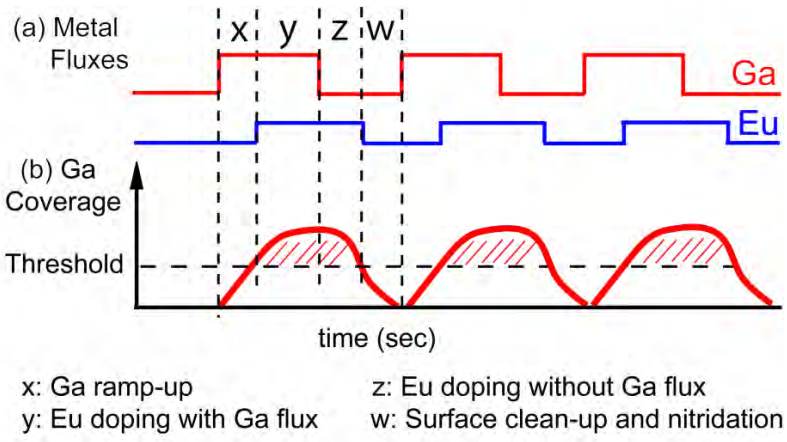

Figure 1.3 Ga surface variation during dynamic growth

As shown in Figure 1.3, nitrogen is always on and not shown. Ga shutter operation is expressed in the form of a red wave. When the Ga shutter is open (at high state), Ga coverage is gradually built up. When the shutter is closed, Ga coverage will gradually drop back to zero. The threshold shown in the figure can be regarded as the optimum Ga ML thickness if the film is grown with convention MBE. With varying surface conditions, it is theoretically possible to have dopant arrives at the surface at a given time when the surface condition is right for doping.

The above discussion is on a theoretical level. In fact, dopant that arrives at the surface is not incorporated immediately. The dopant concentration or density on the surface experiences a similar ramp-up and drop-back transition as with Ga. To avoid confusion, the aforementioned dopant on the surface is not yet incorporated, in other words, no N-dopant bonding has yet occurred. In Chapter 5, we will discuss the transition rate using a mathematical model.

There are also many other dynamic growth schemes for semiconductor epitaxy, in either MOCVD or MBE. In this section, we will focus on the dynamic growth schemes for MBE.

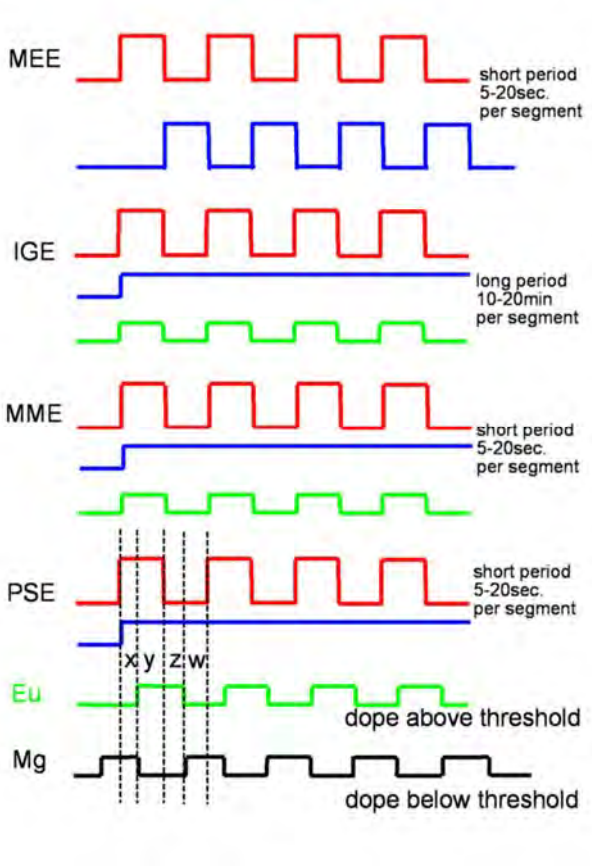

Figure 1.4 Different dynamic growth schemes

In Migration-Enhanced Epitaxy (MEE),[32] both Ga and N flux are modulated. The use of a Ga-only cycle in MME ensures that all Ga sites are taken by Ga. In the N cycle, N is trying to saturate the leftover Ga and decrease N vacancies. This approach is found to result in a high-quality GaN film and a smoother surface. [31]

Interrupted Growth Epitaxy (IGE) [33]is not, strictly speaking, a dynamic growth scheme in that the cycle time is usually from 15 to 30 minutes. In each growth cycle (Ga ON, N ON), the growth condition is close to III/V=1. After the growth cycle, a nitridation cycle occurs in which N flux is used to alter the properties of the already grown film. In Interrupted Growth Epitaxy,

Dopant and Ga shutters open and close at the same time. There are some reports[33] showing that IGE can help improve the photoluminescence efficiency of GaN, but the reason is not quite clear.

Metal Migration Epitaxy (MME) is similar to IGE but each period is much shorter (only 5 to 15 seconds). MME can be regarded as a dynamic growth scheme since there are no or only very short "static states in conventional MBE." The Ga shutter operation and the dopant shutter operation are synchronized, a major difference between MME and PSE. MME has been intensely studied in the doping of Mg in GaN. The reason for using MME is, on the one hand, because the dynamic growth scheme helps improve host quality. On the other hand, the authors claim that the extreme Ga-rich portion of the cycle helps improve Ga incorporation.[17]

In conclusion, of the various dynamic schemes described in this section, Phase Shift Epitaxy alone has been designed to incorporate dopant only at desired surface conditions. In the next chapter, a mathematic model with real world data will be used to help quantify the PSE process.

References

1. H. H. Robert Juza, Zeitschrift fur anorganische und allgemeine Chemie 239-282 (1938)
2. Schoonma.Rc, A. Buhl and J. Lemley, J. Phys. Chem. 69 (10), 3455 (1965).
3. T. L. Chu and F. Y. Jou, J. Electrochem. Soc. 116 (7), C250 (1969).
4. Krasnope.Va and I. S. Fainer, Optics and Spectroscopy-Ussr 26 (2), 166 (1969).
5. S. Nakamura, N. Senoh, N. Iwasa and S. I. Nagahama, Jpn. J. Appl. Phys. Part 2 - Lett. 34 (7A), L797-L799 (1995).
6. Chow, T.P, Ghezzo. SiC power devices. in III-Nitride, SiC, and Diamond Materials for Electronic Devices.
7. Eds. Gaskill D.K, Brandt C.D. and Nemanich R.J., Material Research Society Symposium Proceedings, Pittsburgh, PA. 423 (1996), 69-73.
8. J. H. Ryou, W. Lee, J. Limb, D. Yoo, J. P. Liu, R. D. Dupuis, Z. H. Wu, A. M. Fischer and F. A. Ponce, Appl. Phys. Lett. 92 (10), 101113-101113 (2008).
9. C. B. Soh, S. Y. Chow, S. Tripathy and S. J. Chua, Journal of Physics: Condensed Matter 20 (9), 095210 (2008).
10. K. T. Liu, T. Tezuka, S. Sugita, Y. Watari, Y. Horikoshi, Y. K. Su and S. J. Chang, J. Cryst. Growth 263 (1–4), 400-405 (2004).
11. C.-H. Lin, R. Abe, S. Uchiyama, T. Maruyama and S. Naritsuka, J. Cryst. Growth (0).
12. J. Kamimura, K. Kishino and A. Kikuchi, AIP Advances 1 (4), 042145 (2011).
13. K. Hiramatsu, K. Nishiyama, M. Onishi, H. Mizutani, M. Narukawa, A. Motogaito, H. Miyake, Y. Iyechika and T. Maeda, J. Cryst. Growth 221 (1–4), 316-326 (2000).
14. T. Detchprohm, S. Sano, S. Mochizuki, S. Kamiyama, H. Amano and I. Akasaki, physica status solidi (a) 188 (2), 799-802 (2001).
15. N. Chand, J. Cryst. Growth 97 (2), 415-429 (1989).
16. G. Bacchin, A. Umeno and T. Nishinaga, Applied Surface Science 159–160 (0), 270-276 (2000).
17. H. P. Maruska and J. J. Tietjen, Applied Physics Letters 15 (10), 327-329 (1969).
18. C. G. Van de Walle, C. Stampfl and J. Neugebauer, Journal of Crystal Growth 189–190 (0), 505-510 (1998).
19. J. L. Lyons, A. Janotti and C. G. Van de Walle, Appl. Phys. Lett. 97 (15), 152108-152103 (2010).
20. J. Steckl and R. H. Birkhahn, “Visible emission from Er-doped GaN grown by solid source MBE,” Appl. Phys. Lett., vol. 73, pp. 1700–1702, 1998.
21. J. Steckl, M. J. Garter, R. H. Birkhahn, and J. Scofield, “Green electroluminescence from Er-doped GaN Schottky barrier diodes,” Appl.Phys. Lett., vol. 73, pp. 2450–2452, 1998.
22. M. J. Garter, J.D. Scofield, R. H. Birkhahn, and A. J. Steckl, “Visible and infrared emission from ITO/GaN:Er/Si Schottky diodes,” Appl. Phys. Lett., vol. 74, pp. 182–184, 1999.

23. J. Heikenfeld, M. J. Garter, D. S. Lee, R. H. Birkhahn, and A. J. Steckl,“Red light emission by photoluminescence and electroluminescence from Eu-doped GaN,” Appl. Phys. Lett., vol. 75, pp. 1189–1191, 1999.
24. D. S. Lee and A. J. Steckl, “Room-temperature-grown rare-earth-doped GaN luminescent thin films,” Appl. Phys. Lett., vol. 79, pp. 1962–1964,2001.
25. D. S. Lee and A. J. Steckl, “Lateral color integration on rare-earth doped GaN electroluminescent thin films,” Appl. Phys. Lett., vol. 80,pp. 1888–1890, 2002.
26. J. M. Zavada, S. X. Jin, N. Nepal, J. Y. Lin, H. X. Jiang, P. Chow and B. Hertog, Appl. Phys. Lett. 84 (7), 1061-1063 (2004).
27. Nishikawa, N. Furukawa, T. Kawasaki, Y. Terai and Y. Fujiwara, Appl. Phys. Lett. 97 (5), 051113-051113 (2010).
28. Nishikawa, T. Kawasaki, N. Furukawa, Y. Terai and Y. Fujiwara, physica status solidi (a) 207 (6), 1397-1399 (2010).
29. Wakahara, H. Sekiguchi, H. Okada and Y. Takagi, Journal of Luminescence 132 (12), 3113-3117 (2012).
30. G. Koblmuller, F. Wu, T. Mates, J. S. Speck, S. Fernandez-Garrido and E. Calleja, Appl. Phys. Lett. 91 (22), 221905-221903 (2007).
31. Burnham, PhD thesis 2007
32. S. D. Burnham, G. Namkoong, D. C. Look, B. Clafin and W. A. Doolittle, J. Appl. Phys. 104 (2) (2008).
33. Munasinghe, A.J. Steckl GaN:Eu electroluminescent devices grown by interrupted growth epitaxy Thin Solid Films 496 (2006) 636 – 642
34. A. Thiess, P. H. Dederichs, R. Zeller1, S. Blügel, and W. R. L. Lambrecht, Superparamagnetism in Gd-doped GaN induced by Ga-vacancy clustering Phys. Rev. B 86, 180401(R) (2012)

Chapter 2. MBE system and in-situ characterization techniques

The MBE system consists of several subsystems: gas delivery system, element sources, in-situ characterization tools, sample maneuver system, pumping system, interlock safety system and etc. MBE ultra-high vacuum chamber is usually under constant pumping by one or several cryogenic pumps. Another important component for an ultra-high vacuum system such as MBE is the load lock. The use of load lock effectively reduced the pumping time of the main chamber and prevents water vapor from getting into the main chamber. In the following sections in this chapter, we'll focus on the components that are mostly related to the growth of GaN.

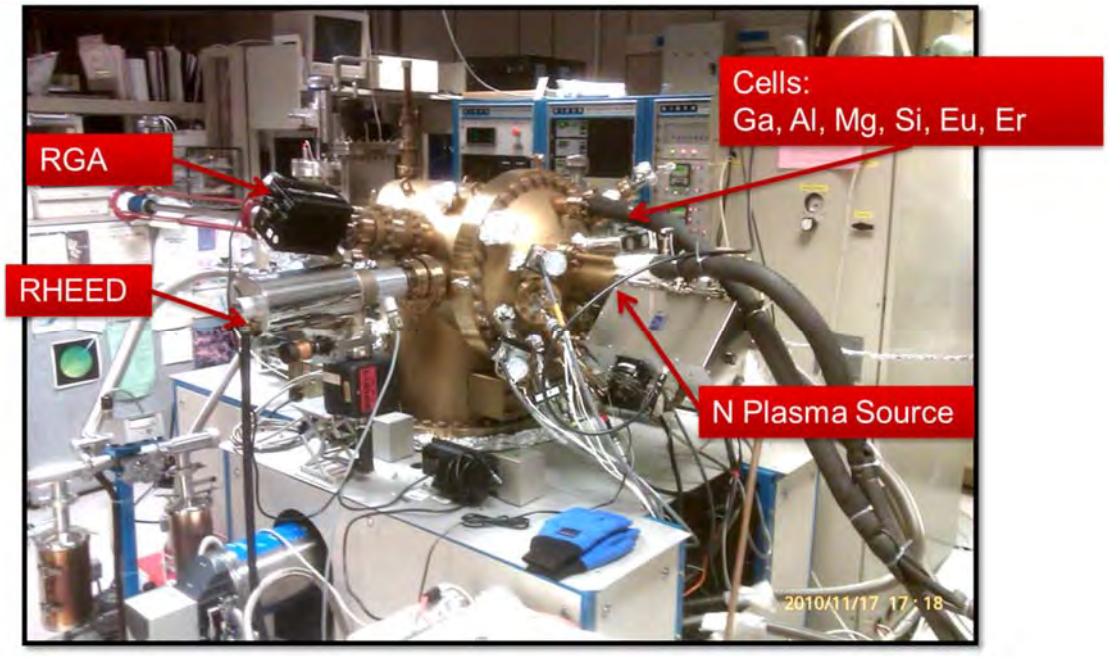

Figure 2.1 Riber 32 MBE system

2.1 Reflection High Energy Electron Diffraction

Reflection High Energy Electron Diffraction (RHEED) is a very important in situ surface characterization tool. In an RHEED setup, high energy electrons (15kev-30kev) beam is directed to the substrate at a very low incident angle and electrons are elastically reflected at the substrate surface. If the growth surface is crystalline (polycrystalline or single crystalline) the electron diffraction will occur, and the diffraction pattern is thus received by a photoluminescent screen.

Suppose the incoming electron beam has an electron wave vector of K_0, due to energy conservation, the electron beam leaving the surface should have a wave vector of K that has the following relationship with K_0, $|K_0|=|K_1|$. Then, we can construct an Ewald's Space [1] with $|K_1|=|K_0|$.

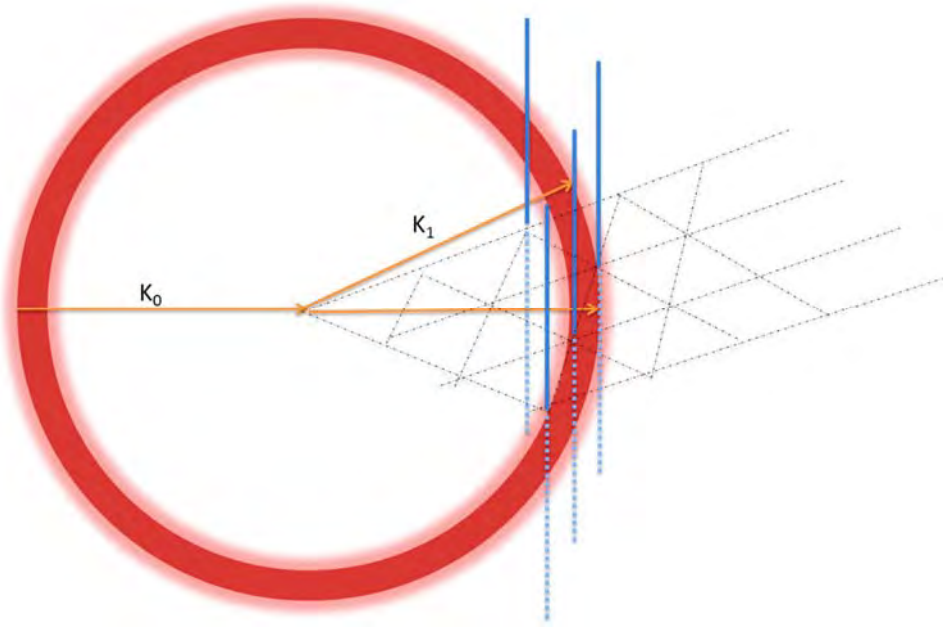

Figure 2.2 Ewald Sphere and reciprocal space of 2D surface

The reciprocal lattices of bulk crystals consist of a set of points in 3D space. However, only the first few layers of the material contribute to the diffraction since electrons are only affected by the surface, so there are no diffraction conditions in the dimension perpendicular to the sample surface. Due to the lack of a third diffraction condition, the reciprocal lattice of a crystal surface is a series of infinite rods perpendicular to the sample's surface (see figure 2.2).

Since the momentum or the wave vector of the incoming electron beam has a certain distribution (rather than a single value), the Ewald's sphere has a certain thickness. For a perfectly flat surface, Ewald's sphere overlaps with the reciprocal lattice, not at individual points but at sets of points that forms several lines. The diffraction pattern is thus streaky.

When the surface is rough, and not only the top layer but several top layers contributes to the diffraction. The electrons are diffracted by a 3D structure and the diffraction pattern is the

determined by the overlap of Ewald's sphere with the reciprocal lattice of a 3D structure, which is a set of individual points in 3D space. The pattern in this case is spotty.

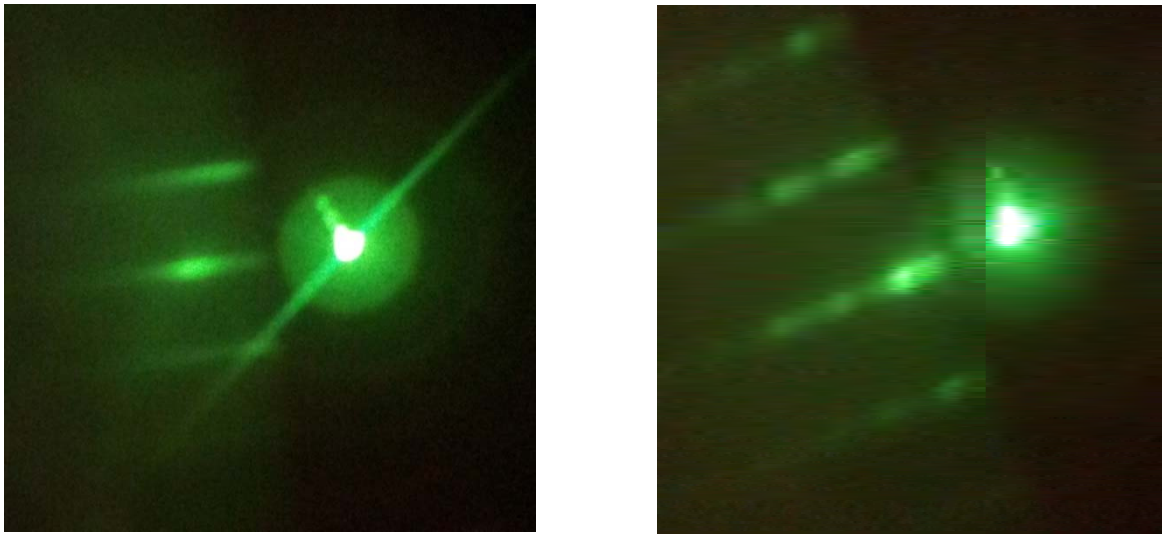

Figure 2.3 1x1 RHEED pattern of GaN smooth surface (left) and Rough surface (right)

As discussed above, by observation of RHEED pattern it is very easy to tell the surface condition, in other words, whether the surface is in Ga rich condition (Ga ML>1) or in N rich condition (Ga ML<1). If Ga ML is too thick, diffraction pattern becomes dim due to the blocking effect of the Ga liquid layer.

The pattern can be recorded and further analyzed in order to get the "real time" lattice constant information. With the knowledge of the electron energy, the space between each line and the distance from the substrate to the photoluminescence screen, people can easily derived the lattice constant. If the lattice constant is known, the strain and stress can then be calculated.

In our experimental setup, the uniformity of the molecular beams and substrate temperature significantly affects the film uniformity. Due to this reason, it is very often that the RHEED

pattern changes from streaky to spotty if one rotates the substrate or adjust the electron beam so that it hits the surface at another location.

2.2 Nitrogen plasma source

Figure 2.4 SVT RF 4.5 nitrogen plasma source. The aperture on this particular plasma source consists of a matrix of small holes.

There are generally two kinds of plasma source that are commonly used in PA-MBE: Electron cyclotron resonance (ECR) plasma source and RF plasma source. ECR plasma source generally results in poorer film quality than RF plasma and thus less studied [2, 3]. In our Riber 32 MBE system, a RF plasma from SVT (SVT RF 4.5) is used. This kind of plasma source provides a growth rate from 500 nm -1000 nm per hour depending on the flux and input plasma power. Gas is guided into a PBN tube and ionized inside. The PBN tube is surrounded by induction coupling copper coils. The coils are water cooled to prevent heat accumulation. The advantage of SVT plasma source is that it has a view port at the backend; thus the optical emission from the plasma can be directly observed. However, it should be noted that the optical spectrum is only an indirect way to approximate the growth rate (a pre-characterization of the relationship between the optical emission intensity and the growth rate is needed). The ratio of each specie inside the

plasma source can also be indicated. However, this ratio inside the plasma tube is different from the ratio of species that is received by the substrate due to the distance quenching effect, in other words, some species have shorter lifetime so that once these species leave the plasma source, the number of these species keep decreasing as they travel. The growth rate is usually measured by using a step profilometer after growth or by measuring RHEED intensity variation frequency in real time. Since different species of Nitrogen contribute to the growth differently, the growth rate or effective N flux cannot be directly interpreted from the emission intensity of the plasma.

2.3 Growth rate and beam equivalent pressure

GaN growth rate depends on Ga flux and N flux, and substrate temperature since it is related to the desorption rate of both Ga and active N. When III/V<1, the growth rate, is Ga flux limited, and it has a linear relationship with Ga flux. And when III/V>1, extra Ga presents on the surface when the surface reaches its static states, the growth in this case is N flux limited and become nearly constant. The growth rate at high substrate temperature could also be reduced by GaN decomposition. Ga decomposition at 700 °C-800 °C is rather low but when extra Ga on the surface or high energy containing particles reaches substrate, the decomposition rate could be significantly increased. These discussions are very general. With different system setup and different plasma source; the result could be different. In the case of Riber 32 MBE system equipped with SVT plasma source, the growth rate decreases significantly at substrate temperature beyond 720 °C and the decrease is most likely due to high energy containing particles from the plasma source. However, most of our experiments are conducted at relatively low substrate temperature and thus we limit the following discussion to low substrate temperature where Ga desorption can be ignored.

In order to determine the N flux for our plasma source, the experiment plan is to grow GaN in N limited condition where the growth rate is not sensitive to Ga flux and measure the thickness of the grown film. GaN density is 6.15 g/cm^3 and N concentration can be calculated by 6.15/84*6.02E23=4.4E22cm^{-3}. The height of each ML of GaN(c-plane) is c/2=0.5185/2 nm=0.25925 nm. thus the surface density or c plan planar density of N is 4.4E22/cm^3x0.25925 nm= 1.14E13 cm^{-2} These parameters are used to built the relationship between different units of growth rate: ML/s, # of atoms/cm^{-2}/s, nm/s. 0.259nm/s=1.14E13cm^{-2}/s=1 ML/s .Our plasma source was optimized to work at 1.5 sccm and 230 W RF power and it provides a growth rate of 0.8 ML/s.

The next step is to characterize Ga flux and it is usually measured with a vacuum gauge and what we get from the gauge reading is the beam equivalent pressure (BEP). The Ga flux is expressed by the nitrogen equivalent pressure and pressure can also be translated to the same unit as growth rate. We of course can use a similar way as characterizing N flux to determine Ga flux in ML/s, and we can so evaluate the ratio between fluxes from different metal sources by using their BEP and ionization energy etc.

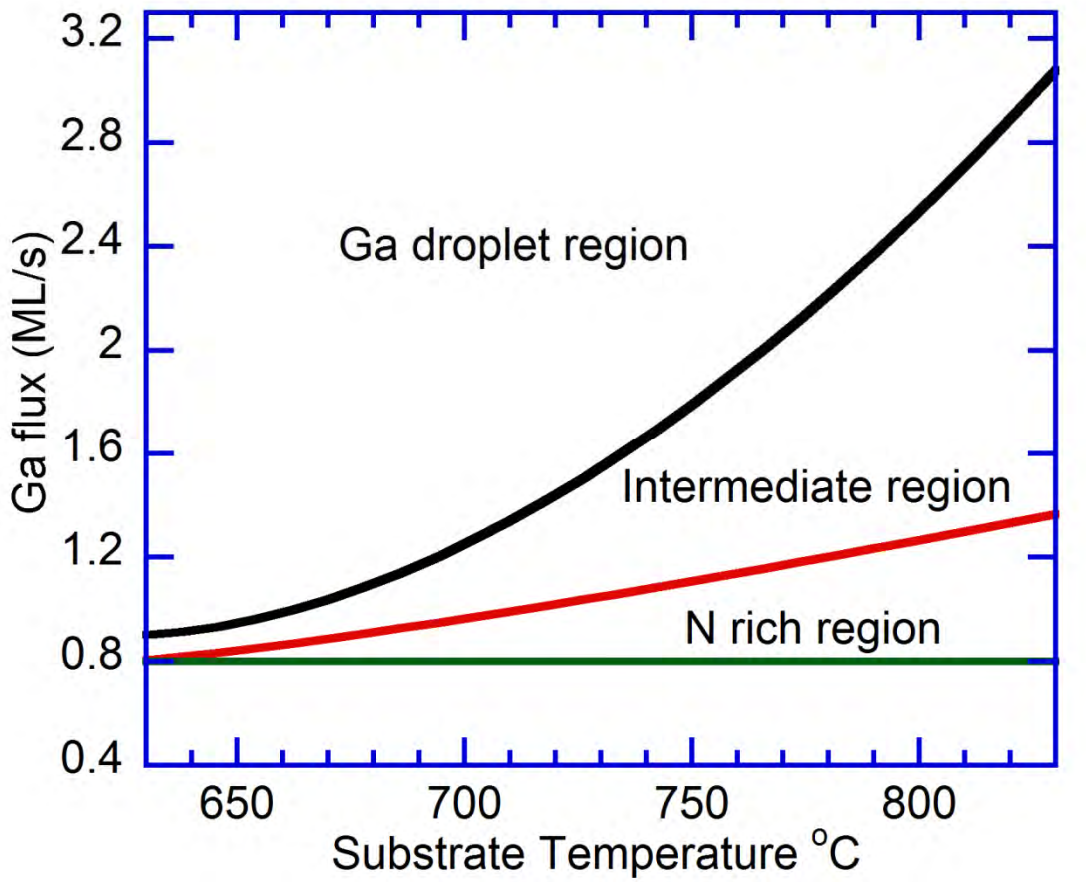

Figure 2.5 Growth regions. With increasing substrate temperature, Ga desorption increases, thus the Ga flux increases to maintain a certain surface Ga coverage. Active nitrogen is considered very reactive with Ga atom; it either leaves the surface with no Ga nearby or combines with floating Ga atom.

$$(2.1)\quad \frac{F_{Mg}}{F_{Ga}} = \frac{P_{Mg}}{P_{Ga}} \bullet \frac{IE_{Ga}}{IE_{Mg}} \left(\frac{T_{Mg}}{T_{Ga}} \bullet \frac{Mass_{Ga}}{Mass_{Mg}} \right)^{0.5} \quad 4$$

In equation 2.1, F is the metal flux; P is the BEP of the metal flux and IE is the ionization energy of each element. T is the cell temperature and the Mass is the atomic mass unit of the metal element.

In our setup, the growth surface takes 2 seconds (RHEED intensity change from bright to dim) to change from N-rich to Ga-rich at the beginning of each cycle after Ga shutter is open and also takes 2 seconds to change from Ga-rich to N-rich after the Ga shutter is closed. However, the variation of the Mg surface concentration cannot be directly observed. Therefore, the model has been developed to simulate this process. The number of "free" Ga or Mg atoms on the surface has a changing rate equal to the incoming flux minus its consumption rate by reaction with N and loss by evaporation, expressed by

. (2.2) $\frac{dM_t}{dt} = F - G - D$

Mt is the metal layer thickness at time t in MLs (ML), F is the incoming metal flux in ML/s, G is the growth rate or dopant incorporation rate in ML/sec and D is the desorption rate also in ML/s. G and D are further defined by "free" metal lifetimes: τ_1 - before reacting with nitrogen; τ_2 - before evaporation (eq.2.3).

(2.3) $G\left(M_t, \tau_1\right) = \begin{cases} \frac{1}{\tau_1} \times M_t, & M_t < 1 \\ \frac{1}{\tau_1}, & M_t \geq 1 \end{cases}$

(2.4) $D = \frac{1}{\tau_2} \times M_t$

When the system reaches steady state (III/V of close to unity) in conventional MBE, M_{Ga} =1ML. D_{Ga} for Ga can be ignored due to the low Ga desorption rate at 600 °C. Thus for Ga is estimated to be 0.72/sec. For Mg,

, (2.5) $$\frac{1-s}{s}=\frac{G_{Mg}}{D_{Mg}}=\frac{1/\tau_1 \cdot M_{Mg}}{1/\tau_2 \cdot M_{Mg}}$$

where s is the Mg sticking coefficient. The Mg sticking coefficient changes with substrate temperature and surface condition. With a rough estimation (although, some literature proposed much lower number [5] of Mg sticking coefficient of 0.1 and assuming (since growth is under kinetic limited region, bonding is considered very quick compared with mass transportation) that Mg shares the same incorporation rate G as Ga , for Mg can be estimated to be 6.48/s. Solving the differential equation gives us the result that only 0.2 s is required for Mg to reach 90% of its peak surface concentration and a similar amount of time is required to remove the Mg surface concentration. The Mg time constants will be larger with higher sticking coefficients, but still much smaller than those for Ga (2~3 s). Hence, Mg can be considered to exhibit instant turn-on on and turn-off.

Figure 2.6 shows the result of metal layer thickness variation on GaN surface. The blue curve shows the variation of Ga. The curve above 1 ML is liner due to constant growth rate in N limited condition. For Mg shown in red, the turn-on (at 6 sec) and turn-off (at 14 sec) is fast compared with Ga. It is worth noting that Mg has very high vapor pressure and very low sticking coefficient, and that is why it can be turn-on and turn-off instantly. If other elements such as Si or Al are being incorporated, the curve should be similar to Ga since the desorption on the surface can be ignored.

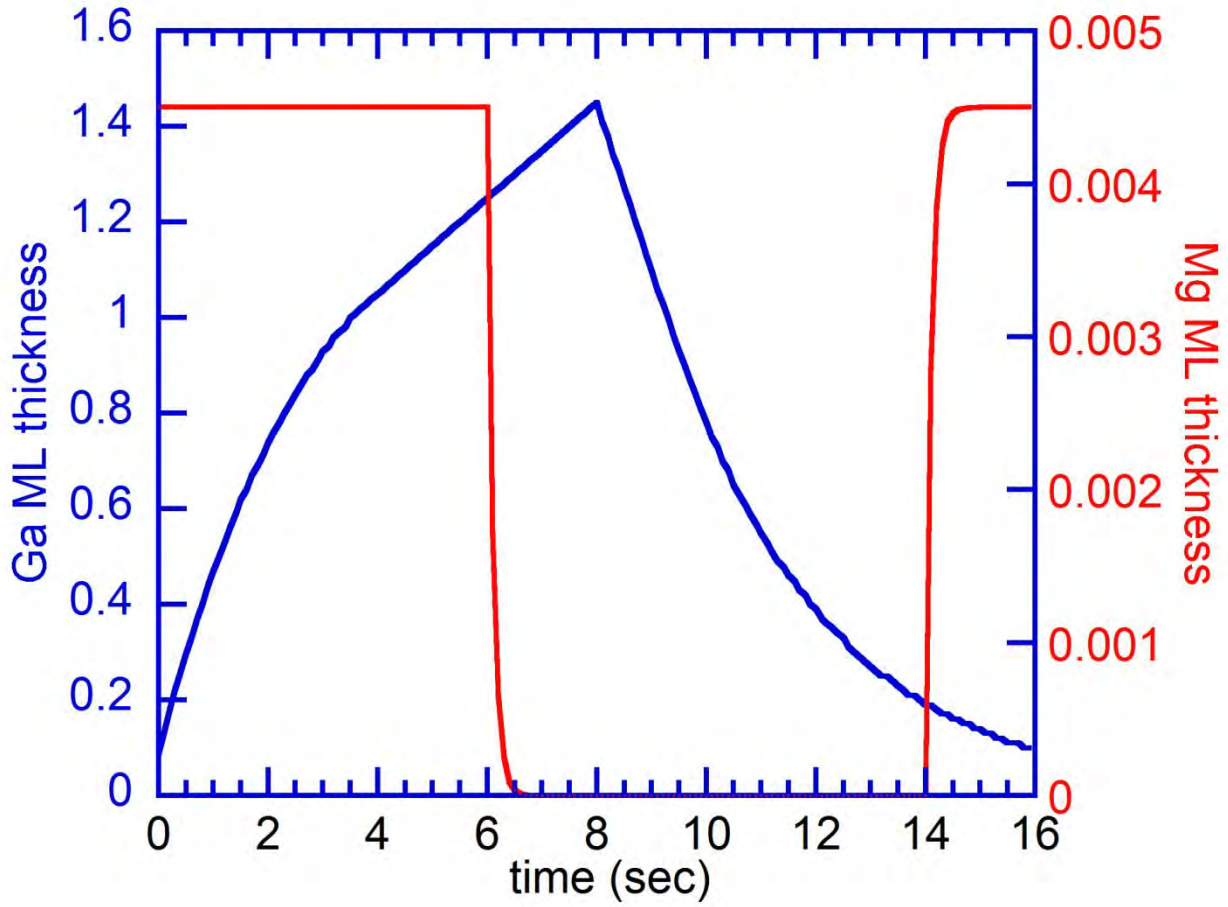

Figure 2.6 Simulation: the change of Ga and Mg surface coverage with a certain shutter operation. Ga shutter turns on at 0 sec and turns off at 8 sec. Mg shutter turns off at 6 sec and turns back on at 14 sec. Mg coverage (red) changes significantly faster than Ga coverage (blue)

These calculations and simulations are very important in that it provides a general method to transfer real world data to simulation. Using the simulation results we can easily determine the surface condition at any time of growth which otherwise cannot be obtained.

2.4 RGA and Leak Check

Another important in-situ characterization tool is Residual Gas Analyzer (RGA). RGA is usually used in leak check and contamination control in high vacuum chambers. RGA can be used as a tool to monitor total pressure and partial pressure of each gas in the chamber. It consists of an ionizer, quadrupole mass spectrometer, and a detector (Faraday cup or Electron Multiplier). Electron Multiplier is often used to increase the signal/noise ratio thus increases the detection limit of RGA. In our setup, an Inficon HM100 RGA is used, and its detection limit can be as low as 1E-14 Torr.

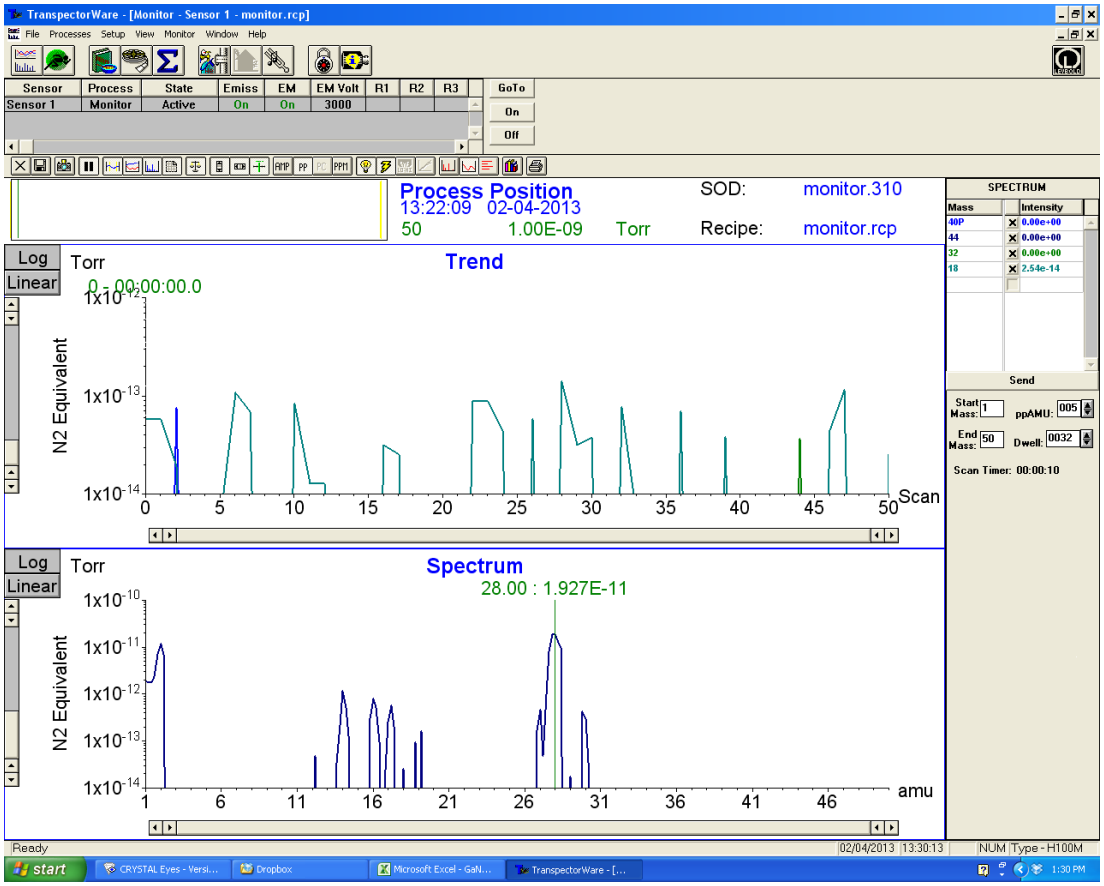

Figure 2.7 RGA spectrum showing ultra-low background contamination in Riber 32 MBE system

RGA is an idea tool for leak detection. Helium is sprayed on possible leak spot, and Helium concentration is monitored. Since Helium molecule is small, it migrates fast in the leakage channel. And Helium has a very low concentration in the atmosphere; thus even a small leak can be picked up by RGA.

There are other ways for leak detection in high vacuum chamber, and it can be used when RGA is not operational. This method is suitable for system that is equipped with an ion pump. In our Riber 32 system, an ion pump is installed at load lock. The ion pump is able to maintain a load lock system pressure of mid-E-9 Torr. The ion pump working principle is to ionize the gas

molecule and than either accelerate the chemically active ions into cathode (made of titanium) or buried gas molecule with Ti (sputtered from cathode) at the anode. The pumping speed of the ion pump for noble gas, however, is very low since noble gas is chemically inert and is not stable in either cathode side or anode side. Leak detection using noble gas such as Ar is thus possible. Probe possible leak spot with Ar spray and if there is a leak, very low pumping rate of Ar would increase the system pressure for a short period of time. Other pumps (such as Cryo pump) can be used at the same time to lower the system base pressure thus increase the detection limit of Ar.

References

1. Ewald, P. P. "Introduction to the dynamical theory of X-ray diffraction". Acta Crystallographica Section A 25 (1969)
2. J. Vac. Sci. Technol. B 13(4) (1995)
3. V. Kirchner, H. Heinke, U. Birkle, S. Einfeldt, D. Hommel, H. Selke and P. L. Ryder, Physical Review B 58 (23), 15749-15755 (1998).
4. G.J.Daives and D. Williams, in E.H.C. Parker (ed.): The Technology and Physics of MBE. Plenum, New York. (1985) p.38
5. Shawn D. Burnham, Improved Understanding And Control Of Magnesium-Doped Gallium Nitride By Plasma Assisted MBE, PhD thesis (2004)

Chapter 3. Ex-situ thin film characterization techniques and the optimization of un-doped GaN by Phase Shift Epitaxy

3.1 X-ray Diffraction

Figure 3.1 Rigaku MiniFlex Desktop XRD unit

X-ray diffraction is a common technique for crystalline quality and structure measurement. In the research of III/N semiconductor, FWHM of a peak is used to value the crystalline quality of the semiconductor thin film. The peak position in a θ/2θ scan is used to calculate the lattice constant of the film. The lattice constant can be used to estimate the composition of an alloy semiconductor, or to analyze the stress and strain in the film. Using Vegard's law, which assumes a linear dependence of lattice parameter on alloy compound semiconductor composition, the Aluminum/Indium concentration can be experimentally determined by these peak positions.

The left figure of Fig. 3.2 shows the XRD θ/2θ scan of the NitronexTemplate, which is GaN grown on Si with several buffer layers. The peak at 28.5° corresponds to Si (111) plane and the peak at 34.8° and 36.4° corresponds to GaN (111) plane and AlN (111) plane respectively. The peaks for two AlGaN layers are at 35° and 35.5° respectively. Fig. 3.2 (right) shows a typical XRD spectrum of MBE grown GaN on Si (111) substrate with a thin AlN buffer layer.

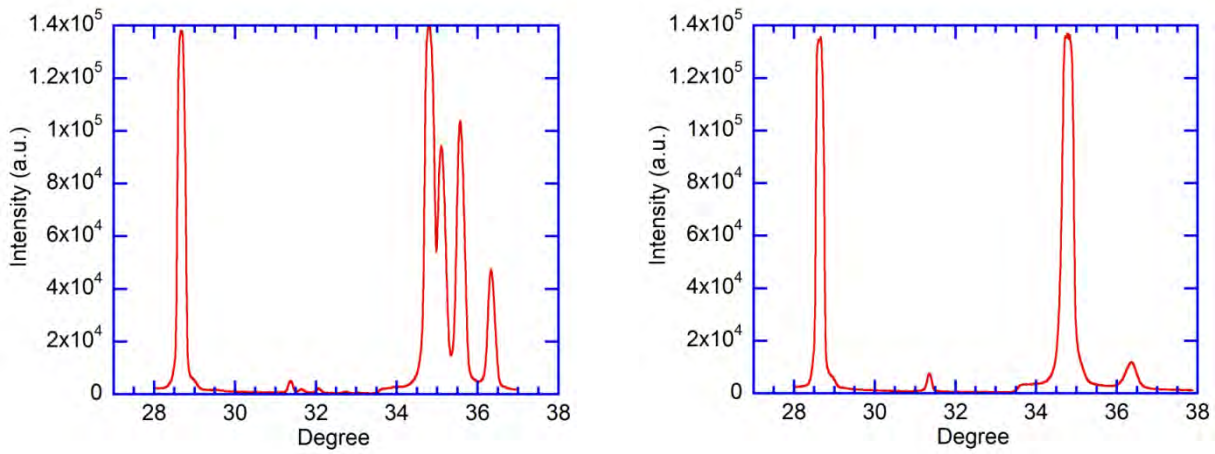

Figure 3.2 XRD results for GaN on Nitronex Template (left) , GaN on Si with AlN buffer (right)

3.2 Photoluminescence

Photoluminescence is another important characterization technique for direct bandgap semiconductor. Generally speaking, in a photoluminescence experiments, light is absorbed by the film and the spectrum of re-emitted light is recorded. Depending on the specific experiment setup, the excitation can be “above bandgap” or “below bandgap”. The light source can be pulsed or continuous.

In our setup, a 30mW HeCd CW laser (325nm, 3.81ev) is used to excite the GaN film. The photons of the laser are of higher energy than the bandgap of GaN (3.4 eV). The electrons are excited from valence band to conduction band, leaving a hole in the valence band. The electron hole pair later recombines and a photon of energy slightly higher than the bandgap energy is emitted (see Figure 3.3).

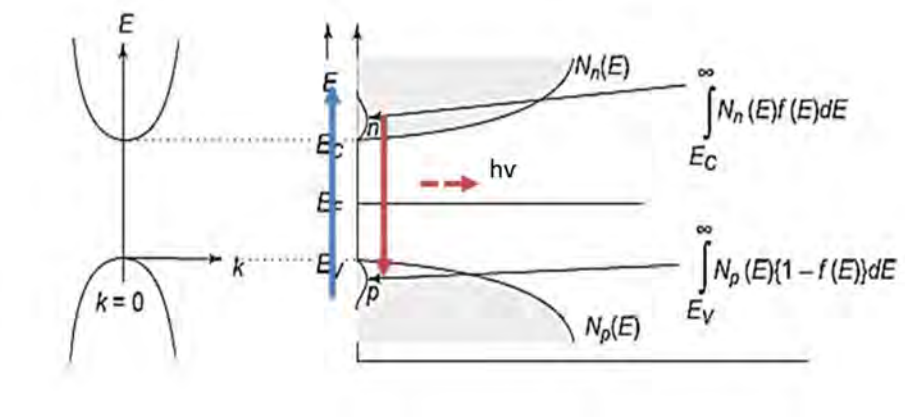

Figure 3.3 Photoluminescence of direct bandgap semiconductor [1]

It is worth mentioning that the incoming beam does not only excite electrons from the valence band to the conduction band; it can also excite electron trapped in some defect levels close to the valence band to the conduction band or excite electron closer to the bottom of the valence band

to some defect levels close to the conduction band. The typical photoluminescence spectrum of GaN by an above band excitation is shown in Figure 3.4, except the band edge peak at 364 nm; there is a broad peak centered on 550 nm. This peak is usually observed from GaN film. The origin of this peak (so called yellow band, yellow luminescence (YL)) is widely studied [2, 3, 4]. It is generally believed that the donor-acceptor pairs are involved in the relaxation process, however, the exact cause is still in debate [6,7].

Photoluminescence is especially sensitive to point defects. Defect density significantly effects the FWHM and the intensity of near bandedge emission, thus it is an effective indicator of the point defect levels in the structure.

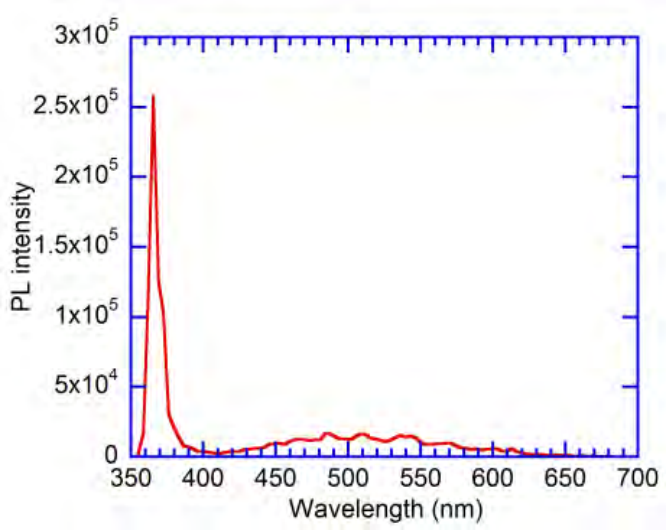

Figure 3.4 Photoluminescence spectrum of GaN at room temperature.

3.3 Secondary Ions Mass Spectrometer (SIMS)

The PHI SIMS 6600 system is used for doping depth profile analysis. This system is equipped with a oxygen duoplasmatron ion gun and a Cs metal source ion gun. High kinetic energy (3-

5KeV) Ion beam is focused onto the surface of the sample. The release of secondary ions caused by the ion-surface impact is then collected and guided into a sphere capacitor analyzer. At the end of the sphere capacitor analyzer, a quadrupole mass spectrometer is used to identify and count each elements (or combinations) .

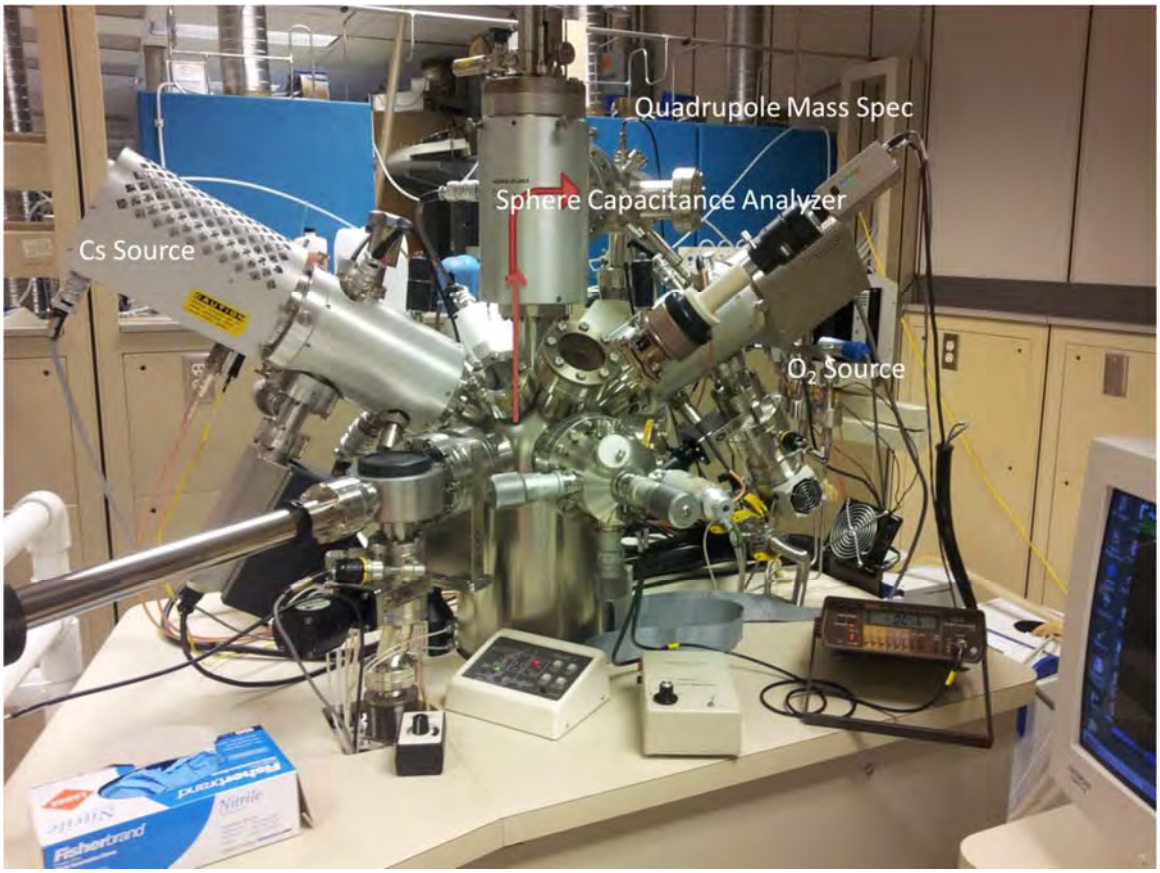

Figure 3.5 PHI SIMS 6600 system in nanolab.

The counts/second of each element is translated into the real concentration with relative sensitivity factor (RSF). A simple expression for RSF is:

(Counts impurity/Counts matrix)×RSF = concentration of impurity

3.4 Hall effect

In our group, hall effect technique is used to measure the electrical properties (resistivity, type of carriers ,carrier concentration, mobility and etc.) of the GaN film. As shown in figure 3.6, with the existence of a magnetic field normal to the surface, the electrons/holes (I) flowing across the film from 1 to 3 will be directed towards different directions by magnetic force, causing a change of the voltage across electrode 2 and 4 (ΔV). The calculation can be found in Reference 1. Hall effect is usually combined with Van der Pauw measurement. In order to make an accurate measurement, ohmic contact should be made at the four electrodes and the film needs to be uniform. The electrodes need to be small compared to the size of the sample, to minimize the error caused by the electrode size difference. If p-type layer sitting on top of the n-type layer is studied, the p-n junction leakage should be minimized to make sure current only flows through the top layer. In the case that leakage through layers is unknown, highly resistive bottom layer should be used.

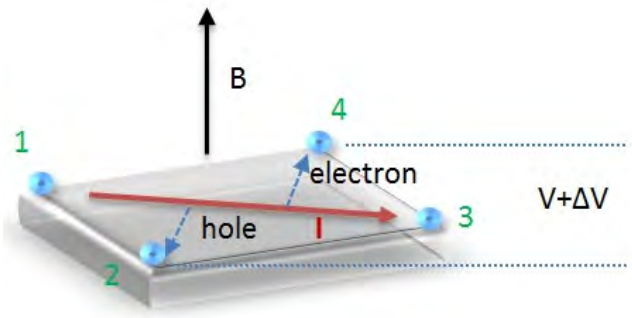

Figure 3.6 Hall effect measurement setup.

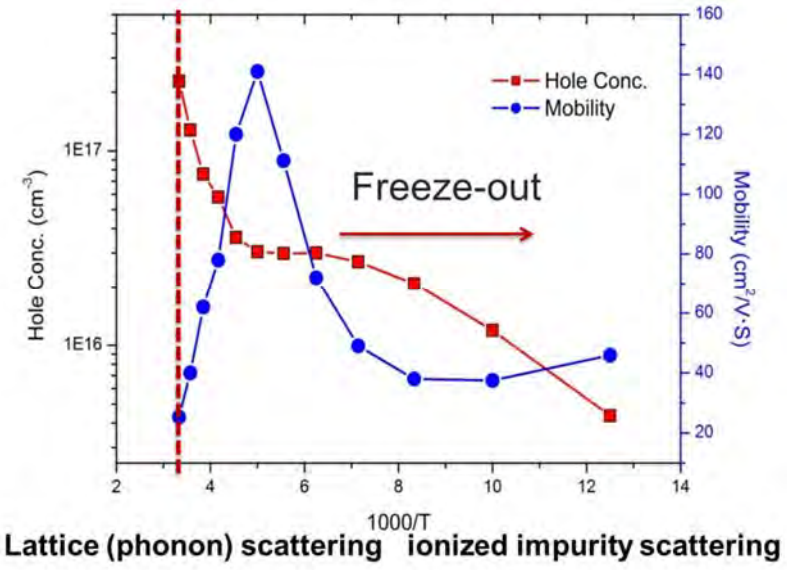

Figure 3.7 Temperature dependent hall effect measurement of a p-type GaN.

Figure 3.7. shows the hole concentration and mobility of a p-type GaN film at different temperature. At intermediate temperatures the carrier density approximately equals the net doping, it increases at high temperatures for which the intrinsic density approaches the net doping density and decreases at low temperatures due to incomplete ionization of the dopants. The mobility decreases at high temperature due to phonon scattering. At low temperature; the mobility decreases due to the dominating ionized impurity scattering.

3.5 Optimization of un-doped GaN by Phase Shift Epitaxy

A GaN:Eu LED, similar to conventional LED, consists of three layers: p type, n type and active layer. Each layer in the device involves a certain doping. As we discussed in the introduction, the advantage of Phase Shift Epitaxy is that the host growth is independent from doping, so the host

growth and doping can be optimized separately. For host lattice growth using PSE, the optimization involves the determination of the following parameters: Ga flux, N plasma condition (N flux, Plasma power, etc.), duty cycles, substrate temperature etc. Previously, similar optimization on Ga flux and substrate temperature has been done in our group. The duty cycle is usually easily determined by RHEED intensity oscillation: the GaOFF cycle need to be long enough to make sure that next cycle starts with zero Ga coverage. Film qualities from duty cycles of 10 s GaON/ 10 s GaOFF and 5 s GaON/5 s GaOFF are very similar. However, nitrogen plasma condition, a parameter that has not been systematically studied in the group before, was found to significantly affect the film quality.

All samples are epitaxially grown on Nitronex substrate (GaN and several buffer layers on Si). Substrate temperature is varied in the range from 600 °C to 650 °C. Below 600 °C, GaN quality is significantly poor and above 650 °C, indium bonding between Si and Nitronex sample is no longer stable. Ga cycle and N cycle is varied in the range from 5 s to 10 s.

In order to characterize the film, XRD and PL are used. However, Nitronex substrate is not uniform, so XRD cannot be used to compare the quality between samples. On the other hand, PL is sensitive to point defects and not sensitive to the threading dislocation density. Therefore, we use PL as a quick and effective indicator of the film quality (point defect density). Our goal for the optimization is to minimize the point defect level in GaN overgrown layer.

There is a variety of species exists in Nitrogen plasma. A typical spectrum taken from the backside view port of SVT 4.5 RF plasma is presented in figure 3.8. If the spectrum is taken from the front side (outlet), the short wavelength part (correspond to second positive, serious N_2) of the spectrum is completely removed. In order to explain this phenomenon, we need to take a

look at the lifetime of these species. From table 3.1, we can see that only the first positive series N_2 and ground state N atom have the lifetime long enough to escape the aperture.

Species	Lifetime
Second positive series N_2	~(μs)[8]
activated N atom	(~ns)[9]
First positive series N_2	~(s)[8]
Ground state N atom	~(s)[10,11]

Table 3.1 lifetimes of different N_2 species

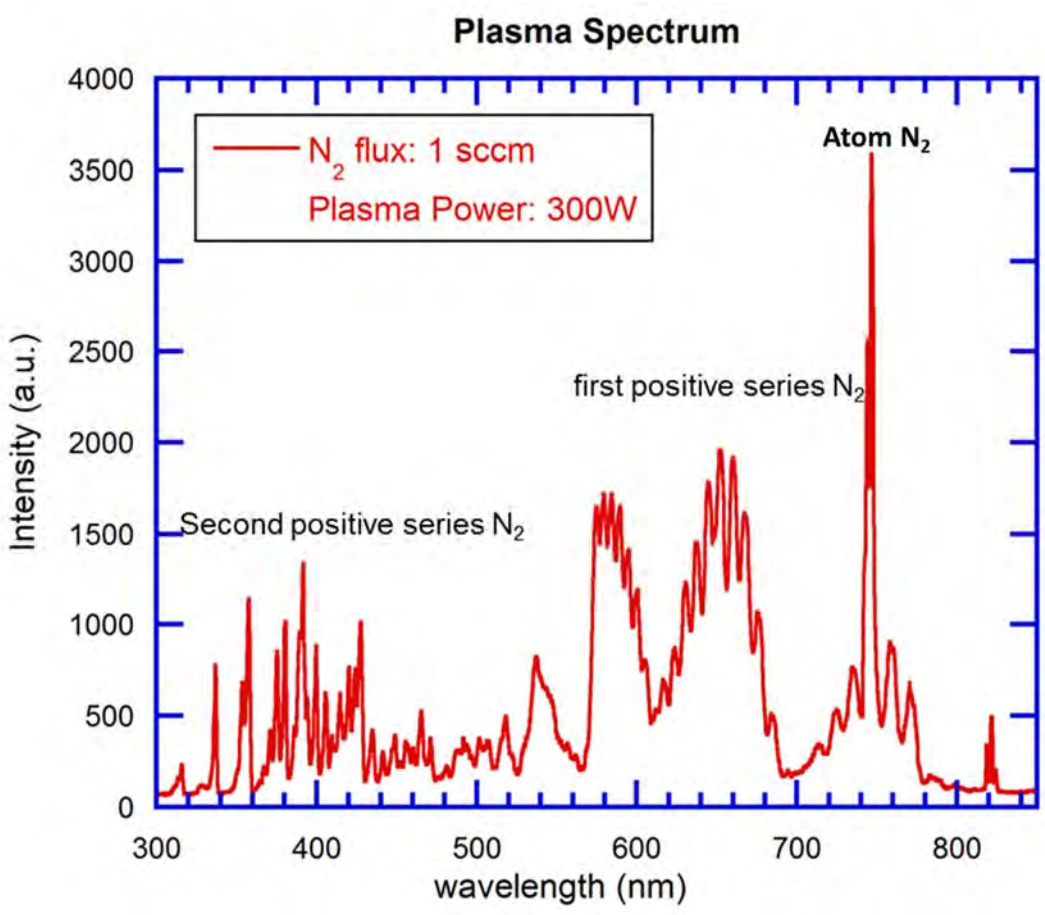

Figure 3.8 typical nitrogen plasma spectrum observed from the backside viewport of SVT 4.5 RF plasma source.

What makes plasma condition optimization time-consuming is that III/V ratio changes with plasma condition, and every time a new plasma condition is used, a corresponding change with respect to Ga flux and ON/OFF cycle needs to be done.

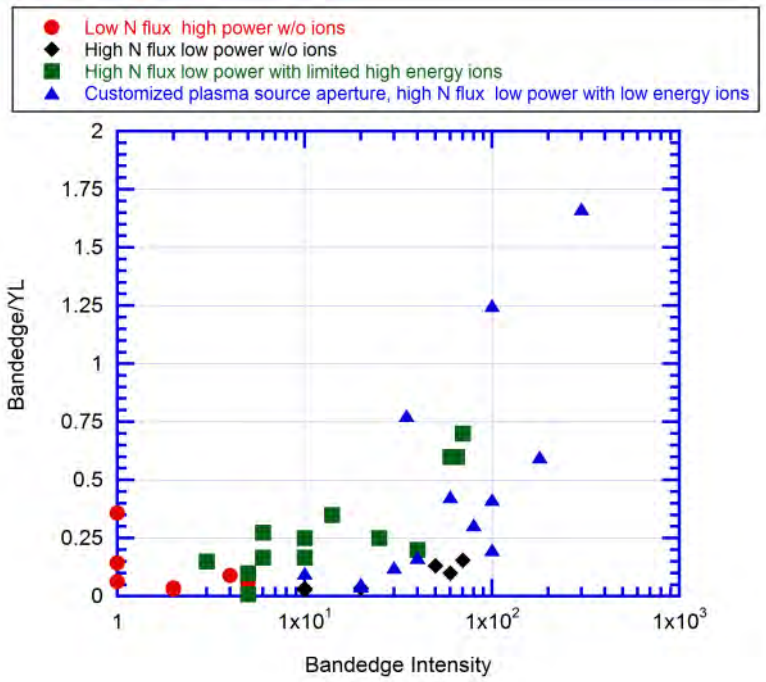

Figure 3.9 Photoluminescence result of four groups of experiments with different plasma conditions. Red: high plasma power/low flux/ions removed; Green: low plasma power/high flux/ions removed; Black: low plasma power/high flux/limited high energy ions; Blue: low plasma power/high flux/limited low energy ions

All data has been summarized into four categories: 1. low N_2 flux high plasma power without ions (ions eliminated by the charge suppression plate). 2. High N_2 flux low power without ions. 3. High N_2 flux low power with limited ions (moderate high voltage added on the charge suppression plate). 4. High N_2 flux low power with self-customized plasma aperture (limited ion flux with lower kinetic energy).

With low N flux (group 1), higher N^*/N_2^* ratio is expected compared with the high N_2 flux case (group 2). In both cases, ions are completely removed by 1000 V charge suppression voltage. In figure 4, band edge emission from the films in group 1 is always significantly lower than group 2. Thus we can conclude that lower N^*/N_2^* is beneficial to the growth.

However, films in both groups 1 and 2 have strong yellow band emission (YL, defect related) compared to band edge emission (BE). In both cases, no matter how you adjust other parameters, there is no significant improvement in BE/ YL ratio. Further optimization of plasma source is needed.

Adatom mobility on the surface is crucial to the growth. It determines if an atom can reach its site effectively during the epitaxy process. In order to get high quality crystal, adatom mobility on the surface should be carefully adjusted by changing substrate temperature or adding surfactant. In PA-MBE, moderate amount of ions can help increase the adatom mobility. These ions can help increase adatom mobility and remove defects.

In group 3, varied voltages (0-500V) were added to charge suppression plates. We can barely get better results than group 2; the data is widely spread. But in a few cases, BE/YL ratio has been improved with suppression voltages around 300 V. The simulation has been done to estimate the ion energy of the ions that reach the substrate. If 300 V can not completely remove ions, it indicates that the ion energy is at least 200 eV. If this is the case, the ions remove defects and create more damages at the same time. This explains why films in group 3 have widely spread distribution of film quality.

As for group 4, a self-customized aperture is added to the plasma source. It consists of a 3×3 array of Φ 0.5mm holes. By changing the aperture, the ion energy is reduced from over 200 eV

to less than 30 eV. The kinetic energy of ions is estimated by adding ion removing voltages and compare the result with films grown with ion completely removed. Group 4 has overall better quality films than any other groups.

The quality of group 4 is still not very satisfactory, probably due to the self-customized aperture, which has a center hole that is bigger than other ones and not in regular shape. Besides, the new aperture decreases the gas conductance, in other words, more gas are trapped inside the tube; thus it is difficult for shorter lifetime particles such as first positive series N_2 to come out of the source, in other words, N^*/N_2^* is increased.

At a relatively low substrate temperature (600°C), the bandedge emission intensity is relatively low compared to yellow band emission intensity. In order to reduce the yellow band emission, we need to understand the origin of this emission. Until today, there are still debates on what causes the yellow emission from GaN.

To summarize, two important conclusions can be made. 1. Low N^*/N_2^* is preferred. 2. Low kinetic energy ions help improve film quality.

Later on, a changed design of customized aperture (6x6, Φ=0. 5mm, no charge suppression added) was used. A purifier is also installed to lower the impurity level in the Nitrogen gas down to <1 ppb. The PL results from growth after these upgrades can be seen on Figure 3.10. All results show a significant decrease of the yellow emission compared with previously without purifier case. In the follow four growths, all III/N ratio is set to be close to 1. As we can see from the PL spectrums, from JT01, 02 and 04, we can find that higher plasma power helps relax the lattice so that the band edge peak position is closer to 364nm. The shapes of these three films are quite similar. JT03 uses highest plasma power and lowest Nitrogen flux, so that the highest

amount of N atom presents in the flux and this condition led to the onset of the blue band. Relatively high N_2 flux usually leads to a more stable plasma operation, and there is no significant different between JT01, 02 and 04. Thus the optimized plasma condition is set to 230 W and 1.8 sccm.

	Sub. T. °C	Ga cell temp °C	N_2 flux sccm	N_2 Power (W)
JT01	600	982	0.8	250
JT02	600	975	0.8	240
JT03	600	962	0.5	300
JT04	600	983	1.8	230

Table 3.2

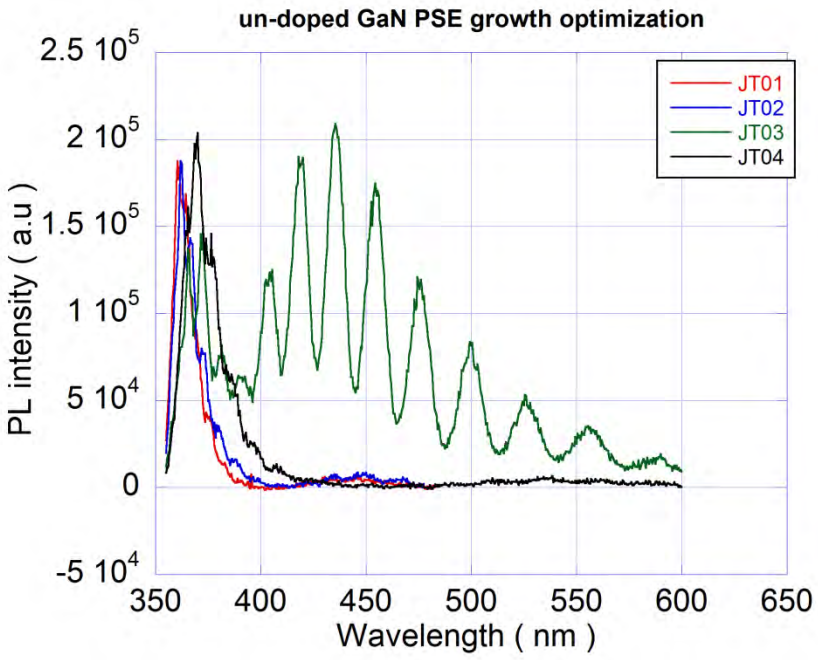

Figure 3.10 photoluminescence spectrum on un-doped GaN grown with 6×6 Φ=0.5mm aperture. Substrate temperature is 600°C.

References

1. Brahmadeo Prasad Singh; Rekha Singh,Electronic Devices and Integrated Circuits Print ISBN-10: 81-7758-978-4
2. G. Li,S. J. Chua,S. J. Xu, and W. Wang, Appl. Phys. Lett. 74, 19 (1999)
3. B. Legrand and D. Stievenard, Appl. Phys. Lett. 75, 4049 (1999)
4. D. C. Reynolds, D. C. Look, B. Jogai, J. E. Van Nostrand, R. Jones and J. Jenny, Solid State Communications 106 (10), 701-704 (1998).
5. J. Bernholc, J. C. Chervin, A. Polian, and T. D. Moustakas, Appl. Phys. Lett. 67, 2188 (1995)
6. P. Kamyczek, E. Placzek-Popko, Vl. Kolkovsky, S. Grzanka and R. Czernecki, J. Appl. Phys. 111, 113105 (2012)
7. A. Sedhain, J. Li, J. Y. Lin and H. X. Jiang, APPLIED PHYSICS LETTERS 96, 151902 (2010)
8. J. Anketell and R .W .Nicholls Rep. Prog. Phys. 33 269 (1970)
9. Richard A. Copeland, Jay B. Jeffries, Albert P. Hickman, and David R. Crosley Radiative lifetime and quenching of the 3p 4D0 state of atomic nitrogen J. Chem. Phys. 86, 4876 (1987)
10. M.A.L. Johnson, N.A. El-Masry, J.W. Cook, J.F. Schetzina, Mater. Sci. Forum 264}268 (1998) 1161.
11. H. Morkoc, IEEE J. Selected Topics Quantum Electron.4 (1998) 537.

Chapter 4. Eu doped GaN by PSE

Because of their strong and narrow photoemission lines at visible and IR wavelengths, RE doped GaN materials have been investigated[1-3] for photonic applications. Eu-doped GaN related light emitting devices were fabricated in our group [4-10]. We found that N-rich surface conditions promote RE incorporation [11], while the slightly Ga-rich condition (which results in the best crystal quality) is more favorable for RE luminescence efficiency (ratio of photoluminescence to RE concentration). However, these conclusions are all based on conventional MBE growth. One can always argue that high RE luminescence efficiency in Ga-rich condition is simply because the host quality is generally better if GaN is growth in slight Ga rich condition. On the other hand, relatively poor crystal structure from N rich growth will surely result in lower efficiency. In this chapter, PSE is used to test previous conclusions.

Various of dynamic growth schemes have been used to improve thin film quality [11-16], In our group, another "semi" dynamic growth scheme was proposed by Munasinghe[17,18] for Eu doping. This proposed "interrupt growth epitaxy (IGE)" has resulted in a ~10× enhancement of Eu^{3+} luminescence in GaN. In each cycle of IGE, film is grown in conventional MBE (III/V=1) for a short time, usually around 15 mins to 45 mins, followed by a nitridation period (15-45 mins). It has to be point out that nitridation period usually lead to an increase of point defects due to the ion damaging effect discussed before.

4.1 Experiment design

The work of this chapter is done during the early stage of our study on PSE. At that time, four segments has been identified in each growth cycle. A fancy name “Phase Shift Epitaxy” is given to this dynamic scheme. Figure 4.1 shows the shutter operations for Ga and Eu. The “rise” and “fall” of Eu has been “shifted” or “postponed” by x seconds and z seconds with respect their correspondence in Ga waveform. A period is then divided into 4 segments: x segment (Ga ramp-up), y segment (Eu doping with Ga flux), z segment (Eu doping without Ga flux) and w segment (surface clean-up and nitridation). In the ideal case, surface condition in y and z segments is Ga rich (above the threshold) and surface condition in x and w segments is N rich. However, without knowing the exact threshold, the ramp up and drop down rate of Ga coverage, one can only experimentally decide the best “phase shift”.

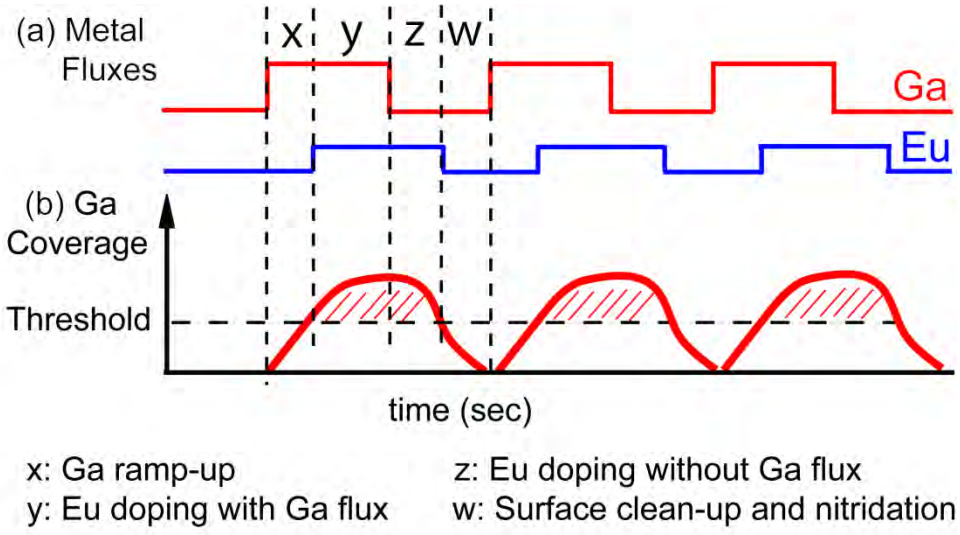

Figure 4.1 Schematics of PSE growth for GaN:Eu. Phase shift exists between Eu and Ga shutter operations. (a) Shutter operations. (b) Corresponding Ga coverage variation

AlGaN templates on p-Si (111) wafers (Nitronex Company, Raleigh NC) are used in these experiments. GaN:Eu grown by conventional MBE grown is used as a comparison to films grown by PSE. The substrate temperature was 650°C. the N2 plasma operated at 1 sccm and 300 W. The Eu cell temperature was 420°C.

Ga cell temperature is set to 900°C, resulting in a beam equivalent pressure (BEP) of 4.4×10-7 Torr. This corresponds to the III/V>>1 case in conventional MBE with the above given nitrogen plasma condition. A single cycle of 22 s consisted of GaON = 14 s and GaOFF = 8 s. The x-parameter was changed from 4 to 1 s, while the z-parameter was changed from 3 to 6 s. A second set of samples was grown with continuous Eu flux, while the Ga flux was pulsed with a constant GaON = 14 s and several values of GaOFF = 8, 10, 12 s. Finally, a third set of films was grown by traditional MBE with various III/V ratios to find the optimized growth condition for GaN:Eu.

The MBE growth lasts 23 min. PSE films had an equivalent Ga ON time that is spread over 90 cycles of 14 s each. All films from three sets of experiments have a very similar thickness of ~150 nm. This allows the direct comparison of the PL emission and PL efficiency from samples grown under different conditions.

Secondary ion mass spectroscopy (SIMS) was used to determine the Eu depth profile and calculate its concentration in the film. PL measurements were performed at 25°C with a 325nm He-Cd laser.

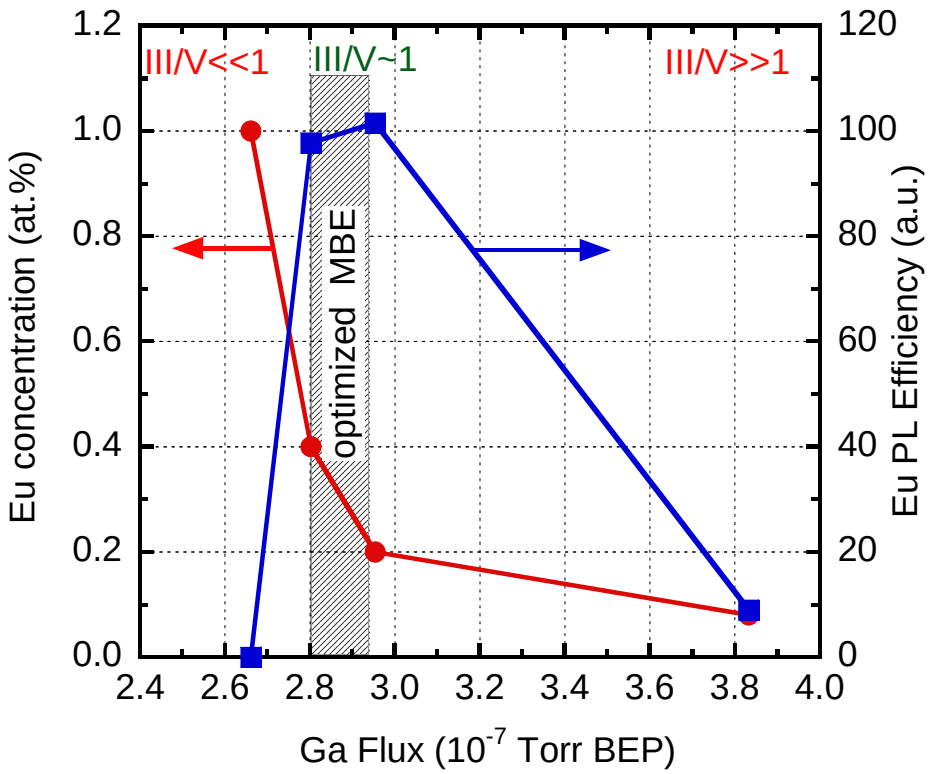

Figure 4.2 GaN:Eu optimization with different Ga fluxes. The optimized condition is shown in the shadow region.

Four MBE samples were grown with different III/V ratios (from <<1 to >>1), as shown in Fig.4.2. The Eu concentration decreases monotonically with increasing Ga flux because of site competition in the Group III sub-lattice of the GaN film, which agrees with previous report[11]. The Eu PL efficiency is calculated by dividing the integrated PL of the Eu peaks around 620 nm by the product of the Eu concentration and the film thickness. The highest efficiency is obtained at III/V = 1 (Ga beam pressure of 2.95×10^{-7} Torr).

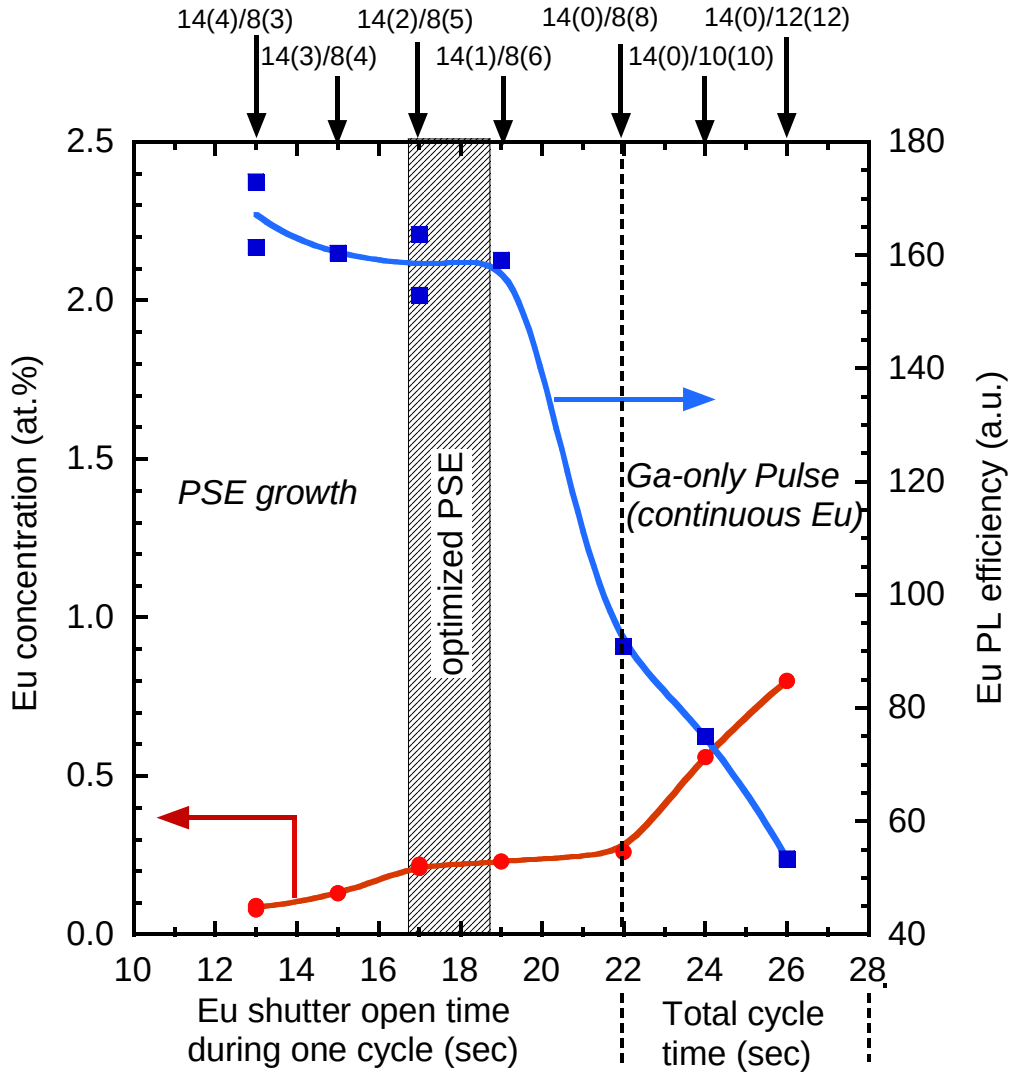

Figure 4.3 GaN:Eu PSE optimization.

In the N-rich case, Ga liquid layer only partially covers the surface, with the uncovered part of the surface exposed to both N and Eu fluxes. This results in a film with high Eu concentration, but low Eu PL efficiency.

In the PSE approach, as shown qualitatively in Fig. 4.1b, during the GaON segment (x+y) the Ga surface concentration increases. The Eu flux is turned on sometime after the turn-on of the Ga beam. This allows the Ga concentration to build up to a certain level before the Eu incorporation

process begins. When the Ga pulse is terminated, Eu doping is still allowed (z-segment) until the Ga surface concentration drops below the threshold. During the last component of the PSE scheme (w-segment) both the Ga and Eu fluxes are turned off. During this time, the N beam removes excess Ga from the surface.

4.2 Results and Discussion

The PSE scheme is denoted by GaON(x)/GaOFF(z), where GaON and GaOFF are the time lengths of the Ga ON and OFF segments, respectively. x and z are the leading and trailing overlaps of the Ga and Eu waveforms, as seen in Fig. 4.1. This notation is later changed to x/y//z/w, which is explained in the next chapter. For this set of experiments, the GaON and GaOFF segments are 14 and 8 s, respectively, for a total cycle of 22 s. The GaOFF segment is used to consume the Ga left on the surface so that another cycle can begin with 'zero' Ga coverage. The x values range from 4 to 1 s and the z values from 3 to 8 s. An assumption is given: Ga rich condition is preferred; Eu doped in Ga rich condition exhibits higher efficiency; doping Eu in N rich condition leads to lower PL efficiency. Suppose this assumption is true, if we start from doping Eu in extremely Ga rich condition, then gradually widen the Eu doping window (y+z), the window will be eventually large enough so that some Eu ions are doped in N rich surface condition. According to the assumption, the PL efficiency of Eu should drop. In Figure 4.3, as Eu doping window (y+z) increases, from 13 to 22 s, Eu concentration shows a gradual increase from 0.13 to 0.23 at. %. Eu PL efficiency however, stays almost the same at low Eu concentration (or narrower Eu doping window). For the Eu shutter time of 22 s

[14(0)/8(8)] the PL efficiency experiences a sharp reduction. In this case; the Eu flux is on continuously and therefore much larger amount of Eu is doped during the w-segment (very low Ga coverage) of the cycle. This efficiency confirms our assumption that doping Eu in N rich condition leads to lower Eu PL efficiency.

Increasing the total cycle time from 22 to 26 s by extending the GaOFF time and keeping the Eu flux on continuously (in other words Eu shutter time/cycle=GaON + GaOFF) results in a sharper rise in Eu concentration and a further reduction in Eu PL efficiency. For the GaOFF period of 8 s (cycle time of 22 s), a 1×1 RHEED pattern persists throughout the growth. However, for longer GaOFF times, the RHEED pattern disappeared shortly after the start of the growth, indicating that longer GaOFF segments lead to poor crystal quality. As shown in Fig. 4.2, for these three samples the Eu concentration increased from 0.26 to 0.8 at. % (still well below the concentration quenching limit[5] of Eu of 2.2 at.%), while the PL efficiency dropped from 94 to 54. Clearly, Eu ions incorporated during low Ga coverage results in low PL efficiency, degrades the lattice structure. Parameters near 14(1)/8(6) represent optimized PSE conditions.

Compared with optimum conventional MBE samples (dashed region in Figure. 4.2) at similar Eu concentration, the optimum PSE growth (dashed region in Fig.4.3) provides a ~50% increase in Eu PL efficiency.

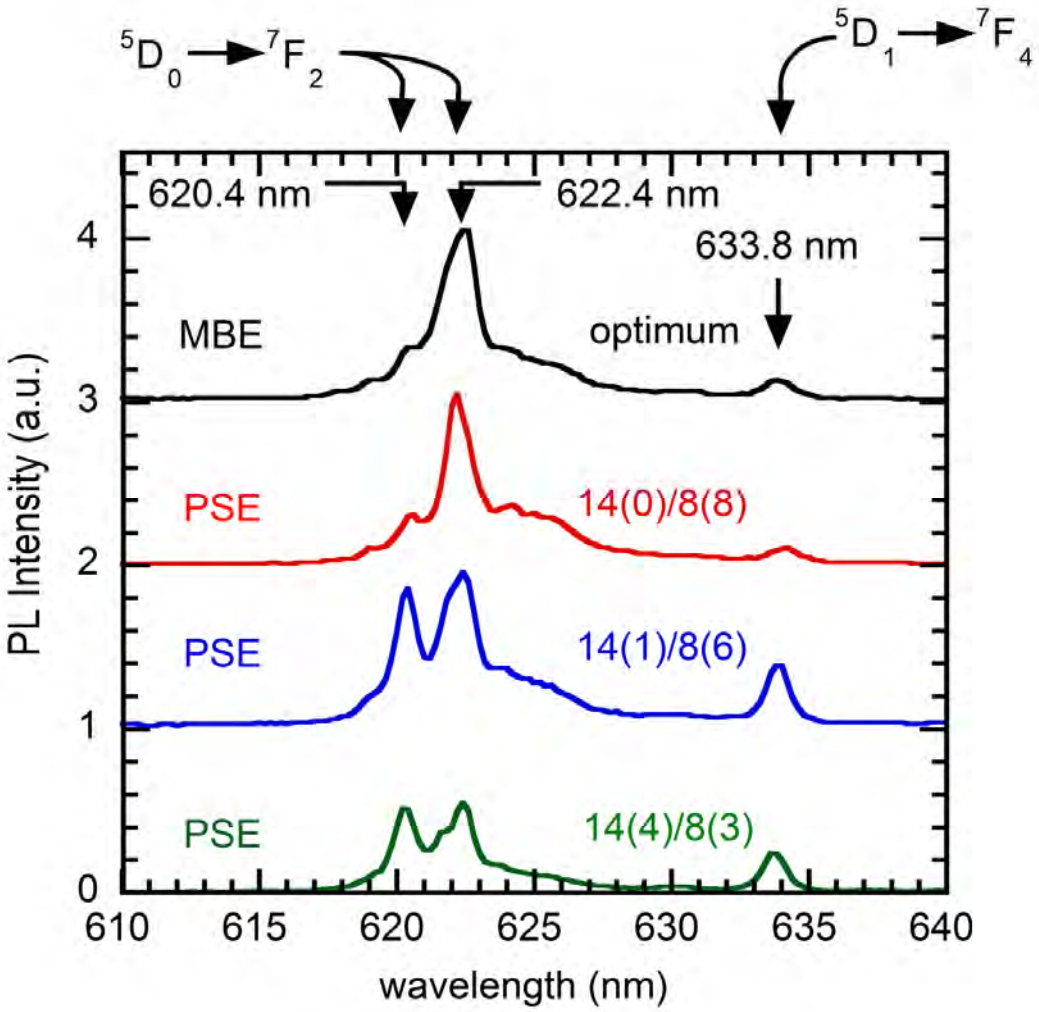

Figure 4.4 Room Temperature Photoluminescence spectrum taken on different samples. Black: optimized MBE grown sample. Red: un-optimized PSE grown sample (some Eu doped in N rich condition). Blue: optimized PSE grown sample. Green. Optimized PSE grown sample with lower Eu concentration.

PL spectra in the vicinity of the main Eu intro-4f transition ($5D_0 \rightarrow 7F_2$) obtained from samples grown under several conditions are shown in Fig. 4.4. The MBE sample grown under optimized conditions (III/V ≈ 1) exhibits a large peak at 622.4 nm and a much smaller peak at 620.4 nm.

These two peaks have been previous reported[23] and represent the two main Eu incorporation sites. Samples grown under optimum PSE conditions (Eu doped in Ga rich condition) display significantly enhanced 620.4 nm peak and simultaneously higher PL efficiency. This peak is believed to be from a different Eu site [14,24,25]. The rise of the 620.4 nm peak can be explained by a combination of additional Eu incorporation into the second site and reduction of defects that affect the efficiency of this site. The sample grown as the PSE special case with continuous Eu flux [14(0)/8(8)] produces a spectrum similar to that of the MBE-grown sample, with a peak at 620.4 nm very much reduced. The sharp decrease of 620.4 nm peak intensity between the 14(1)/8(6) and 14(0)/8(8) samples are probably due to Eu-related defects incorporated during segments of the cycle when Ga coverage is low. This explanation is supported by the gradual disappearance of the RHEED pattern under increasingly low Ga coverage growth conditions [14(0)/10(10) and 14(0)/12(12)]. Furthermore, in the absence of Eu flux, growth under low Ga coverage conditions still exhibits streaking RHEED patterns.

4.3 Conclusion

In summary, the PSE growth technique was presented and applied to the growth of GaN:Eu films. Adjusting the phase shift between metal fluxes during growth enables the incorporation of dopants during the optimum segments of the growth cycle. The PSE technique displays its potential to enhance the doping of GaN and other semiconductors with optoelectronic, magnetic and electronic impurities. The GaN:Eu layer grown by PSE will later be applied in GaN:Eu LEDs as the active layer.

References

1 A. J. Steckl and J. M. Zavada: MRS Bull. **24** (1999) 33.

2 A. J. Steckl, J. C. Heikenfeld, D. S. Lee, M. J. Garter, C. C. Baker, Y. Q. Wang, and R. Jones: IEEE J. Sel. Top. Quantum Electron. **8** (2002) 749.

3 A. J. Steckl, J. H. Park, and J. M. Zavada: Mater. Today **10** (2007) 20.

4 J. Heikenfeld, M. Garter, D. S. Lee, R. Birkhahn, and A. J. Steckl: Appl. Phys. Lett. **75** (1999) 1189.

5 Z. Q. Li, H. J. Bang, G. X. Piao, J. Sawahata, and K. Akimoto: J. Cryst. Growth **240** (2002) 382.

6 M. Pan and A. J. Steckl: Appl. Phys. Lett. **83** (2003) 9.

7 J. H. Park and A. J. Steckl: Appl. Phys. Lett. **85** (2004) 4588.

8 J. H. Park and A. J. Steckl: J. Appl. Phys. **98** (2005) 056108.

9 K. Wang, R. W. Martin, K. P. O'Donnell, V. Katchkanov, E. Nogales, K. Lorenz, E. Alves, S. Ruffenach, and O. Briot: Appl. Phys. Lett. **87** (2005) 112107.

10 A. Nishikawa, T. Kawasaki, N. Furukawa, Y. Terai, and Y. Fujiwara: Appl. Phys. Express **2** (2009) 071004.

11 R. Wang and A. J. Steckl: J. Cryst. Growth **312** (2010) 680.

12 N. Kobayashi, T. Makimoto, and Y. Horikoshi: Jpn. J. Appl. Phys. **24** (1985) L962.

13 J. J. Huang, K. C. Shen, W. Y. Shiao, Y. S. Chen, T. C. Liu, T. Y. Tang, C. F. Huang, and C. C. Yang: Appl. Phys. Lett. **92** (2008) 231902.

14 Y. Horikoshi: J. Crys. Growth **202** (1999) 150.

15 Y. Horikoshi, M. Kawashima, and H. Yamaguchi: Jpn. J. Appl. Phys. **25** (1986) L868.

16 D. Sugihara, A. Kikuchi, K. Kusakabe, S. Nakamura, Y. Toyoura, T. Yamada, and K. Kishino: Jpn. J. Appl. Phys. **39** (2000) L197.

17 C. Munasinghe, A. Steckl, E. E. Nyein, U. Hommerich, H. Y. Peng, H. Everitt, Z. Fleischman, V. Dierolf, and J. Zavada: Mater. Res. Soc. Symp. Proc. **866** (2005) 41.

18 C. Munasinghe and A. J. Steckl: Thin Solid Films **496** (2006) 636.

19 S. D. Burnham, W. Henderson, and W. A. Doolittle: Phys. Stat. Soli.(c) - Current Topics in Solid State Physics, Vol 5, No 6 **5** (2008) 1855.

20 S. D. Burnham, G. Namkoong, D. C. Look, B. Clafin, and W. A. Doolittle: J. Appl. Phys. **104** (2008) 024902.

21 M. Moseley, D. Billingsley, W. Henderson, E. Trybus, and W. A. Doolittle: J. Appl. Phys. **106** (2009) 014905.

22 G. Namkoong, E. Trybus, K. K. Lee, M. Moseley, W. A. Doolittle, and D. C. Look: Appl. Phys. Lett. **93** (2008) 172112

23 E. E. Nyein, U. Hommerich, C. Munasinghe, A. J. Steckl, and J. M. Zavada: Mater. Res. Soc. Symp. Proc. **866** (2005) 67.

24 E. E. Nyein, U. Hommerich, J. Heikenfeld, D. S. Lee, A. J. Steckl, and J. M. Zavada: Appl. Phys. Lett. **82** (2003) 1655.

25 H. Peng, C. W. Lee, H. O. Everitt, C. Munasinghe, D. S. Lee, and A. J. Steckl: J. Appl. Phys. **102** (2007) 073520.

Chapter 5. Mg doped GaN by PSE

Mg has a notoriously high activation energy of around 120-250 meV [1-3] in GaN. Thus, the activation efficiency is usually less than 10% at room temperature making high hole concentration doping in GaN very difficult. In order to achieve high hole concentration, one strategy is to increase the activation efficiency by reducing compensation donors and trap densities. High hole concentration of ~3×10^{18} cm^{-3} has been demonstrated with MBE in both Ga-rich [4] and N-rich growth conditions [5]. Although significantly different growth conditions were applied, the resulting films had similar Mg concentrations, limited to low 10^{19} cm-3 range in order to minimize Mg self-compensation or other kind of defects. The other straightforward method is to increase the magnesium concentration. However, greater Mg concentration leads to defects due to the low solubility of Mg in Ga [6]. Mg self-compensation [7] and even GaN polarity inversion [8,9] are usually reported when higher Mg flux is applied.

The group of Alan Doolittle at Ga Tech [10] has developed a dynamic MBE growth scheme - modulated metal epitaxy (MME) - to promote Mg incorporation. During MME, the condition of the growth surface varies periodically with a short period (5 – 10 s), with the shutters for the metal sources (Ga and dopants) opening and closing simultaneously while the N shutter is open throughout the growth. Hole concentration as high as $4.5\times10^{18}cm^{-3}$ with an accompanying mobility of 1.2 $cm^2/V\cdot s$ has been achieved with MME [10].

MME and other similar growth schemes, such as metal enhanced epitaxy (MEE) [11], periodically saturate the growth surface with Ga so that even at relatively low growth temperatures (which result in low Ga surface mobility) excess Ga minimizes Ga vacancy concentration. Subsequent

excess N flux conditions remove N vacancies and prevent Ga droplet formation, resulting in a smooth GaN surface. It should be pointed out that prolonged growth process and varying surface conditions can introduce more contaminants (such as O, C) into the film. Ptak et al. have reported that both extreme Ga-rich or N-rich condition favor oxygen incorporation [12]. Only with a very clean growth environment and ultra high purity gases, can the contamination levels be well controlled.

Phase shift epitaxy (PSE) takes advantage of the variable surface conditions (specifically, Ga ML thickness) during growth. Using PSE, a suitable doping window can be found during the periodic variation of surface conditions for a selected dopant. More specifically, the dopant shutter schedule is designed to be open during a certain period of time in a dynamic cycle so that the dopant is introduced when the growth surface is either Ga-rich or N-rich. The timing sequences of different dynamic growth schemes are shown in Fig. 5.1. A more detailed description these dynamic growth techniques can be found in previous publications [10,13,14,15].

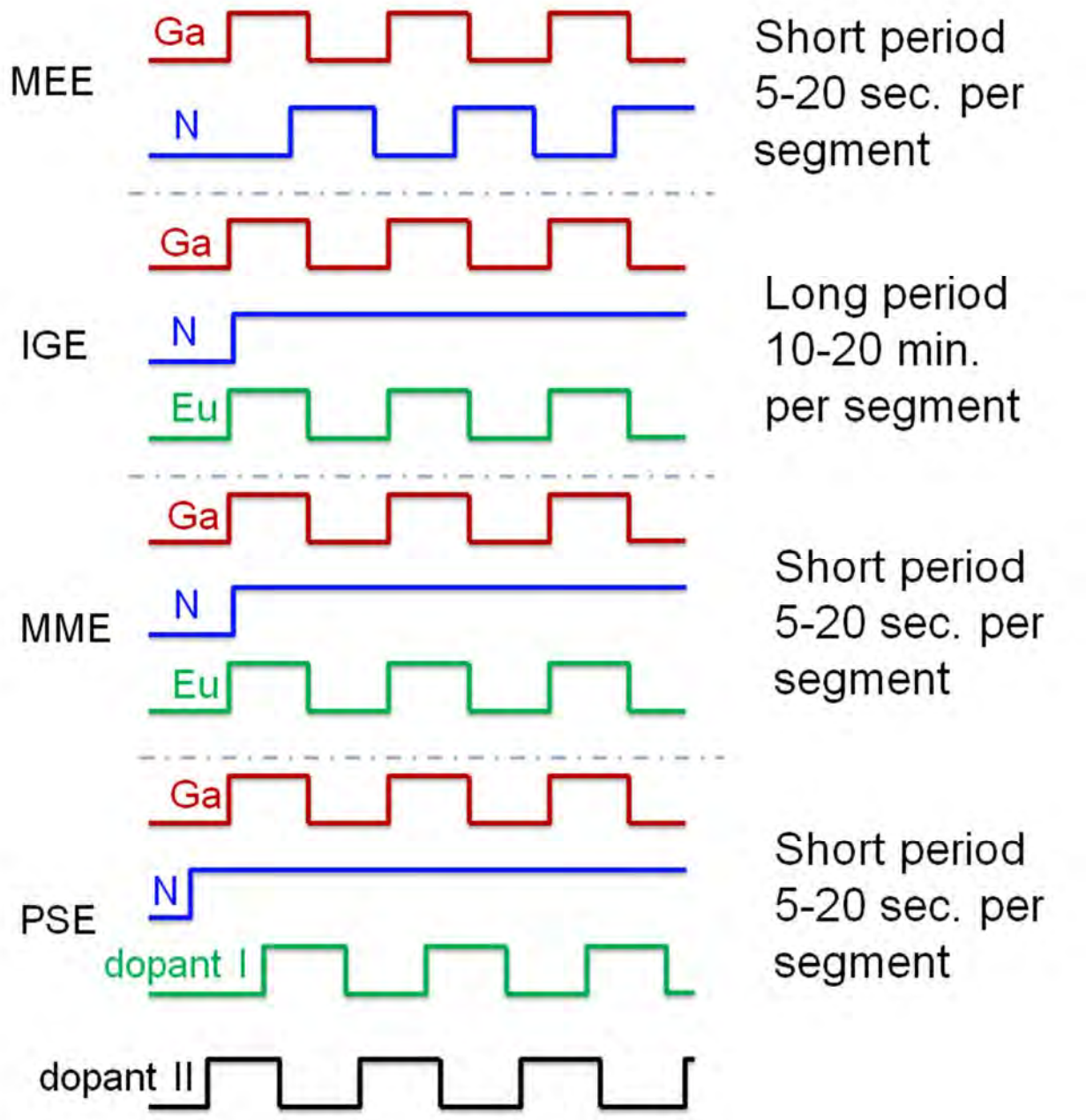

Fig. 5.1 Diagram of different modulated growth schemes. (Migration Enhanced Epitaxy [11], Interrupted Growth Epitaxy [14], Metal Migration Epitaxy [10], Phase Shift Epitaxy [15])

Using PSE to dope Eu in GaN under Ga-rich conditions has been previously shown [15] to lead to a 10-fold enhancement of specific Eu site luminescence efficiency. In this paper, high hole concentration in Mg-doped GaN is achieved by adjusting the doping window in PSE in order to suppress Mg self-compensation at high Mg concentration.

5.1 Experimental Conditions

The experiments are carried out on Nitronex templates (with a 100 nm highly resistive GaN top layer on Si) in a Riber 32 MBE system. High purity N_2 (>6N) is used with an SVT 4.5 RF plasma source with ion removal control. The N_2 source condition (1.8 sccm flow, 230 W plasma power) produces a maximum growth rate of 0.72 ML/s using conventional (i.e. continuous) MBE growth conditions. A thermocouple attached to the back of the substrate holder indicates a temperature of 600 °C. During each cycle, the Ga shutter is open for 8 s to allow Ga to build up on the surface and closed for the next 8 s to deplete the excess Ga atoms on the surface. The Mg shutter also opens for 8 s in each cycle, but is not synchronized with the Ga shutter. The Ga flux is kept at 9×10^{-7} Torr beam equivalent pressure (BEP) (equivalent to 1.1 ML/s) for all growth experiments (except if otherwise specified), while the Mg flux is varied from 2×10^{-10} to 3×10^{-9} Torr BEP.

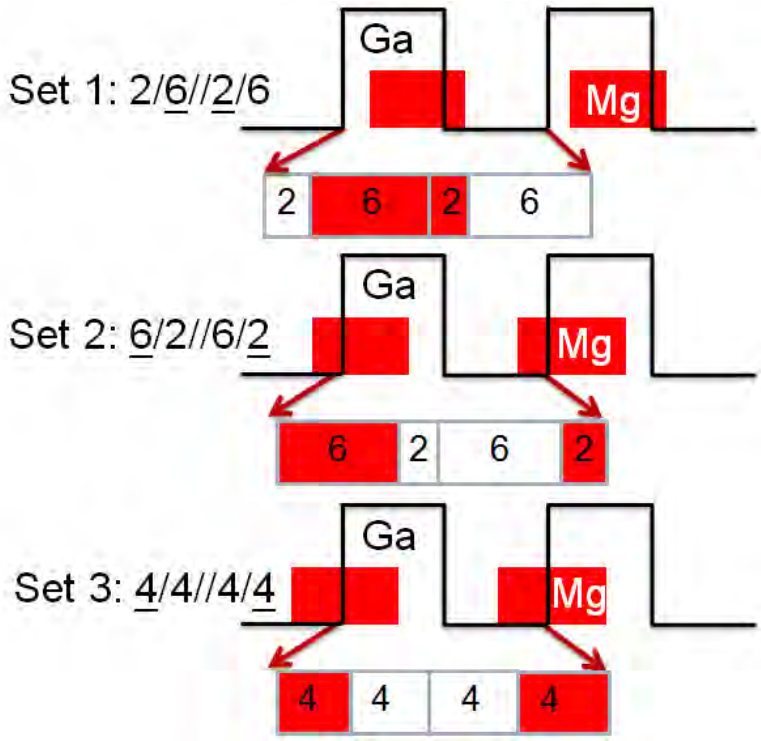

Fig. 5.2 PSE growth schemes for optimum doping condition identification.

In order to determine the favorable surface condition for Mg doping, three sets of growth timing experiments (shown in Fig. 5.2) were performed. The PSE timing schedule is described by x/y//z/w, where "/" separates each segment in each period, "//" separates the Ga ON cycle and Ga OFF cycle and "_" is used to indicate that the Mg shutter is open during the segment.

Since PSE is a dynamic process, each metal beam takes a certain time to turn on and for the corresponding surface coverage to reach maximum. From RHEED intensity variations [16], it is relatively easy to estimate the Ga turn-on time. In our setup, the growth surface takes 2 seconds to change from N-rich to Ga-rich at the beginning of each cycle after the Ga shutter is open and also takes 2 seconds to change from Ga-rich to N-rich after the Ga shutter is closed. However,

the variation of the Mg surface concentration cannot be directly observed. Therefore, the model has been developed to simulate this process. The number of "free" Ga or Mg atoms on the surface has a changing rate equal to the incoming flux minus its consumption rate (by reaction with N) and loss by evaporation, expressed by

$$\frac{dM_t}{dt} = F - G - D. \tag{1}$$

M_t is the metal layer thickness at time t in MLs (ML), F is the incoming metal flux in ML/s, G is the growth rate or dopant incorporation rate in ML/s and D is the desorption rate also in ML/s. G and D are further defined by "free" metal lifetimes: τ_1 - before reacting with nitrogen, eq. (1); τ_2 - before evaporation (eq.2):

$$G\left(M_t, \tau_1\right) = \begin{cases} \frac{1}{\tau_1} \times M_t, \ M_t < 1 \\ \frac{1}{\tau_1}, \ M_t \geq 1 \end{cases} \tag{2}$$

$$D = \frac{1}{\tau_2} \times M_t \tag{3}$$

When the system reaches steady state in conventional MBE with a III/V of close to unity, M_{Ga} =1ML and $\frac{dM_{Ga}}{dt} = 0$ and $\frac{1}{\tau_2} \approx 0$ for Ga due to its low desorption rate at 600 °C. Thus $\frac{1}{\tau_1}$ for Ga is estimated to be 0.72/s. For Mg,

$$\frac{s}{1-s} = \frac{G_{Mg}}{D_{Mg}} = \frac{{}^{1}\!/_{\tau_1} \cdot M_{Mg}}{{}^{1}\!/_{\tau_2} \cdot M_{Mg}} \tag{4}$$

where *s* is the Mg sticking coefficient. The Mg sticking coefficient changes with substrate temperature and surface condition. With rough estimation of the Mg sticking coefficient of 0.1 (although some literature proposed much lower number [17]), and Since the growth is under kinetic limited condition, bonding is considered fast compared with mass transport, one can assume that the Mg has the same incorporation rate *G* as Ga. Then $\frac{1}{\tau_2}$ for Mg can be estimated to be 6.48/s. Solving the differential equation gives the result that only 0.2 s is required for Mg to reach 90% of its peak surface concentration and a similar amount of time is required to remove the Mg surface concentration. The Mg time constants will be larger with higher sticking coefficients, but still much smaller than those for Ga (~2-3 s). Hence, Mg can be considered to exhibit practically instant turn-on on and turn-off.

5.2 Results

During the growth, the surface starts with a streaky 1×1 RHEED pattern and changes to a slightly spotty pattern, as also observed by Namkoong et al. [18]. No polarity inversion is found even at our highest Mg flux. The polarity of the film is indicated by the 2×2 RHEED pattern (Fig. 5.3) during the cool down process after the growth. Hole concentration (solid curves) and Hall mobility (dotted curves) from all three sets of experiments are shown in Fig. 5.4 as a function of Mg concentration (obtained by SIMS (Figure 5.5)) and corresponding Mg flux BEP. The data points in the region where the hole concentration drops in each curve are repeated to confirm the trend. A theoretical curve of hole concentration vs. Mg concentration is also shown based on background donor concentration of 3×10^{18} cm^{-3} and Mg activation energy of 130 meV.

Figure 5.3. 2×2 RHEED reconstruction during the cool down process after growth

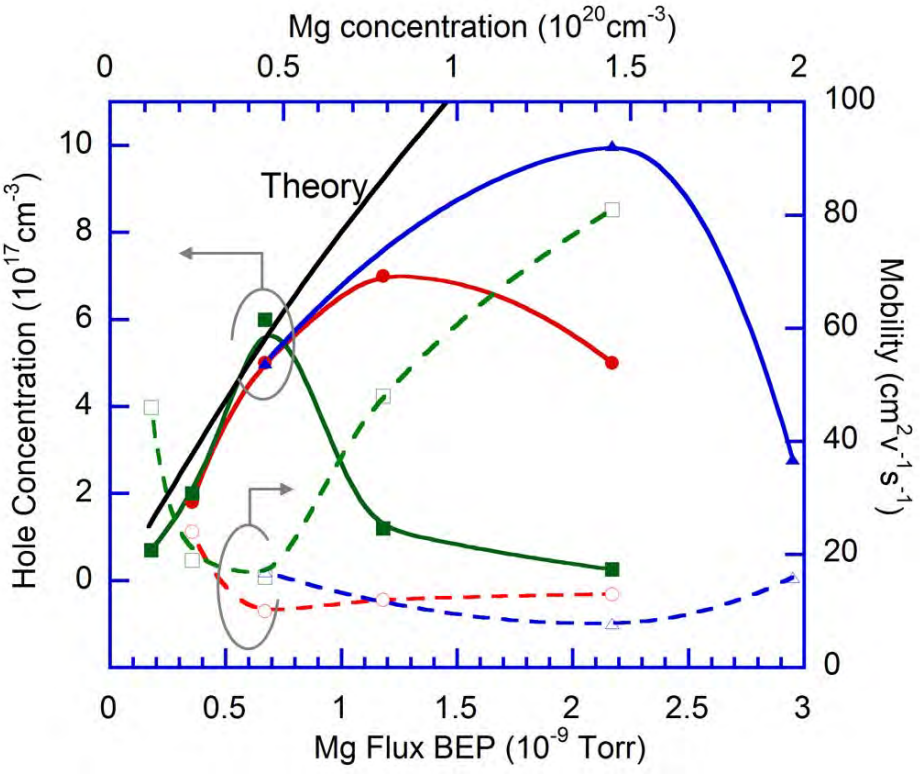

Fig. 5.4 Relationship between hole concentration/mobility and Mg flux/concentration for three sets of experiments (Set 1: ■□, Set 2: ●○, Set 3: ▲△).

In the low Mg flux region (less than ~5×10^{19} cm^{-3}), the hole concentration curves for the three growth conditions are very similar and agree well with the theoretical curve. However, as the Mg flux increases into the high 10^{19} and the 10^{20} cm^{-3} range, Set 1 samples experience a steep drop in hole concentration. The highest hole concentration at the turning point is 6×10^{17} cm^{-3} at a Mg flux BEP of 8×10^{-10} Torr, corresponding to a Mg concentration of 5×10^{19} cm^{-3} . The hole concentration of Set 2 peaks at 7×10^{17} cm^{-3}, produced by a Mg concentration of 8×10^{19} cm^{-3}, corresponding to a Mg flux of ~ 1.4×10^{-9} Torr. In Set 3, the Mg shutter opened for the longest time in the N-rich condition (low Ga ML thickness) of all three sets, and the peak hole concentration increases to 1×10^{18} cm^{-3} produced by a Mg concentration of 5×10^{19} cm^{-3}. All three sets experience a drop in hole concentration at higher Mg fluxes, probably due to Mg self-compensation effect. Doping in the N-rich condition clearly helps postpone the onset of hole concentration dropping at higher Mg flux levels.

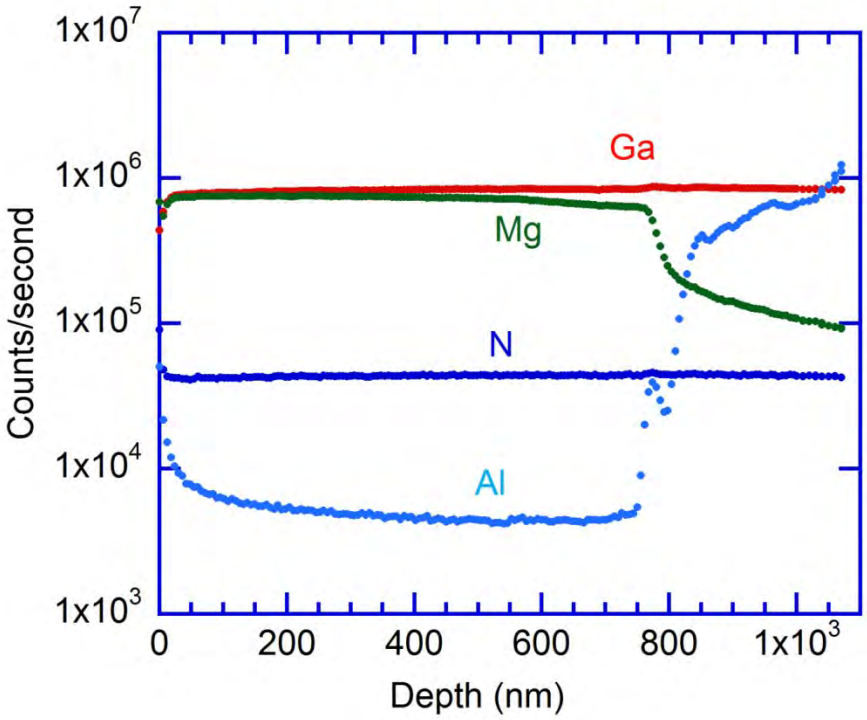

Figure 5.5. SIMS depth profile for p-type GaN doped with Mg (6/2//6/2). Mg flux used in this sample is 6×10^{-10} Torr BEP and Mg concentration is $4\times10^{19}cm^{-3}$.

Inspired by these results, we pursued Mg doping in an even more N-rich condition (3/5//5/3 and reduced Ga flux). This resulted in the highest hole concentration of $2.4\times10^{18}cm^{-3}$ obtained at a Mg flux BEP is 3.5×10^{-9} Torr.

The lowest resistivity among these samples is 0.5-0.7ohm-cm, occurring for samples in Sets 1 and 2, while the sample with the highest hole concentration (from Set 3) shows a resistivity of 1.0 ohm-cm because of lower mobility. The overall relationship between the mobility and the hole concentration for all samples is plotted in Fig. 5.6. Data from all three sample sets follow a

very similar trend, with the mobility monotonically decreasing with increasing hole concentration, which agrees with previously published results [19].

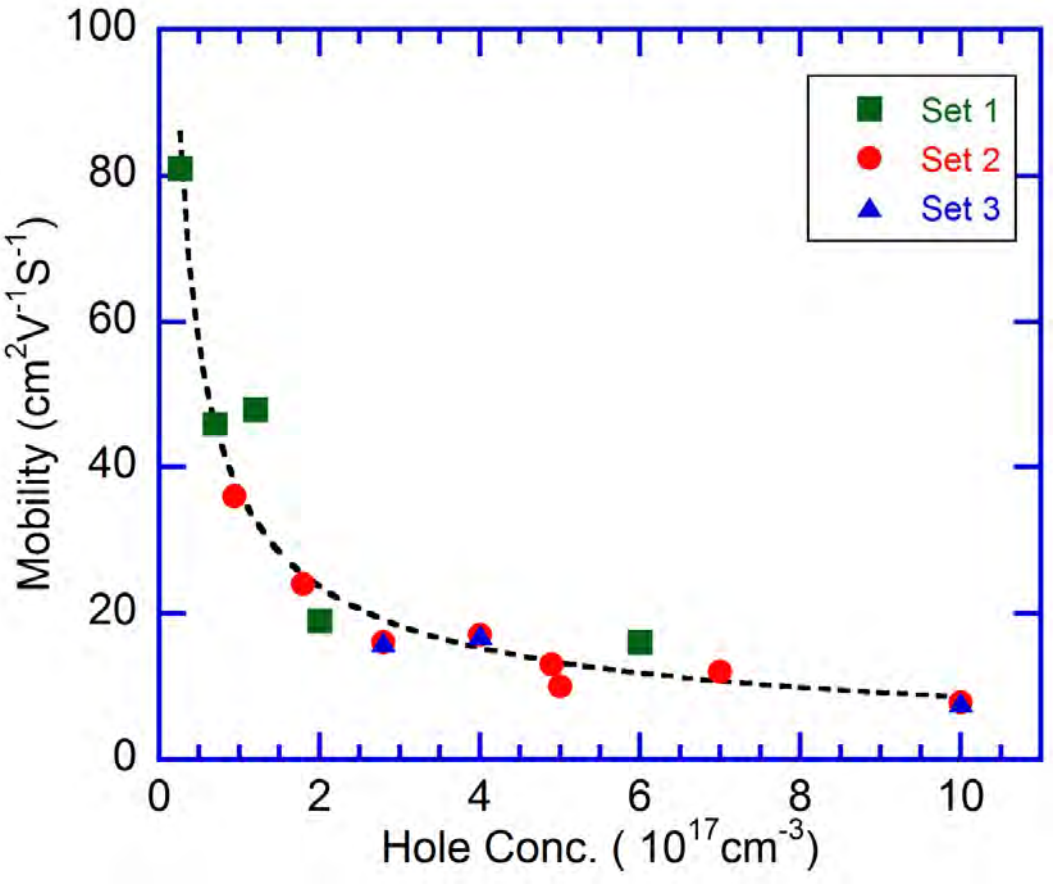

Fig. 5.6 Relationship between hole concentration and mobility for all samples in the three sets of experiments.

Sample #	Growth Scheme	Mg flux BEP (Torr)	Hole Conc. (cm^{-3})	Mobility (cm^2/v-s)	FWHM (002) (arcsec)	FWHM (015) (arcsec)
JT32	2/6//2/6	2.2×10^{-9}	2.60×10^{16}	81	1206	979
JT34	4/4//4/4	2.2×10^{-9}	1.00×10^{18}	7.8	900	846
Template	NA	NA	NA	NA	1022	1098

Table 5.1. Double X-Ray Diffraction test result for selected samples

Two samples (see Table 5.1) with different growth schemes, but similar Mg concentrations, were selected for double crystal x-ray diffraction (XRD) analysis and the Nitronex template is used as a reference. Note that the XRD signals from the template will also be collected during the analysis. However, since the overgrown GaN PSE layer is somewhat thicker compared to the GaN layer in the template (450 nm vs. 400 nm), the signal from the PSE p-type layer will not be overwhelmed by its substrate, and the comparison is still valid. Representative XRD results are shown in Fig. 5.6 and summarized in Table 1. Sample JT34 in set 3 grown under N-rich conditions (growth scheme - $\underline{4}/4//4/\underline{4}$) exhibits narrower peaks than sample JT32 in Set 1 grown under Ga-rich conditions ($2/\underline{6}//\underline{2}/6$) in both (002) and (015) planes indicating lower density of both screw and edge type dislocations. These results agree very well with the Hall effect measurements. The reciprocal map (figure 5.8) from these samples shows a similar trend, and no significant distortion has been found. Furthermore, in the case of sample JT34 the crystal quality indicated by the XRD results represent an underestimate since some of the linewidth broadening is due to the underlying template In general, the quality of the PSE p-type GaN overlayer is limited by the growth template and therefore further improvements in the p-type layer will be achieved as the template growth is improved.

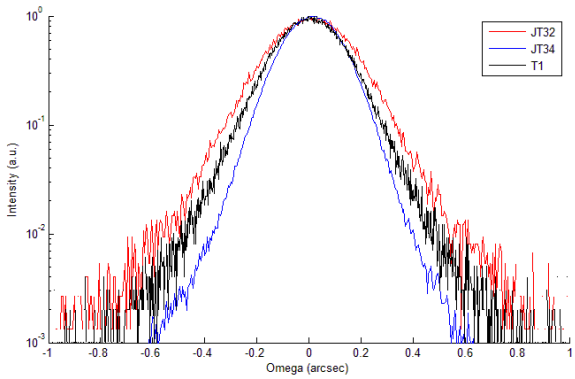

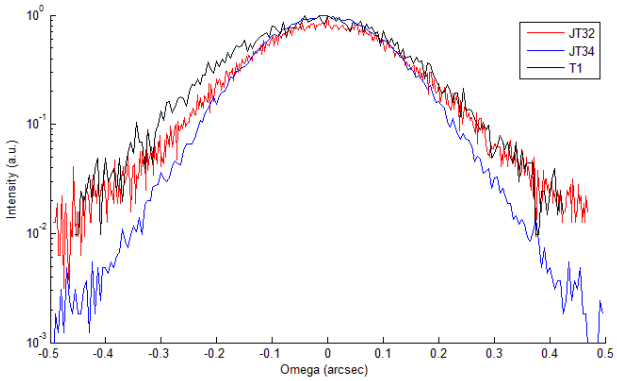

(002) Omega scan FWHM:
JT34: 900 arcsec JT32 1206 arcsec T1:1022 arcsec

(015) Omega scan FWHM:
JT34: 846 arcsec JT32:979 arcsec T1:1098 arcsec

Figure 5.7 XRD peak for (002) and (015) planes.

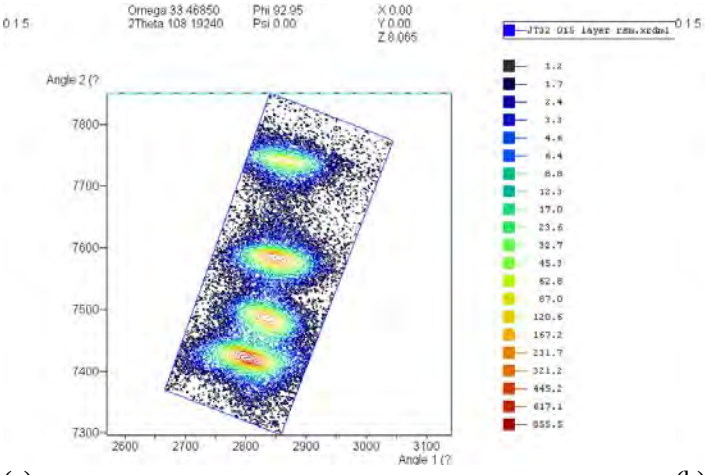

(a)

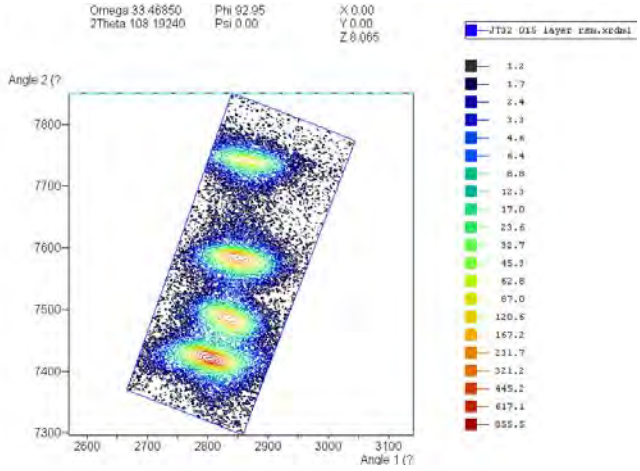

(b)

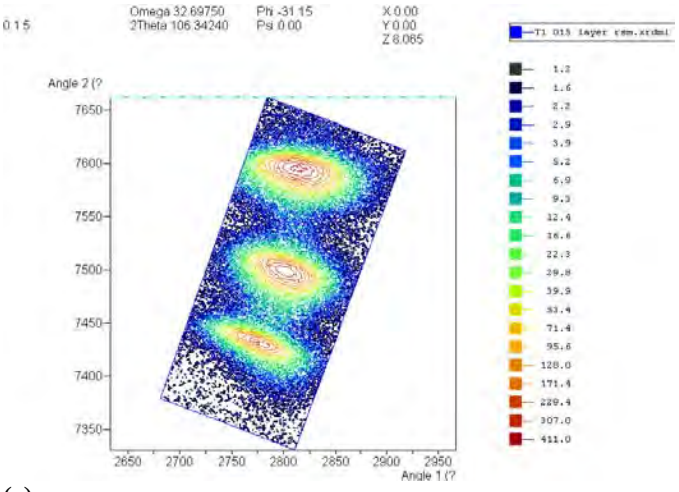

(c)

Figure 5.8 (partial) reciprocal mapping of (a) JT 32 , (b) JT32 and (c) T1

GaN p-n junctions were fabricated on Nitronex templates using the following structure: p ($5\times10^{17}cm^{-3}$)/n ($2\times10^{17}cm^{-3}$)/n^+ ($2\times10^{18}cm^{-3}$). The p-type layer was doped under PSE N-rich condition (8//5/3). Relatively higher growth temperature than previous p-type doping experiments was used to control the leakage current. The leakage current reduction with high growth temperature is tentatively explained by a combination of reduction of trap concentrations and improvement of film structural quality. The thermocouple substrate temperatures for n- and p-type growth are 700 and 680℃, respectively. Increasing the substrate temperature beyond 680℃ during p-type layer growth is found to roughen the surface significantly, especially when high Mg concentration ($>1\times10^{20}\,cm^{-3}$) is used, possibly due to unwanted GaN decomposition of the p-type layer or limited Mg solubility in GaN. ITO and a large Ga pad are used as simple p- and n-type electrodes. For the p-type layer growth, the Mg shutter is turned on for 3 s and then turned off before re-opening the Ga shutter. Thus, Mg is considered being doped completely in extreme N-rich condition. The I-V and J-V characteristics (figure 5.9) show a typical reverse leakage [20] behavior due to a high density of substrate threading dislocations. High threshold voltage of 5 volts and series resistance of 1 Ωcm^2 compared with a published value of 6.3 $m\Omega cm^2$ [21] are due to non-ideal ohmic contacts to both p and n-GaN. p-type surface polarity was tested using NaOH etching [22]. The surface is resistant to the etching indicating that no polarity inversion occurs during the growth, even though Mg is doped without Ga flux, which usually leads to the conjecture that Mg_3N_2 formation will take place [23].

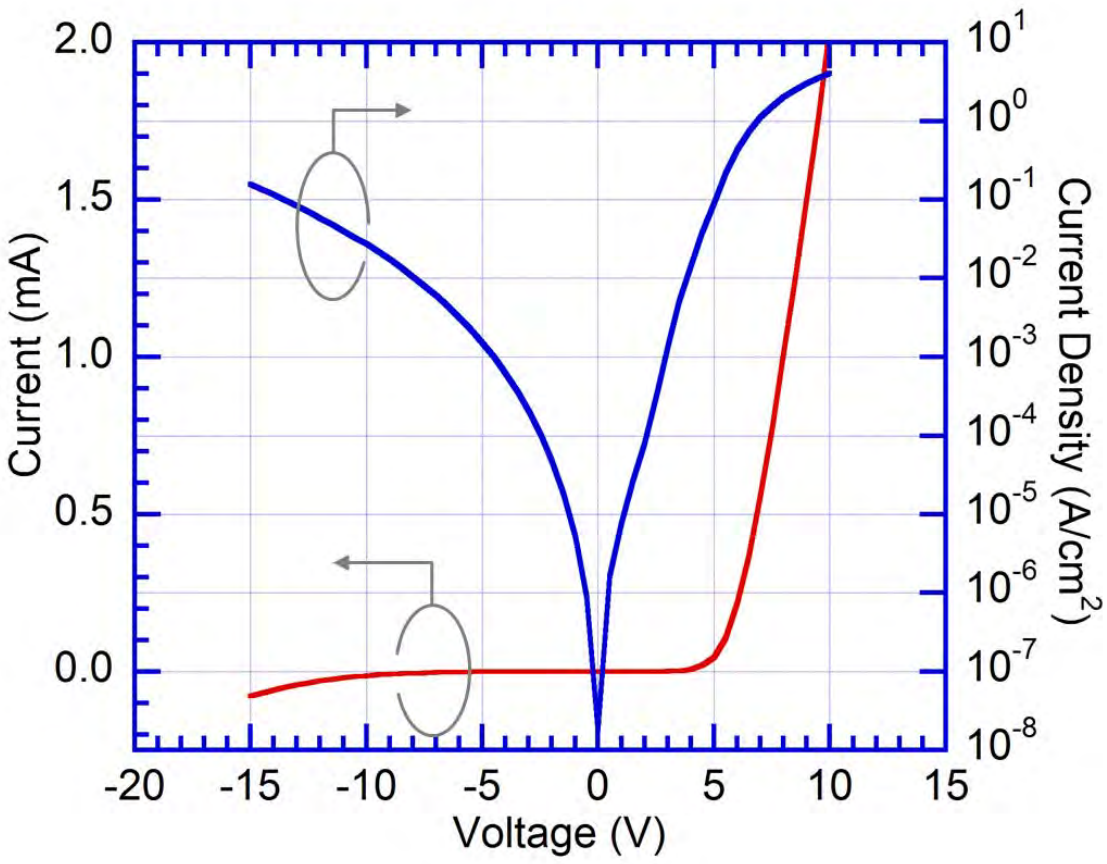

Fig. 5.9 Current-voltage characteristics for p-n GaN diode with p-type layer doping (Mg) in PSE extreme N-rich condition.

5.3 Further Discussion

In MBE growth of compound semiconductors such as GaN, the manner in which dopants are incorporated into the lattice is strongly affected by the surface condition of the host material. During conventional MBE growth of GaN, ~1-2 liquid Ga MLs exist on top of the surface. Mg incorporation into Ga sites is limited by the solubility of Mg in Ga. When complete solubility is not satisfied, excess Mg atoms tend to stay on the surface as surfactants [24] or to form defect

structures such as inversion domains (ID) [6,23]. A Ga pre-wet layer is required to suppress ID formation [23]. On the other hand, when the Ga ML coverage is very low, or there is no Ga on the surface, Ga atoms and dopant atoms behave as separate individual species rather than liquids, so that a complete solubility condition and pre-wet layer are not required. In addition, operating in the extreme N-rich condition significantly reduces adatom mobility so that Mg atoms are not likely to be incorporated jointly as self-compensating donors. While the Ga-rich condition with Ga pre-wet layer helps suppress defect formation it also limits Mg incorporation, especially with high substrate temperature when Mg solubility in Ga is low. To the contrary, when most Mg is incorporated in a Ga-free environment, no noticeable polarity inversion is observed, and higher hole concentration can be achieved due to higher Mg concentration.

5.4 Conclusions

The advantages of PSE over other dynamic schemes and conventional MBE are: (1) it helps distinguish favorable surface condition for designated dopant related structure; (2) desynchronizes doping incorporation from host growth conditions, thus breaking the trade-off between optimum conditions for host growth and doping. In the case of Mg, doping desires extreme N-rich condition while host quality is usually much better when grown at slightly Ga-rich condition. The above advantages make PSE a very effective tool in thin film doping and give PSE the potential to achieve much higher quality doped films than other growth schemes.

References

1 W. Gotz, N. M. Johnson, J. Walker, D. P. Bour, and R. A. Street, Appl. Phys. Lett. **68** (5), 667-669 (1996).

2 J. W. Huang, T. F. Kuech, H. Q. Lu, and I. Bhat, Appl. Phys. Lett. **68** (17), 2392-2394 (1996).

3 W. Kim, A. Salvador, A. E. Botchkarev, O. Aktas, S. N. Mohammad, and H. Morkoc, Appl. Phys. Lett. **69** (4), 559-561 (1996).

4 A. Bhattacharyya, W. Li, J. Cabalu, T. D. Moustakas, D. J. Smith, and R. L. Hervig, Appl. Phys. Lett. **85** (21), 4956-4958 (2004).

5 M. Zhang, P. Bhattacharya, W. Guo, and A. Banerjee, Appl. Phys. Lett. **96** (13), 132103-132103 (2010).

6 C. G. Van de Walle, C. Stampfl, and J. Neugebauer, J. Cryst. Growth **189**, 505-510 (1998).

7 D. J. Dewsnip, J. W. Orton, D. E. Lacklison, L. Flannery, A. V. Andrianov, I. Harrison, S. E. Hooper, T. S. Cheng, C. T. Foxon, S. N. Novikov, B. Y. Ber, and Y. A. Kudriavtsev, Semi. Science and Technology **13** (8), 927-935 (1998).

8 S. Pezzagna, P. Vennéguès, N. Grandjean, and J. Massies, J. Cryst. Growth **269** (2–4), 249-256 (2004).

9 V. Ramachandran, R. M. Feenstra, W. L. Sarney, L. Salamanca-Riba, J. E. Northrup, L. T. Romano, and D. W. Greve, Appl. Phys. Lett. **75** (6), 808-810 (1999).

10 S. D. Burnham, G. Namkoong, D. C. Look, B. Clafin, and W. A. Doolittle, J. Appl. Phys. **104** (2), 024902 (2008).

11 Y. Homma, H. Yamaguchi, and Y. Horikoshi, Appl. Phys. Lett. **68** (1), 63-65 (1996).

12 A. J. Ptak, L. J. Holbert, L. Ting, C. H. Swartz, M. Moldovan, N. C. Giles, T. H. Myers, P. Van Lierde, C. Tian, R. A. Hockett, S. Mitha, A. E. Wickenden, D. D. Koleske, and R. L. Henry, Appl. Phys. Lett. **79** (17), 2740-2742 (2001).

13 Y. Y. Wong, E. Y. Chang, Y. H. Wu, M. K. Hudait, T. H. Yang, J. R. Chang, J. T. Ku, W. C. Chou, C. Y. Chen, J. S. Maa, and Y. C. Lin, Thin Solid Films **519** (19), 6208-6213 (2011).

14 C. Munasinghe and A. J. Steckl, Thin Solid Films **496** (2), 636-642 (2006).

15 M. Y. Zhong and A. J. Steckl, Appl. Phys. Express **3** (12), 121002 (2010).

16 M. Moseley, D. Billingsley, W. Henderson, E. Trybus and W. A. Doolittle, J. Appl. Phys. **106** (1), 014905-014907 (2009).

17 S. D. Burnham, Improved Understanding and Control of Magnesium Doped Gallium Nitride by Plasma Assisted MBE, Ph. D. Thesis in Electrical and Computer Engineering, 2007, Georgia Institute of Technology, Atlanta. p. 26.

18 G. Namkoong, E. Trybus, K. K. Lee, M. Moseley, W. A. Doolittle and D. C. Look, Appl. Phys. Lett. **93** (17), 172112-172113 (2008).

19 U. Kaufmann, P. Schlotter, H. Obloh, K. Kohler, and M. Maier, Phys. Rev. B **62** (16), 10867-10872 (2000).

20 S. W. Lee, D. C. Oh, H. Goto, J. S. Ha, H. J. Lee, T. Hanada, M. W. Cho, T. Yao, S. K. Hong, H. Y. Lee, S. R. Cho, J. W. Choi, J. H. Choi, J. H. Jang, J. E. Shin, and J. S. Lee, Appl. Phys. Lett. **89** (13), 132117-132113 (2006).

21 T.Tanabe, S.Hashimoto, Y.Yoshizumi, and M.Kiyama, SEI Tech. Rev. **64** (21), (2007).

22 A. R. Smith, R. M. Feenstra, D. W. Greve, M. S. Shin, M. Skowronski, J. Neugebauer, and J. E. Northrup, Appl. Phys. Lett. **72** (17), 2114-2116 (1998)

23 D. S. Green, E. Haus, F. Wu, L. Chen, U. K. Mishra, and J.S. Speck J. Vac. Sci. Technol. B **21**, 1804 (2003)

24 E. Monroy, T. Andreev, P. Holliger, E. Bellet-Amalric, T. Shibata, M. Tanaka, and B. Daudin, Appl. Phys. Lett. **84** (14), 2554-2556 (2004).

Chapter 6 PN junction and leakage control

The success in the growth of p type GaN makes fabrication of p-n junction possible. GaN p-n junction fabrication faces significant challenges under our current experiment/growth conditions. One major challenge comes from the substrate (GaN on Si template). The template has a threading dislocation density around 1E9cm^{-3} to 1E11cm^{-3}, which caused by lattice mismatch between GaN and Si. These threading dislocations act as leaky pathways so that the performance of the device is significantly reduced[1,2]. At the beginning of p-n junction device fabrication, all devices shows linear I-V behavior. P-n junctions are shorted by the high leakage current. The goal in this chapter is to reduce the leakage pathways for better current efficiency and reliability of the devices.

6.1 Growth and Fabrication

The Nitronex template used for the p-n junction growth has GaN grown on Si with several buffer layers. The high threading dislocation density in the template is a major source of leakage current. Another leakage origin is the thermal carrier recombination and generation[3], which is related to point defects in the depletion region. A 2 μm thick un-doped GaN layer is grown on the template before the p-n junction growth. After that, 500 nm higly doped n-type GaN with Si (Si cell temperature=1100°C) is grown. This highly doped n-type layer is used to enhance current spread. Then, Si cell temperature is reduced to 1040°C to grow a lightly doped n-type layer of 500 nm After that, shutter for Si source is closed, and a 100 nm unintentionally doped GaN layer is

grown. In the end, 100 nm p-type GaN is grown with PSE (8//5/3, Ga cell temperature = 970°C, Mg cell temperature =270°C).

The fabrication of p-n junction takes simply six steps:

1. Surface cleaning: the sample, is cleaned with HCl solution ($HCl:H_2O=3:1$) to remove the Ga droplets left on the surface. Afterwards, the sample is immersed in saturated NaOH solution for 5 min to etch out inverted polarity region (if there is any). Then, sample is cleaned with an organic solvent and finally rinsed by DI water.

2. Sample is baked in the oven for 1 min at 90 °C to remove water vapor then it is quickly transferred to sputter system for ITO (thickness=150 nm) sputtering. Our sputtering system does not have the substrate heating and in-situ etch option. After ITO sputtering, the sample is annealed in RTA at 450°C for 4 min. ITO conductivity after the heat treatment is greatly increased.

3. Photolithography is then used to pattern top p-type electrode (ITO).

4. The sample is put into HCl solution (HCl: H2O=3: 1) for 45 min for ITO wet etching. This step is to fabricate the ITO top electrode (to p-type GaN).

5. Sample is then dry etched in ICP system (Plasma therm 790). Note that photoresist from the previous step was not removed. The photoresist and the ITO electrode act as a mask in this step.15 sccm Cl_2 and 5 sccm Ar gas are supplied into the chamber, and the operating pressure is maintained at 5 mtorr by controlling the throttle valve. RIE power is set to be 100 W, and ICP power is set to 400 W. The corresponding etching rate is around 600 nm/min. The anisotropic

etching lasts 1 min 10 second, and highly doped n-type GaN layer is exposed after the ICP etching.

6. The sample is cleaned with an organic solvent to remove photoresist. Then, saturated NaOH solution is used to remove damages on the sidewall. Then, the sample is then put on a hot plate (~200 °C), so that Indium can be melted on the exposed highly doped n-type GaN to form n-type electrode.

Please note that ITO and Indium do not form state of art ohmic contact for p type and n type GaN. The reason to choose these materials is simply their availability to us. The SEM images show the top view (at a certain angle) of the structure.

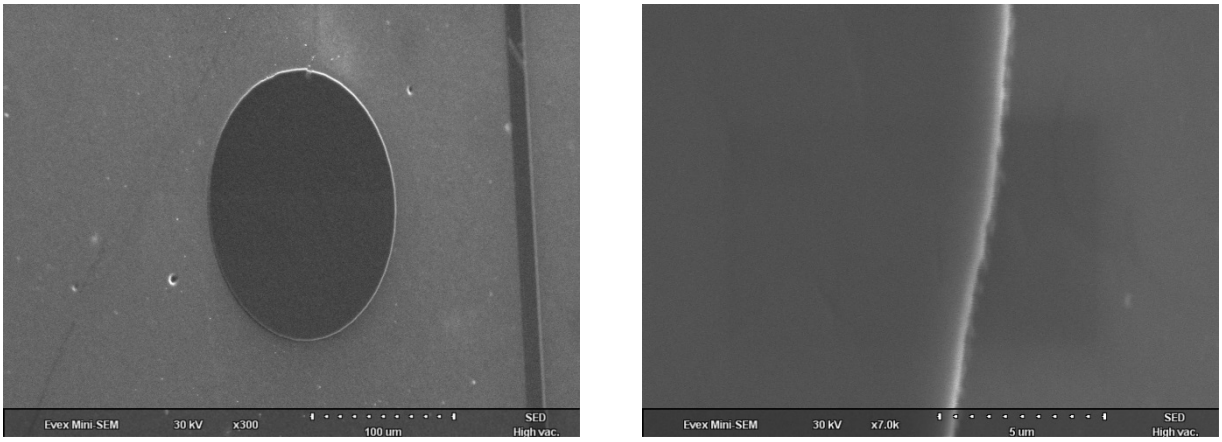

Figure 6.1 SEM images of final p-n junction structure.

6.2 Leakage current

Early experiments use low temperature (600 °C) for the p-n junction growth. There is unfortunately no rectifying I-V behavior found. During the growth, Ga has very limited desorption rate, and thus Ga is easily trapped in the threading dislocation and forms conductive pathway. Furthermore, defect structure is relatively stable at low substrate temperature. Higher trap density is thus believed to be another significant contributor to the leakage current. Low temperature grown p-n junctions are of high leakage, and there is no rectifying IV curve observed. In order to reduce the leakage current of a low temperature grown p-n junction, 2 min post growth annealing at 700 °C with RTA in N_2 environment is carried out. High temperature annealing help passivate leakage pathways, but the exact reason is unknown. Figure 6.2 is the IV curve from the annealed p-n junction.

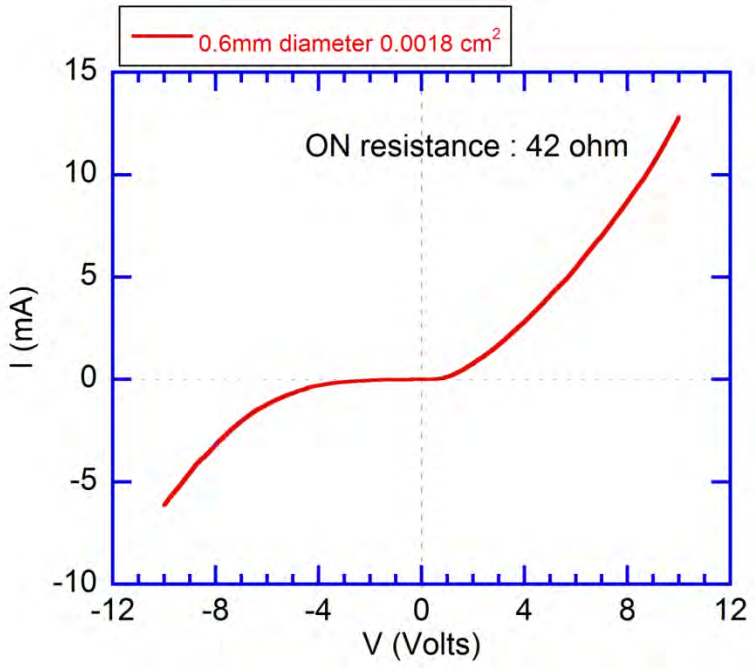

Figure 6.2 IV curve of a GaN p-n junction grown at low substrate temperature (600°C) and post-annealed at 700°C

In order to further improve device's leakage performance, high temperature growth is carried out. Previously, the sample (10x10mm) is indium bonded to a 2 inch Si wafer. Indium bonding is found unstable at high substrate temperature over 650 °C. Currently, to further increase substrate temperature, the small sample is physically secured on to a moly block by Titanium wires. The temperature uniformity is very poor. The edges where sample touches the moly block are of lower temperature. The center of the sample on the other hand, is hotter than the edges. Another problem is that the Ti wires are very likely to be contaminated in the process of "sewing" thus the contamination (especially at the sample edge) is not under control and the repeatability of the experiments is poor.

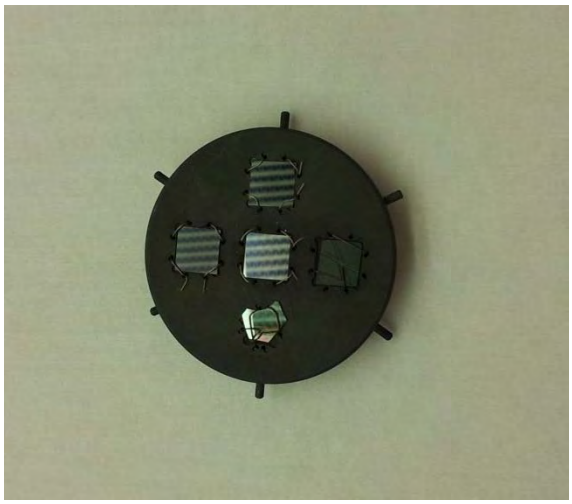

Figure 6.3 sample transfer set-up for high temperature growth

Regardless of the difficulties, I am able to grow a few GaN diodes with reasonably low leakage current. Different III/V resulted in different leakage behaviors. The growth is carried out using previously optimized Nitrogen plasma condition (230 W 1.8 sccm) to minimize the plasma-induced defects. At high temperature, Ga desorption leads to the change (reduction) of effective III/V ratio thus an optimization of III/V ratio is performed by adjusting Ga flux.

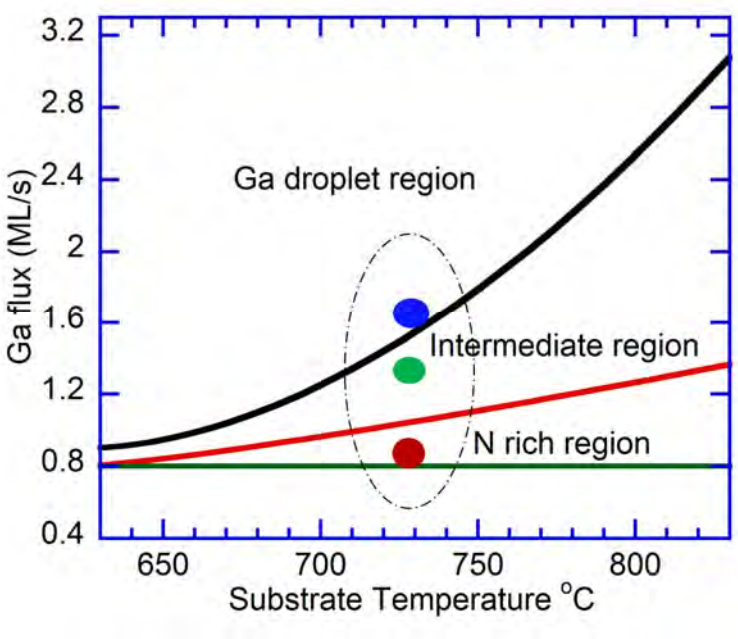

Figure 6.4 Ga flux/surface conditions for n-type GaN in three GaN p-n junctions

Three p-n junctions are grown. p type layers for these diodes are PSE grown under the same condition (substrate temperature= 680 °C, Ga flux =1.1 ML/s , PSE =(8//5/3) and Mg cell temperature =270 °C), but n type layer is grown under conventional MBE with different III/V ratio. These III/V ratios are shown in Figure 6.5: PN7 is grown under N rich condition, PN8 is grown in Ga droplets region and PN9 is grown with effective III/V slightly larger than 1. Figure 6.5 shows the relationship between voltages and current densities of these diodes. For the red curve (PN7), the lowest Ga flux (shown in the red dot in Figure 6.4) is used, and the growth falls into the nitrogen rich condition. This diode has the highest reverse leakage current among three devices. The second highest reverse bias leakage comes from the blue curve (PN8) with n-type layer grown in Ga droplets region (shown in blue dot). The best device in terms of reverse leakage is grown with Ga flux in the intermediate region. Its JV curve is shown in green, and its Ga flux is shown as a green dot. These conclusions agree with previously published results[6]. The

high turn-on currents from PN7 and PN8 do not necessarily mean that these devices perform better when turned on. The forward bias current is enhanced by the forward leakage bias. If we compare the ON-OFF ratio at ±10 V, PN 9 has the highest ON-OFF ratio.

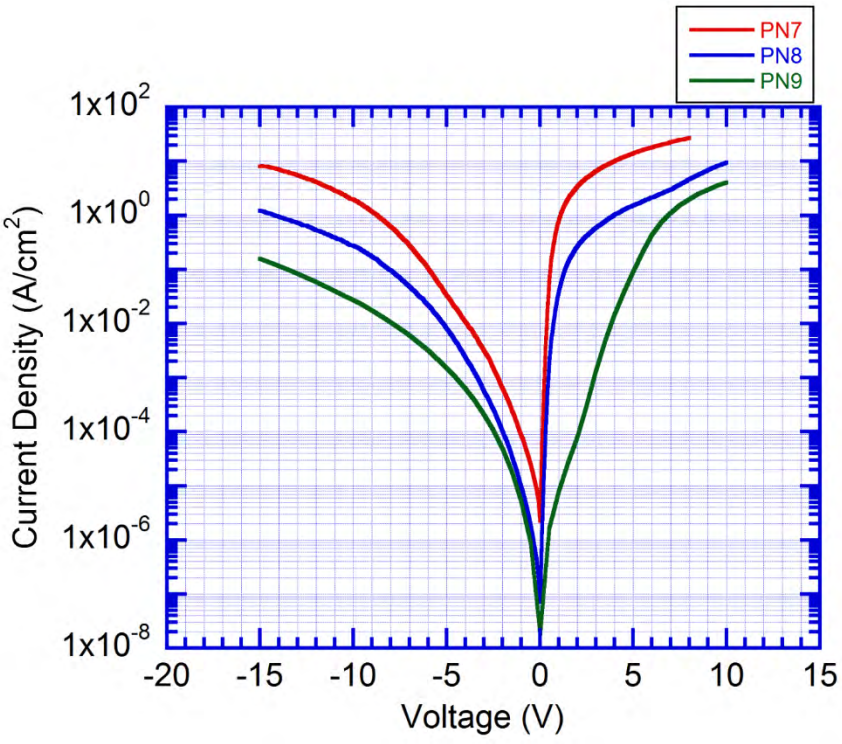

Figure 6.5 current-voltage relationships for three GaN p-n junctions with n type grown in different growth conditions. Green curve: Ga flux just below Ga droplet region; Red curve: Ga flux is in N rich condition; Blue curve: Ga flux sets in droplet region.

References

1. H. Kim, J. Cho, Y. Park and T.-Y. Seong, Appl. Phys. Lett. 92 (9), 092115-092113 (2008).
2. X. L. Fang, Y. Q. Wang, H. Meidia and S. Mahajan, Appl. Phys. Lett. 84, 484 (2004)
3. P. Kozodoy, J. P. Ibbetson, H. Marchand, P. T. Fini, S. Keller, J. S. Speck, S. P. DenBaars, and U. K. Mishra, Appl. Phys. Lett. 73, 975 (1998)
4. Jay S. Brown, Gregor Koblmüller, Feng Wu, Robert Averbeck, Henning Riechert and James S. Speck, J. Appl. Phys. 99, 074902 (2006).

5. V. Sampath, G. A. Garrett, C. J. Collins, P. Boyd, J. Choe, P. G. Newman, H. Shen, M. Wraback, R. J. Molnar and J. Caissie, Journal of Vacuum Science & Technology B: Microelectronics and Nanometer Structures 22 (3), 1487-1490 (2004).

Chapter 7 GaN:Eu LED fabrication and device characterization

RE doped GaN optoelectronic devices have been previously studied in our lab as well as around the world. These devices usually exhibit low quantum efficiency [1-4]. Similar to conventional quantum well LED, the device design (layer thickness, addition of electron/hole blocking layer) is found to affect the performance of the device. Growth conditions significantly different from "normal" conditions are found to enhance the efficiency [5-7]. So far, the reported GaN:Eu LED with the highest efficiency has a Eu doped layer grown in atmosphere MOCVD. In addition, in this device, the active layer thickness ranges from 500 nm to 900 nm, much thicker than quantum well LED active layer (usually less than 200 nm and wall thickness is less than 10 nm). These MOCVD grown devices show rectifying I-V behavior. Other devices grown by MBE [3,4]shows much lower efficiency and in some cases, reverse bias shows even stronger luminescence and higher efficiency [8].

In already published reports[9], reverse bias luminescence from MBE grown device is explained by the hot carrier collision to Eu ions. MOCVD grown samples have rectifying IV curves and people claim that electron hole recombination is responsible for the Eu luminescence [5-7]. Unfortunately, it is hard to judge the quality and defect levels in both MBE and MOCVD grown samples, either conclusion is questionable at this point. In this chapter, optimum growth conditions for p type, n type and Eu doped active layer are used in the GaN:Eu LED. The leakage due to thread dislocations are minimized, all layers are assume to be close to idea. In other words, no defect levels other than those related to the dopants are expected to exist in film.

7.1 Thin film growth and device fabrication

In figure 7.1, schematic structure diagram of the GaN:Eu LED is shown. It has a 30 nm active layer. The growth is carried out in low substrate temperature (600 °C), same temperature used in the optimization of each layer (see Chapter 3-5).The fabrication steps are similar to the p-n junction fabrication described in chapter 6.

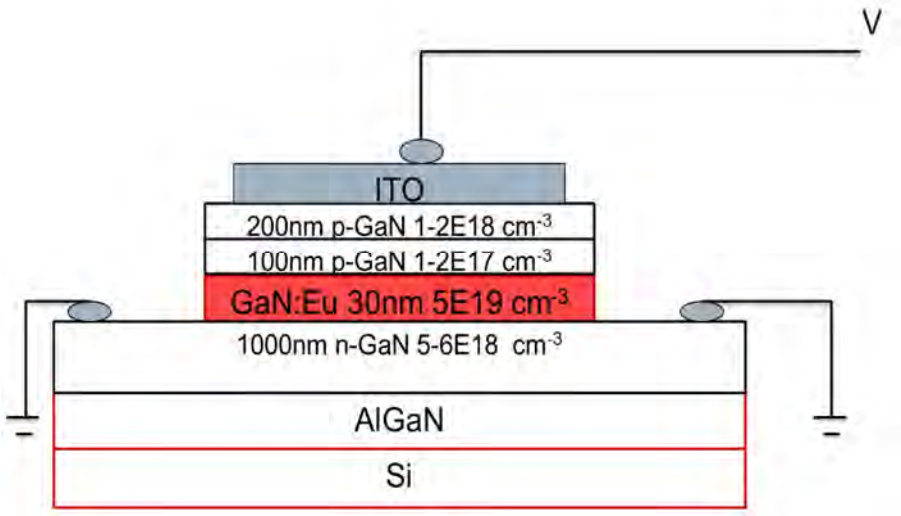

Figure 7.1 schematic structure diagram of the GaN:Eu LED

This device grown at low substrate temperature (600 °C) is found to be leaky (ohmic, straight line IV curve) and only the edge is lit up by electroluminescence under forward bias. The highly doped depletion region and high dislocation density are believed to be big contributors to the leakage current. As described in the last chapter, the low temperature grown p-n junction is very leaky, so we are not able to determine the dominant contributor to the leakage at this point. We are also not sure if the edge-emitting phenomenon relates to the leakage current or the low substrate temperature.

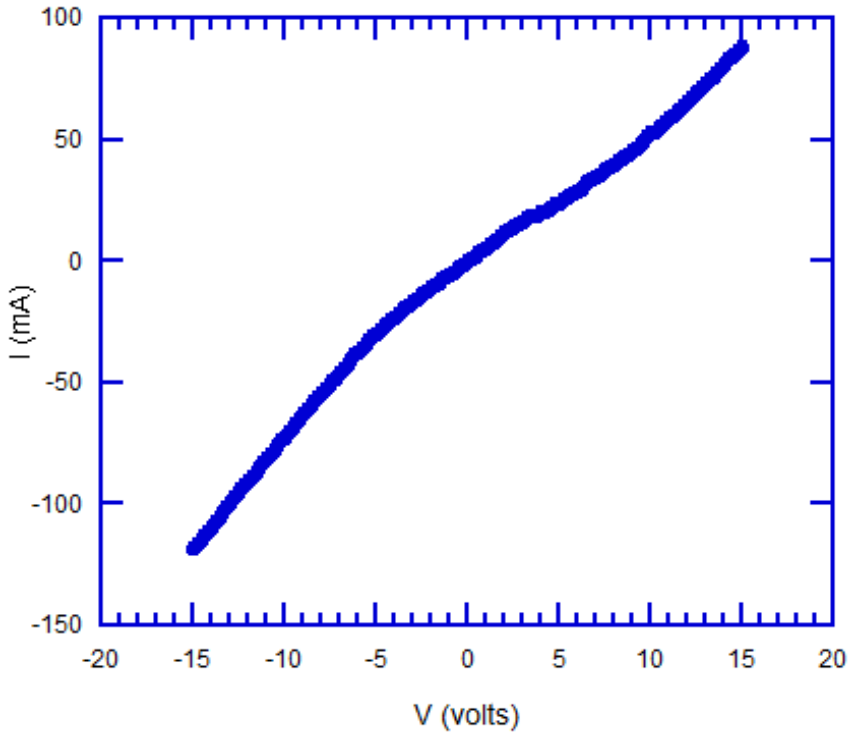

Figure 7.2 I-V curve of the GaN:Eu LED grown at 600 °C

Figure 7.2 is the I-V curve of this device. The I-V curve indicates that the structure is electrically leaky. Light output-voltage relationship is shown in Figure 7.3, the light output is taken on the edge of sample, where the emission is the strongest. The light output saturates at around 15 Volts. The Photoluminescence is also tested; the signal from GaN:Eu layer is extremely weak due to the low thickness of this layer. The electroluminescence spectrums (Figure 7.4) with different forward bias are presented and as the voltage increases, 622 nm peak shows a red shift. This is because that the nature of this transition is an electric dipole transition, which is very sensitive to the intensity of the electrical field. $5D_0$-$7F_2$ line originates from electric dipole (ED) transitions while $5D_0$-$7F_1$ line (around 635nm) originates from the magnetic dipole transition. According to the Judd-Ofelt theory[10], ED transition is only allowed in the absence of inversion symmetry and is sensitive to the local electric field[11].

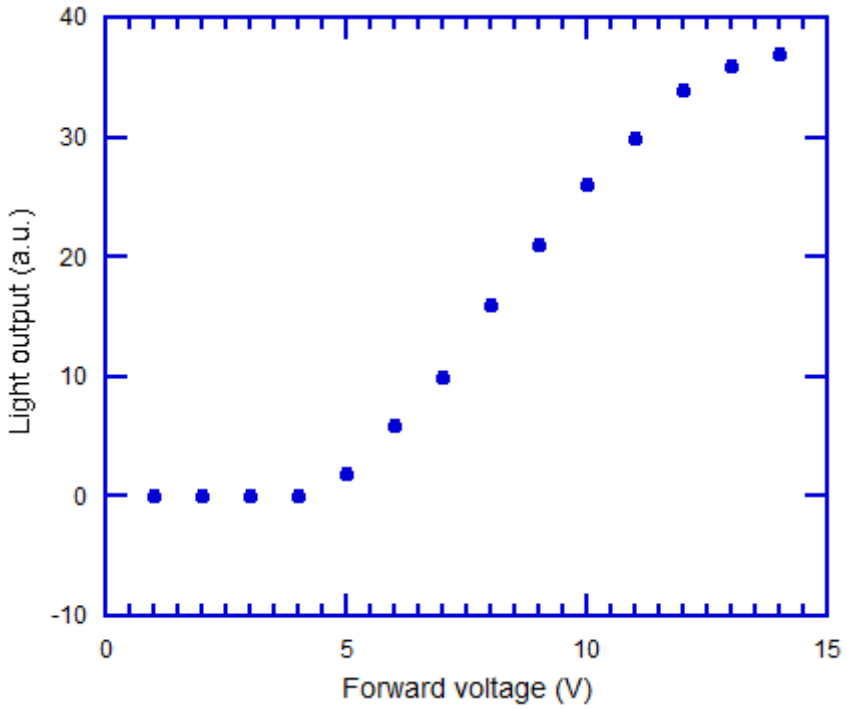

Figure 7.3 light output relationship with forward voltage of GaN:Eu LED grown at 600 °C

The splitting of electric field sensitive $5D_0$-$7F_2$ transition indicates that Eu^{3+} exists in at least two local structural environments differing in symmetry.

The fact that only edge is emitting is very interesting. The edge of the LED structure is believed to have the highest defect density since it is damaged during the dry etching. It is thus possible that defects at the edge promote the energy transfer from band edge to Eu ions.

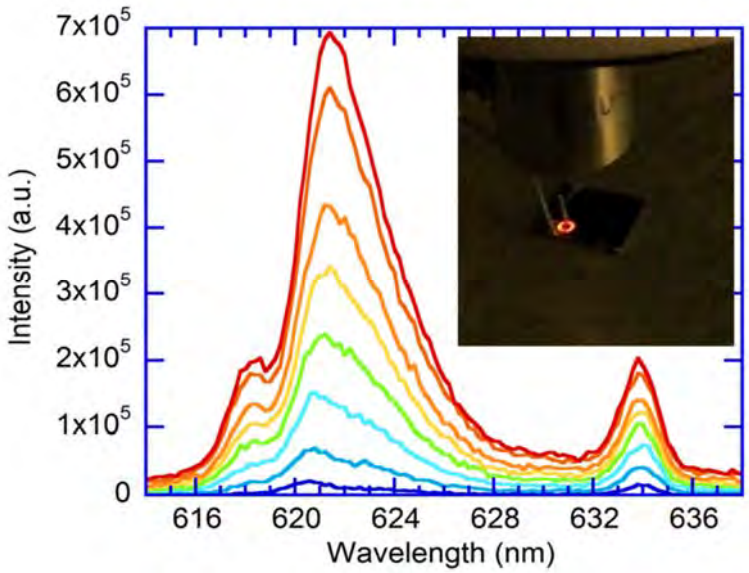

Figure 7.4 Spectrums from GaN:Eu EL. The blue curve (lowest) corresponds to 5 V forward bias, and the red (highest) curve corresponds to 15 V forward bias.

7.2 High substrate temperature growth

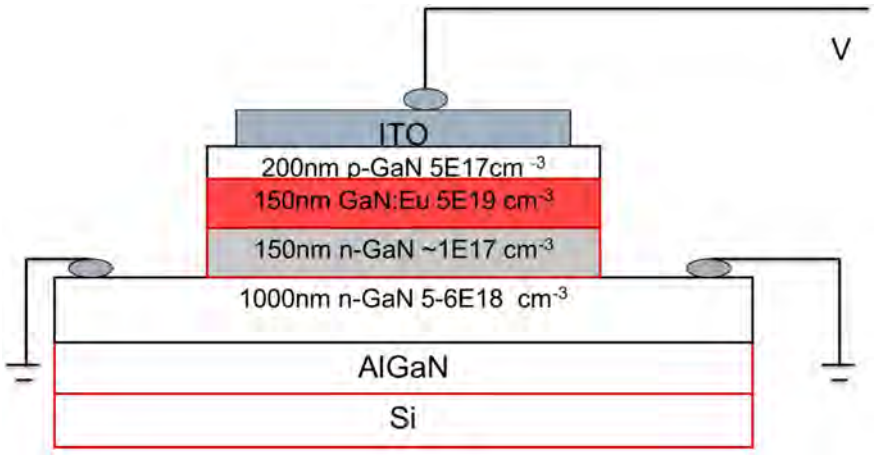

Figure 7.5 schematic structure diagram of the GaN:Eu LED (high temperature grown)

The growth of all three layers (P,I,N) are optimized (dopant incorporated in preferred surface conditions which are determined previously), and the growth temperature is 680 °C for p type and 720 °C for n type and Eu doped layer. There is no electron or hole-blocking layer added at this time. These films have the best film quality we can get from our MBE system. We can thus assume very low defect levels in these films. The Eu doped GaN layer is 150 nm and strong Photoluminescence from Eu ions can be recorded (excitation light source: 325 nm, 30mw HeCd laser). After ICP dry etching step, n-type GaN is exposed and PL is taken from the n type layer. The PL spectrums are shown in figure 7.6. Strong band-edge emission has been observed. The PL results indicate that the films have a very good optical quality. However, the device turns out to be leaky, as seen on its I-V curve (figure 7.7); the reverse current starts to shown ohmic behavior at -3 V. Since the p-n junction leakage has been previously minimized, the leakage current of this LED is believed to result from the high trap density (Eu) in the active layer. The mid gap defect bands caused by Eu ions allow majority carriers to flow through the depletion region to reach the other side of the junction. The device emits red light under both polarities while, under forward bias, only the edge is emitting, similar to the low temperature grown the

device. However, under reverse bias, unlike the low temperature case, the whole structure is emitting.

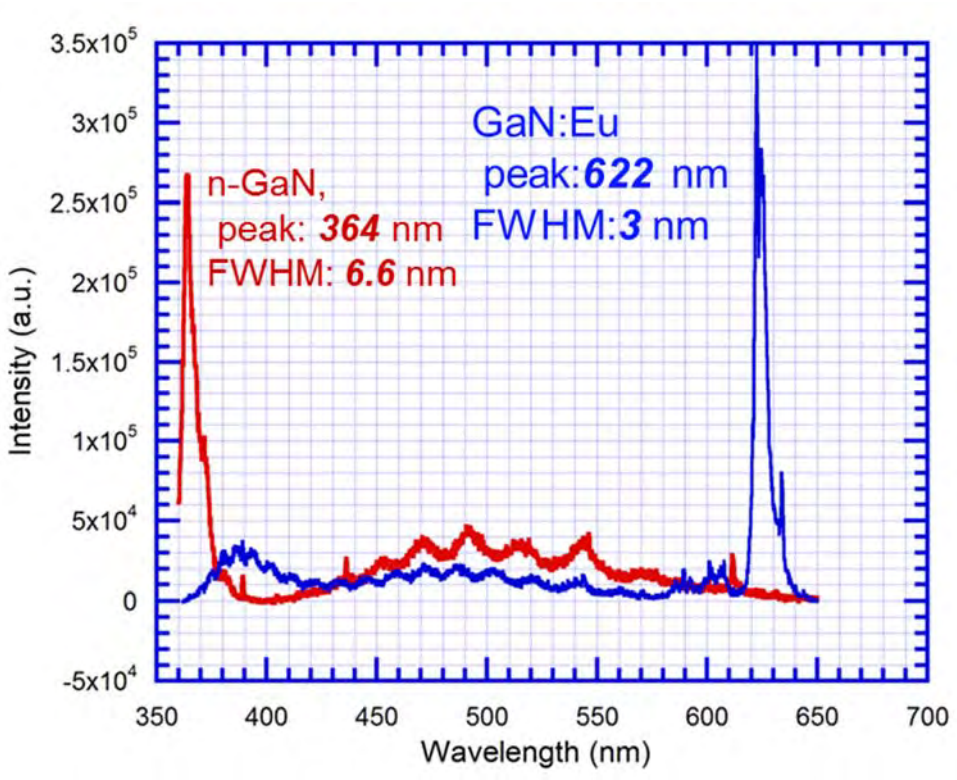

Figure 7.6 Photoluminescence spectrums were taken on n-GaN layer (red) and on p-GaN layer (blue). Since p-GaN is only 100 nm, the underlying GaN:Eu spectrum can also be taken at the same time.

Two LEDs are put in series (see Figure 7.8) with a PN-NP configuration and 45 V is added across two p-electrodes (ITO). Since the LEDs have high reverse leakage current, at high voltages, these devices are considered to have ohmic behavior so that we can assume that two LEDs have around 22 V positive and negative bias respectively.

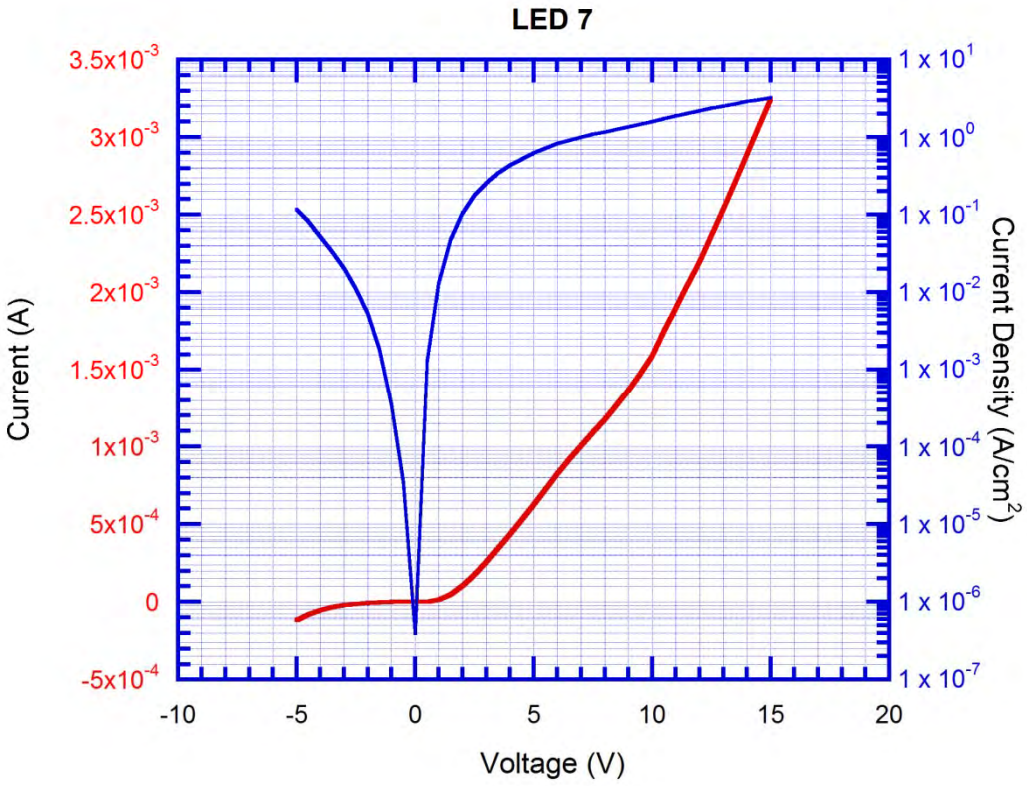

Figure 7.7 Current(current density) –voltage curve of high temperature grown GaN:Eu LED

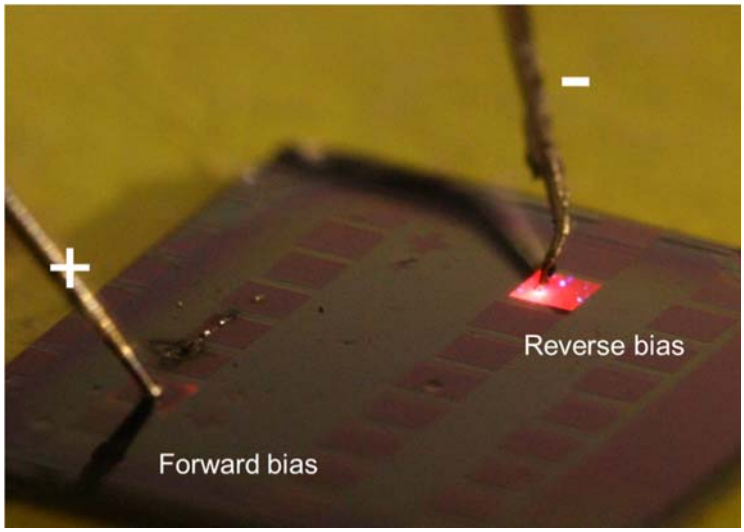

Figure 7.8 Two GaN:Eu LEDs in series with (+PNNP-) configuration. The upper right LED is under reverse bias and the lower left LED is under forward bias.

Discussion

It is very hard to draw any solid conclusions from the characterizations of those devices. In order to explain the results, we can start from the similar behaviors of these two kind devices. They all have edge emission under forward bias. The emission is not from relatively higher quality region but damaged edge indicates that defects play an important role in Eu ion electroluminescence. Let's consider the carrier trapping in a p-n junction in a C-V measurement. Under reverse bias, the carriers are extracted from the traps, and under forward bias, these levels are re-filled. Under forward bias, the defect level is usually filled. If the back filling from valence band to Eu ground state is faster than the luminescence related relaxation, the Eu EL efficiency will be very low. Another possible reason is that the electrons do not have high kinetic energy to activate these Eu ions by impact with forward bias. Under reverse bias, Eu ground state is cleared allowing the "electron-Eu ground state" to happen. The electron may from the conduction band, or from a certain defect band close to conduction band. In the low temperature grown samples, the dominant leakage from low temperature growth related leakage pathways significantly reduced the efficiency so that no emission is observed under reverse bias in that device. There are still many experiments to do to confirm the assumptions, however, the reliability and repeatability of our experiment carried out at high substrate temperature need to be improved.

References

1. D. S. Lee and A. J. Steckl, Appl. Phys. Lett. 79 (13), 1962-1964 (2001).
2. J. Heikenfeld, D. S. Lee, M. Garter, R. Birkhahn and A. J. Steckl, Appl. Phys. Lett. 76 (11), 1365-1367 (2000).

3. J. Heikenfeld, M. Garter, D. S. Lee, R. Birkhahn and A. J. Steckl, Appl. Phys. Lett. 75 (9), 1189-1191 (1999).
4. J. Steckl, M. Garter, D. S. Lee, J. Heikenfeld and R. Birkhahn, Appl. Phys. Lett. 75 (15), 2184-2186 (1999).
5. Nishikawa, T. Kawasaki, N. Furukawa, Y. Terai and Y. Fujiwara, physica status solidi (a) 207 (6), 1397-1399 (2010).
6. Nishikawa, N. Furukawa, T. Kawasaki, Y. Terai and Y. Fujiwara, Appl. Phys. Lett. 97 (5), 051113-051113 (2010).
7. N. Furukawa, A. Nishikawa, T. Kawasaki, Y. Terai and Y. Fujiwara, physica status solidi (a) 208 (2), 445-448 (2011).
8. J. M. Zavada, S. X. Jin, N. Nepal, J. Y. Lin, H. X. Jiang, P. Chow and B. Hertog, Appl. Phys. Lett. 84 (7), 1061-1063 (2004).
9. J. Steckl, D. S. Lee, J. Heikenfeld, C. Munasinghe, M. Pan, Y. Wang, Z. Yu, J. Park, C. Baker and R. Jones, presented at the Compound Semiconductors, 2003. International Symposium (2003)
10. B. M. WALSH JUDD-OFELT THEORY: PRINCIPLES AND PRACTICES (2006)
11. R. Reisfeld, E. Zigansky, and M. Gaft, Mol. Phys. 102, 1319 (2004).

Chapter 8 Conclusions and Future work

8.1 Conclusions

In the first part of this chapter, I would like to review what has been achieved in this thesis and the thinking that led to each critical judgment in my research. Not only the successes, but also the failures will be presented. The research on RE-doped GaN has a history of more than ten years. These thin film materials have been prepared by MOCVD [1-3]as well as MBE on different substrates (sapphire, Si, SiO_2, SiC,etc)[4-7]. People in our group have tried to build DC [8] and AC [9] ELD devices using GaN:RE as an active layer. Different RE excitation mechanisms[1,4] were also purposed. However, the quality of the MBE-grown GaN layer (doped and un-doped) in our group remains low. Optimization efforts were made but the improvements on the thin film quality as well as on PL efficiency were very limited. The high point defect level in the film prevented achieving p-type doping and building efficient devices. All devices previously made in the group had no p-type layer, thus the current injection efficiency were low. This may also explain the poor external quantum efficiency of these devices. In the early stage of my research, my attention was therefore given to the MBE thin film growth process. New areas that were not attempted before in our group were explored; three more variables (nitrogen plasma power, nitrogen flux, and ion current density) were added to the DOE (design of experiment) optimization process; a dynamic approach was also chosen to improve the thin film quality. The decision to proceed with a dynamic approach was based on a few initial experiments that showed

promising results. The goal of these new efforts was p-type doping of GaN, which would lead to the fabrication of an efficient p-n junction device and P-I-N LED.

Combining doping with dynamic growth is very interesting but nothing new. High hole concentrations were already reported using MME: a dynamic approach for doping. In MME, the action of metal shutters (Ga and Mg) was always synchronized, but there was no explanation as to why the synchronization of shutters is required. We gave the name "Phase Shift Epitaxy" to a dynamic growth scheme with desynchronized shutter operations, and Eu doping of GaN using desynchronized shutter operations was carried out as a test to see if shutter opening times matter at all. Eu doping was chosen due to its availability to our group and because we have a long history of studying Eu doping with conventional MBE. To our surprise, results showed higher PL efficiencies if doping Eu in Ga-rich condition in PSE; we observed a peak around 620 nm in these samples. Such a strong peak was never observed before in our group. It is a great encouragement to me that PSE, which is a novel way to combine doping with a dynamic growth scheme, shows advantages over conventional MBE. Moreover, we found that it does in fact matter with doping whether shutters are synchronized or not.

Next, I turned my attention to the p-type doping of GaN with Mg. This is considered a milestone in our pursuit of the fabrication of PIN structure GaN:RE LED. However, our efforts to conduct p-type doping all led to highly resistive films. My focus was then drawn back to the un-doped GaN. As explained previously, PSE is able to desynchronize the host growth and doping; high-quality un-doped GaN grown by PSE is therefore a pre-step of p-type doping of GaN by PSE. With minimized ion energy, optimized N_2*/N and purified nitrogen gas, the un-doped GaN quality was significantly improved and p-type GaN was demonstrated in our group for the first time.

Interestingly, the first p-type GaN was grown in a Ga-rich condition with PSE. I expected at the beginning that the optimum surface condition for Mg was a Ga-rich condition, the same as with Eu doping. However, we found that Mg doping in a PSE Ga-rich condition usually led to highly resistive films and that with high Mg flux, partial polarity inversion was observed. Higher Ga flux (more Ga-rich) made conditions even worse. N-rich PSE was later carried out, and again contrary to my expectations the results showed a mild improvement; a higher hole concentration was measured. Ironically, the comparison of this slightly N-rich (6/2//6/2) condition with the original Ga-rich condition (2/6//2/6) was at first considered unfair; I expected the formation of Mg_3N_2 when opening the Mg shutter with no Ga flux arriving at the substrate. Mg doping experiments in an even more N-rich condition were carried out. The results showed an even lower Mg self-compensation level. After several repeats, I found similar trends: An N-rich condition is more favorable for Mg doping.

P-n junctions and LEDs are then grown and fabricated. Unfortunately, one challenge I have to face is the high threading dislocation density (TDD) on the template (GaN on Si). To minimize the leakage current resulting from the high TDD level, I used a substrate temperature that was higher than previously used in single-film growth. Actually, the high substrate temperature created more problems than it solved. Indium bonding could no longer be used and we did not have an effective way to secure the sample to its holder. A high substrate temperature resulted in poor repeatability of the growth. The research thus came to a stop, but the results surely proved the feasibility of using PSE-grown films in a device fabrication.

I hope the above paragraphs explain how the research began and at what point it concluded. To summarize this thesis, it describes a new dynamic growth and doping technique called Phase Shift Epitaxy, which has been successfully applied to Eu and Mg doping of GaN. This technique

is useful in studying the effect of surface condition and doping concentration on thin-film quality without altering the growth conditions of the host material.

The luminescence from a specific Eu site in the GaN lattice is enhanced 10 times by doping Eu under a Ga-rich PSE condition. This also indicates that the formation energy of various Eu sites can be adjusted with the help of PSE.

This technique is further tested in Mg doping of GaN. Not only was the first p-type GaN sample achieved using this technique in our group, but we were also able to get a very high hole concentration (2.4E18 cm^{-3}), comparable to the best numbers ever published. This is achieved by doping Mg in an N-rich condition in the PSE cycle, which helps suppress the notorious Mg self-compensation effect.

The success of p-type GaN growth enabled us to build a device with a P-I-N structure and conduct initial experiments on these devices. The leakage current of these devices was significantly reduced by growing these devices at high substrate temperature. A prototype GaN:Eu LED with low defect density has been fabricated. With forward bias the devices were found to emit light only on the edge, but with reverse bias the whole structure can be lit up.

8.2 Future Work

In the study of Mg doping of GaN with PSE, we found that incorporating Mg in an N-rich condition greatly suppressed the self-compensation effect. The self-compensation effect is a

result of the formation of Mg clusters. In other words, doping Mg in an N-rich condition helps uniformly distribute Mg, increasing the formation energy of the clusters.

In high indium-content InGaN, indium clusters contribute to the carrier localization [12-14] and greatly reduce the current efficiency of an InGaN quantum-well LED at high current density. This problem is similar to Mg doping of GaN, except that indium content could be as high as 40-50 atomic percentage. Phase Shift Epitaxy with Indium incorporation under N-rich conditions provides the possibility of improving the uniformity of indium distribution. Therefore, high indium-content "green" and "red" quantum-well LEDs can contribute to higher efficiency at improved current densities.

References

1. Wakahara, H. Sekiguchi, H. Okada and Y. Takagi, Journal of Luminescence 132 (12), 3113-3117 (2012).
2. Nishikawa, T. Kawasaki, N. Furukawa, Y. Terai and Y. Fujiwara, physica status solidi (a) 207 (6), 1397-1399 (2010).
3. Nishikawa, N. Furukawa, T. Kawasaki, Y. Terai and Y. Fujiwara, Appl. Phys. Lett. 97 (5), 051113-051113 (2010).
4. J. Steckl, D. S. Lee, J. Heikenfeld, C. Munasinghe, M. Pan, Y. Wang, Z. Yu, J. Park, C. Baker and R. Jones, presented at the Compound Semiconductors, 2003. International Symposium on, (2003)
5. J. Steckl, M. Garter, D. S. Lee, J. Heikenfeld and R. Birkhahn, Appl. Phys. Lett. 75 (15), 2184-2186 (1999).
6. J. Heikenfeld, D. S. Lee, M. Garter, R. Birkhahn and A. J. Steckl, Appl. Phys. Lett. 76 (11), 1365-1367 (2000).
7. J. Heikenfeld, M. Garter, D. S. Lee, R. Birkhahn and A. J. Steckl, Appl. Phys. Lett. 75 (9), 1189-1191 (1999).
8. J. Heikenfeld and A. J. Steckl, "Electroluminescent devices on glass using a high temperature stable GaN-based phosphor and thick film dielectric," IEEE Trans. Electron Devices, (49) 557–563 (2002)

9. J. Heikenfeld, and Andrew J. Steckl, IEEE TRANSACTIONS ON ELECTRON DEVICES, 49 (9) 1545 (2002)
10. R. Wang, A. J. Steckl, E. E. Brown, U. Hommerich and J. M. Zavada, J. Appl. Phys. 105 (4), 043107-043103 (2009).
11. D.-g. Lee, A. Nishikawa, Y. Terai and Y. Fujiwara, Appl. Phys. Lett. 100 (17), 171904-171903 (2012).
12. J. Wang, L. Wang, W. Zhao, Z. Hao and Y. Luo, Appl. Phys. Lett. 97 (20), 201112-201113 (2010).
13. Y. J. Wang, S. J. Xu, Q. Li, D. G. Zhao and H. Yang, Appl. Phys. Lett. 88 (4), 041903-041903 (2006).
14. S. Hammersley, D. Watson-Parris, P. Dawson, M. J. Godfrey, T. J. Badcock, M. J. Kappers, C. McAleese, R. A. Oliver and C. J. Humphreys, J. Appl. Phys. 111 (8), 083512-083516 (2012).
15. Veeco Application Note March 1997 • Note No. 1/97